NUCLEAR INTERACTIONS OF THE SOLAR AND GALACTIC COSMIC RAYS WITH INTERPLANETARY MATERIALS

By

Madhukar B. Potdar

A THESIS
SUBMITTED FOR DEGREE OF DOCTOR
OF
PHILOSOPHY OF THE
GUJARAT UNIVERSITY
AHMEDABAD

OCTOBER 1981

PHYSICAL RESEARCH LABORATORY
AHMEDABAD 380009 (INDIA)

CERTIFICATE

I hereby declare that the work presented in this thesis is original and has not formed the basis for the award of any degree or diploma by any university or institution.

Madhukar B. Potdar

Madhukar B. Potdar
(Author)

Certified by:

N. Bhandari
(Thesis Adviser)
October 1981

To

My Wife
KAVERI

And

My Daughter
VARSHA

TABLE OF CONTENTS

ABSTRACT

In this thesis the dependence of production rates of cosmogenic nuclides ^{10}Be, ^{26}Al, ^{21}Ne, ^{22}Ne and ^{60}Co in meteorites and lunar samples on size and depth has been evaluated. Based on these investigations, the long-term flux and spectrum of the solar and galactic cosmic rays are deduced. Several physical processes which govern the nuclide production depth profiles in meteorites and lunar samples, such as mass erosion due to micrometeorite impacts, collisional fragmentation resulting in multiple exposures to cosmic rays, and the ablation of meteorites in the earth's atmosphere are studied in order to evaluate the depth and size dependent production rates. The effect of solar modulation of galactic cosmic ray intensity has been taken into account by calculating the annual average GCR fluxes during all the years covering solar cycle 20. We have used the documented lunar samples of known exposure history, shielding depth and irradiation geometry and the meteorite samples with known shielding depth, so that cosmic ray effects can be correlated with these parameters.

The ^{26}Al depth profile in a 50 cm radius Dhajala chondrite has been determined to deduce the spectra of nuclear active particles as a function of depth within the framework of a model used for calculating production rates. Several features of variations of GCR and the secondary

nucleons can be understood by a comparison of measured and calculated profiles, for example, the experimental ^{22}Na depth profile in Dhajala when compared with the calculated profile shows a significant excess, a part of which can be attributed to high GCR fluxes during solar cycle 20. The measured ^{60}Co production profile is used to calculate the slowing down density of the 0.5-300 eV integrated epithermal neutrons in a 50 cm radius body. The slowing down density is less than the model calculations based on the fast neutron source function deduced from cosmogenic ^{4}He depth profiles. It is found that the production ratio ($^{10}Be/^{60}Co$) is sensitive to the shielding depths and can be used to determine the preatmospheric size of meteorites.

The measured activities of radionuclides ^{10}Be, ^{26}Al and ^{60}Co in a sample of Kirin chondrite ($R_E \sim 100$ cm) are found to be consistant with the expected production. The depth profiles of cosmogenic nuclides viz. ^{21}Ne, ^{22}Na, ^{26}Al, ^{53}Mn, ^{54}Mn and ^{60}Co are reconstructed.

The depth and size dependent production rates of ^{21}Ne and ^{22}Ne are calculated for chondrites with $R_E > 6$ cm. These calculations allow us to establish a criterion based on track production rates and $(^{22}Ne/^{21}Ne)_{sp}$ correlation diagram for identification of chondrites with complex exposure history. Several chondrites with complex exposure history are identified. Based on an assumed irradiation shielding depth in parent bodies, the model exposure ages have been calculated.

One of the important physical processes which introduces uncertainty in the preatmospheric size and velocity of meteorites and hence in their heliocentric orbits is the atmospheric ablation. The Baldwin-Sheaffer (1971) ablation model is used with some variations to deduce the preatmospheric velocities of several meteorites. The velocities can be estimated within an uncertainty of ± 0.5 to ± 2 km/sec.

The ^{26}Al depth profile measurements in lunar rocks 61016,287, 69935,14 and soil 67481,7 are consistent with long-term average SCR flux given by the parameters (Js,Ro) = (125,125). The long-term average flux is higher than the solar cycle 20 average of (90,85) and lower than the cycle 19 average of (378,100-130). This higher long-term average can be reconciled with the several periodicities in solar flare activity.

ACKNOWLEDGEMENTS

I express my deep sense of gratitude to Prof.Narendra Bhandari for introducing me to this exciting field of extraterrestrial sciences and guiding me throughout the course of this investigation.

I am indebted to Prof.D.Lal, K.Gopalan, M.N.Rao, B.L.K. Somayajulu, S. Krishnaswami and O.P.Agrawal for numerous useful discussions and constant encouragement throughout.

I had great pleasure in working with several of my collegues Drs. S.K. Bhattacharya, P.N.Shukla, H.R.Prabhakara, T. Raman and A.K.Singhvi. The help rendered by Dr.P.N.Shukla in lunar radiochemistry is gratefully acknowledged. I am thankful to Mr.M.M.Sarin for atomic absorption measurements.

I am indebted to NASA(USA) for lunar samples, to the USSR Academy of Sciences for Luna-24 core soil sample and to the Academica Sinica for Kirin sample. Also, I am indebted to Dr.R.C.Agrawala (Govt.Museum, Jaipur) and to Dr.B.P. Sinha (Patna Museum) for meteorite samples.

In this thesis, I have used unpublished data from several sources. I am grateful to Drs. L.A.Rancitelli, G. Heusser, M. Honda, D. Lal, J.N.Goswami, E.L. Fireman, R.M.Lindstrom, K.Nishiizumi for communicating their unpublished data.

I have benefited by numerous fruitful discussions with Dr.Robert Reedy of Los Alamos Scientific Laboratory and to Dr.Barret Baldwin of NASA/Ames Research Center.

I am grateful to M/s N.R.Manchanda, A.R.S. Pandian and G.D.Panchal for developing new NIM modules and maintaining the electronics.

I am thankful to my friends Drs.Prem Sagar, P.Sharma, D.V.Borole, V.N. Nijampurkar, Sheela Kusumgar, T.R.Venkatesan, R.K.Pant, Ravi Korisetter and M/s C.M.Nautiyal, R.Jha, J.T. Padia, N.Hussain, J.R.Trivedi, M.Bhaskaran, P.Sharma, R. Rengarajan, R.Ramesh, V.G.Shah, Deo Murari, K.M. Suthar, Chhaya and Nirzari for their kind co-operation. Also my thanks are due to Dr.D.R.Kulkarni and Mr.C.S.R.Murty for their encouragements.

My sincere thanks are due to Mr.Shanti Bhavsar, Mr.Jagdish Vora and D.R.Ranpura for their co-operation in drafting, xeroxing and photography, and to Mr.J.P.Bhavsar for his assistance in chemistry. My thanks are also due to Mr.K.V. Haridas for carrying out the arduous task of typing the manuscript.

Finally, my thanks are due to numerous PRL collegues who have directly and indirectly helped me in accomplishing this task.

Madhukar B. Potdar

LIST OF FIGURES

LIST OF TABLES

CHAPTER-I

INTRODUCTION

In this thesis, the nuclear interactions of the solar and galactic cosmic rays with interplanetary materials viz. meteorites and Moon samples resulting in production of stable and radioactive nuclides are studied. Based on depth and size dependent production rates of cosmogenic nuclides, the long-term characteristics of solar and galactic cosmic rays are deduced. A brief introduction to the nature of cosmic rays and the nuclear interactions followed by a section on scope of the thesis are given in this chapter.

A. The nature of the Cosmic Rays :

The interplanetary medium of our solar system is permeated by energetic charged particles of both the solar and extra-solar origin. The Galactic Cosmic Rays (GCR) originate in high energy stellar processes in our milky-way galaxy and are subsequently accelerated and scattered in the interstellar magnetic fields before impinging on the heliosphere. They arrive from all directions and isotropically. Only the ultra-high energy cosmic rays ($E > 10^{19}$ eV) are expected to show anisotropy in their arrival directions giving clues to their sources (Wdowczyk and Wolfendale 1980). Because of higher general magnetic field strength in heliosphere ($\sim$5 gammas) compared to local interstellar magnetic field ($\sim$0,3 gammas), only high energy GCR with gyroradii greater than the dimension of heliosphere ($\sim$70-100 A.U.) can penetrate the heliosphere.

This results in solar modulation of the galactic cosmic rays. The interplanetary magnetic field decreases with heliocentric distance and consequently, low energy GCR flux increases with heliocentric distance. Contemporary GCR mainly consists of 93% protons, 6% helium nuclei, 1% metals ($Z > 2$). The VH ($20 \leq Z \leq 28$) nuclei abundances peaks at Fe nuclei and VVH (≥ 30)/VH$\sim 1.3\times10^{-3}$ (Bhandari et al.1973). This does not necessarily represent source composition, because source composition changes significantly due to spallation reactions of GCR with the interstellar matter(ISM).

The VH and VVH nuclei in cosmic rays slow down by ionization energy loss producing solid state damage in meteoritic and lunar rock minerals which can be revealed as tracks by suitable chemical etching. The tracks seen in extra-terrestrial bodies are mostly due to VH nuclei.

The differential energy spectrum of GCR particles above 100 MeV in the inner solar system is described by a power law in kinetic energy, E, of the form

$$\frac{dJ(E)}{dE} = K(\alpha + E)^{-\gamma} \qquad \ldots.(I.1)$$

where dJ(E) is the number of GCR particles with K.E. between E and E+dE, and

K, α and γ are constants. γ is defined as the spectral index, and α as the spectral hardness or spectral shape parameter. At $E < 100$ MeV/n, the SCR particles and at $E > 100$ MeV/n, the GCR particles dominate the interplanetary space. They are very effective in inducing nuclear reactions in their interaction

with solid bodies in the interplanetary space, such as asteroid surface materials, micro-and macro-meteoroids, planetary surfaces and atmospheres. As the GCR primary particles traverse the matter, they are attenuated due to ionization energy loss and energetic particles induce nuclear interactions resulting in secondary nucleonic cascade which, in turn, are potential source of further nuclear reactions. In these nuclear interactions, a large number of both the stable and radioactive isotopes are produced. A detailed study of production of radionuclides in earth's atmosphere has been done by Lal and Peters (1967) and in moon rocks by Reedy and Arnold (1972).

The solar particles are divided into two groups. Solar wind (SW) particles and solar flare cosmic rays (SCR). The SW is a continuous stream of charged particles due to the hydro-magnetic expansion of the outer solar corona, and this stream carries with it the "frozen-in" magnetic field from the sun which is responsible for the general magnetic field of the interplanetary medium. The physical properties of quiet-time SW are : Kinetic Energy $\sim$ a few KeV, proton flux $\sim 2.4 \times 10^8$ protons/(cm^2.sec) and SW velocity $\sim$ 400 km/sec (Hundhausen 1972). The average solar wind velocity remains relatively constant over a solar cycle. (Gosling et al 1971, Intrigillator 1975). During solar sunspot minimum, there are more high velocity (upto $\sim$ 800 km/sec) solar plasma streams dominating the interplanetary medium and stretching radially the interplanetary magnetic field. The GCR particles diffuse along this radial component of the magnetic

field more easily than along transverse component resulting in the higher GCR flux in the interplanetary medium. The general interplanetary magnetic field increases during peak sunspot activity.

The SW ions cannot induced nuclear reactions by virtue of their low energy, but they penetrate matter to depth of a few tenths of microns and are implanted on the surfaces of extra-terrestrial objects.

The SCR are emitted in sporadic solar outbursts occurring in the solar chromosphere called solar flares. About 0.1-1.0% of the total solar flare energy is transformed into $\geq$ 10 MeV particles (Lin and Hudson 1976). These particles travel into interplanetary medium before interacting with solid objects in the solar system. The proton fluence (flux integrated over the time duration of flares which is of the order of 1000 secs) in solar flare varies between $10^7 - 2\times10^{10}$ depending on the total magnetic field energy of the sunspots involved.

The SCR constitute of 90% protons, 9% helium nuclei and $\sim$ 1.0% metals (Z> 2). Neutrons and positrons are also detected in solar flares (Chupp et al 1973). However, there are no observational evidences of detection of neutrons and positrons in SCR (Chupp 1971). The VVH to VH abundance ratio is $\sim 1.4\times10^{-2}$ (Bhandari et al, 1973). The energy spectrum of SCR is well represented by a power low in rigidity (Freier and Webber 1963).

$$\frac{dJ(R)}{dR} = \frac{dJ}{dR}(t)\exp\{-R/R_o(t)\} \qquad .....(I.2)$$

where R is the particle rigidity = $\frac{pc}{Ze}$

i.e. momentum per unit atomic number or energy per unit charge,

R_o is the characteristic rigidity for solar flare particles,

dJ(R) = number of particles between rigidity R and R+dR, and

t = time since the onset of the solar flare.

An alternative form of the spectrum is the power law in particle kinetic energy and is given by

$$\frac{dJ(E)}{dE} = K(t)E^{-\gamma} \qquad ....(I.3)$$

where K(t) = constant and function of time, t, since the onset by solar flare and γ is the spectral index.

The characteristic rigidity (R_o) is found to vary between 40-400 MV from flare to flare and generally decrease with time after the start of the solar flare (Freier and Webber 1963). The occurrence of solar flares of very high rigidity and high fluence is very rare. The largest solar flare observed so far lasted for several days and produced a fluence at 1 A.U. of more than $\sim 10^{10}$ protons/(cm^2.E> 10 MeV/n), and total energy released was $\sim 10^{32}$ ergs in accelerating particles, an amount comparable to energy emitted in visible light in the associated solar flare (Lin and Hudson 1976).

The SCR protons have steep energy spectrum ($\gamma \sim$ 3-4) and consequently their nuclear interaction effects are limited to

depth of matter of $\sim$ 20 g.cm^{-2} from the surface. Thus SCR produced nuclides can be easily distinguished by the characteristic gradient in their concentrations.

(B) Meteorites and Moon Samples:

Meteorites are the interplanetary solid bodies in heliocentric orbits which have survived complete ablation during their high velocity entry into the earth's atmosphere. Due to the aerodynamical stress, the meteoroids, usually, undergo fragmentations and they fall as a few fragments or some times as showers. Added to above are their unknown preatmospheric shapes and heliocentric orbits. Unlike meteorites, the Moon samples are ablation free, well-documented, handpicked and brought safely to Earth by Apollo astronauts. Moon samples are the solar system material from a well defined heliocentric distance of 1 A.U. whereas meteoriod orbits extend to 3 to 4 A.U.

Meteorites are divided into four chemical catagories viz. Chondrites, Achondrites, Irons and Stony-Irons (Wasson 1974). Major elemental composition of a particular class of chondrites are similar to each other. The relative amounts of non-volatile elements in chondrites are remarkably similar to those found in the solar atmosphere and in atmospheres of sun-like stars.

Achondrites are differentiated mateorites containing no chondrules. Achondrites are divided into two groups (i) Ca-rich achondrites and (ii) Ca-poorachondrites. Angrites, Nakhlites, Eucrites and Howardites belong to the first group, and Aubrites, Diogenites, Chassignites and Ureilites belong to the later group.

Stony-Iron meteorites contain relatively higher amount of siderophile elements. Pallasites, Siderophyres, Lodranites and Mesosiderites are Stony-Iron meteorites. Iron meteorites contain different phases of Fe-Ni alloys, Kamacite and Taenite being the major phases.

The chondritic meteorites have been subclassified infour different types viz (1) Enstatite chondrites (2) Olivine-Bronzite chondrites, (3) Olivine-Hypersthene chondrites and (4) Carbonacous chondrites. The Olivine-Bronzite and Olivine-Hypersthene chondrites are known as ordinary chondrites. Depending on Fe/Si ratios, these ordinary chondrites are divided into 3 types, (i) H-group, high Fe-content, (ii) L-group, low Fe content and (iii) LL-group, Low Fe and Low metal phase content. The three most common silicate minerals are Olivines $(Mg, Fe)_2SiO_4$, Pyroxenes $(Mg,Fe)SiO_3$, $(Mg,Fe,Ca)SiO_3$ and Plagioclase feldspars ($NaAlSi_3O_8$ - $CaAl_2Si_2O_8$).

The cosmic ray exposure ages of chondrites are much lower ($\sim$10 Myr) than their formation ages ($\sim 4.6\times10^3$ Myr). The meteorites must have, therefore, remained shielded from cosmic rays for a major part of their time in the interplanetary space. There are meteorites with unsaturated ^{26}Al activity and the largest exposure stony meteorite so far known is Norton County (T=220 Myr).Exposure age histogram shows peaks at 4 Myr for H chondrites, 15 Myr for LL chondrite and the exposure ages of carbonacous chondrite are < 15 Myr. L chondrite exposure ages show a continuous spread below 100 Myr. Iron meteorites have

exposure ages considerably greater than Stony meteorites and the histogram peaks around 600 Myr.

The Lunar Samples are available in two types (1) Lunar Regolith (Soil) and (2) Lunar Rocks. The Lunar Mare basalts consist, chiefly, of Pyroxenes, Ilmenite ($FeTiO_3$) and Plagioclase feldspar. The Mare regions are surrounded by older and more densely cratered terrains, known as Highland regions. The highland rocks are found to be rich in Plagioclase feldespar and poor in Ilmenite. Many of the highland rocks are Breccias resulted from physical compaction of fragments from many sources. The Mare basalts ages are the times of impact cratering and partial melting of rocks beneath the lunar crust which erupted these rocks to the lunar surface. The solidification ages of highland rocks are the times of last cratering events on the Moon, known as Early Heavy Bombardment about 4 Byr ago.

(C) Cosmic Ray Induced Reactions:

Cosmic ray particles interacting with matter in space can produce a wide variety of product nuclei. The production rate, $P_i(X,R_E)$ of a nuclide, i, at depth X in a body of preatmospheric size, R_E, is given by

$$P_i(X,R_E) = \sum_j N_j \sum_k \int_{E_T^k}^{\infty} \sigma_{ij}^k(E) \frac{dJ^k(E)}{dE} \cdot dE \qquad \ldots(14)$$

where J represents the target nucleus,

N_j the target element concentration (atmos per unit mass)

and, k the nuclear active particle (either proton or neutron)

$\sigma_{ij}^{k}(E)$ is the excitation function of reaction between projectile k with target nuclide, j, resulting in product nuclide, i.

$\frac{dJ^{k}(E)}{dE}$ is the differential energy spectrum of nuclear particle k at depth X, which depends on incident primary spectrum and the depth X in body of radius R_E,

and

E_T^k is reaction energy threshold.

In the present work we are mainly concerned with the reactions induced by SCR and GCR particles with meteorites and moon. Therefore some of the parameters which determine the production rates of nuclides are discussed below.

(i) Nuclear Active Particles: Most primary protons undergo nuclear interactions in traversing matter before they are slowed down by ionization energy loss. Many secondary particles such as neutrons, protons, pions etc.are produced for each incident primary proton of energy E> 1 GeV which in turn undergo further nuclear interactions producing additional particles. The dominant strongly interacting particles with E < 100 MeV in a large body are the neutrons, since most charged particles with E < 100 MeV are stopped by ionization energy losses before they can interact with target nucleii. At high energies (E > 100 MeV), all particles interact in similar ways

and most of the nuclear reactions of interest the excitation functions, $\sigma(E)$, at these high energies, do not depend critically on the nature of the particles. Moreover, the excitation function at high energies do not vary much with energy (Silberburg and Tsao 1973) and proton and neutron induced excitation functions are same. Most of these neutrons of a few MeV energy are produced in evaporation processes from excited nuclei and the higher energy ($\sim$ 10 MeV) neutrons are produced by knock on processes.

Because of the relatively low energy of SCR protons a major fraction of these protons are stopped by ionization energy losses before they can induce nuclear reactions. A 50 MeV proton has nuclear interaction mean free-path of 100 $g.cm^{-2}$ while the range is only $\sim$ 3 $g.cm^{-2}$. Only a few SCR protons undergo nuclear interactions resulting in insignificant secondary production.

(ii) Energy Threshold: Spallation reactions are high energy endothermic reactions resulting in partial breakup of the target nucleus into lower mass particles after forming an excited compound nucleus (within time 10^{-15}-10^{-16} sec) in collision with an energetic projectile nucleus. During the de-excitation of the compound nucleus, prompt gamma rays along with protons, neutrons, alpha particles and other higher mass nuclei are emitted, resulting in either a stable or a radioactive nuclide.

Because of the radioactive decay, unlike stable isotopes, the radioactive isotope concentration does not build up with time.

If the production rate of a radionuclide remains constant, eventually the decay rate and the production rate become equal and secular equilibrium is established. Then the measured activity of such an isotope is equal to the production rate, which depends only on the averaged cosmic ray intensity over such a time period.

Spallation reactions have $Q < 0$. The spallation reactions are possible at energies greater than E_T, i.e. threshold kinetic energy of the nuclear active particles, which is given by

$$E_T = \frac{M+m}{M} | Q | \qquad \ldots.(I.5)$$

where M = mass of the target nucleus, and

m = mass of the projectile nucleus

The major target elements are:

O, Na, Mg, Al, Si, Ca, Fe, Mn, Ni etc.

In table I-1 the energy threshold for the production of some radio-and stable-nuclides in the interaction of cosmic ray primary and secondary protons and neutrons with major target elements in extraterrestrial samples are given.

(iii) The GCR Intensity in the past : The energy spectrum of the contemporary cosmic rays is given by equation I.1 with average integral proton flux (above E=1 GeV) of 1.7 protons/(cm^2.sec.4π sr). The GCR intensity variation due to solar cycle modulation is well known. Long-term variations in the GCR intensity are due to:

TABLE-I.1

Production Nuclear Reactions and Energy Threshold of some Cosmogenic Radio and Stable Nuclides

Isotope (1)	Half-life (yr) (2)	Target (3)	Particles (4)	Cosmogenic Nuclear Reactions Neutron Induced Reaction (5)	E_T(MeV) (6)	Proton Induced Reaction (7)	E_T(MeV) (8)
^{10}Be	1.5×10^6	O	GCR	$^{16}O(n,4p3n)$	67	$^{16}O(p,5p2n)$	69.5
				or $(n,^7Be)$	26.6		
		Mg	GCR	$^{24}Mg(n,8p7n)$	140	$^{24}Mg(p,9p6n)$	143
		Al	GCR	$^{27}Al(n,9p9n)$	167	$^{27}Al(p,10p8n)$	170
		Si	GCR	$^{28}Si(n,10p9n)$	179	$^{28}Si(p,11p8n)$	183
^{21}Ne	Stable	Mg	SCR,GCR	$^{24}Mg(n,\alpha)$	2.76	$^{24}Mg(p,3pn)$	32.8
		Al	SCR,GCR	$^{27}Al(n,3p4n)$	60	$^{27}Al(p,4p3n)$	63.50
				or $(n,^7Li)$	19	or $(p,^7Be)$	20.8
		Si	SCR,GCR	$^{28}Si(n,4p4n)$	72.3	$^{28}Si(p,5p3n)$	76.00
				or $(n,2\alpha)$	13.1	or $(p,^8B)$	32.7
		Ca	SCR,GCR	$^{40}Ca(n,10p10n)$	180	$^{40}Ca(p,11p9n)$	184.90
				or $(n,^{20}Ne)$	14.5		
^{22}Ne	Stable	Mg	SCR,GCR	$^{25}Mg(n,\alpha)$	0.51	$^{24}Mg(p,3p)$	21.8
		Al	SCR,GCR	$^{27}Al(n,3p3n)$	28.5	$^{27}Al(p,4p2n)$	32.0
				or $(n,3d)$	42		
		Si	SCR,GCR	$^{28}Si(n,4p3n)$	61.4	$^{28}Si(p,5p2n)$	65.1
				or $(n,^7Be)$	21.9	$^{28}Si(p,^7B)$	34.0
		Ca	SCR,GCR	$^{40}Ca(n,10p9n)$	170	$^{40}Ca(p,11p8n)$	175.0

Table-I.1 (Contd.)

(1)	(2)	(3)	(4)	(5)	(6)	(7)	(8)
^{22}Na	2.56	Mg	SCR, GCR	$^{24}Mg(n,p2n)$	25.3	$^{24}Mg(p,2pn)$	28.6
				or (n,Dn)	22.0	or $(p,T)^{22}Mg$	21.3
				or $(n,^{3}H)$	16.3	or $(p,^{3}He)$	17.1
				$^{25}Mg(n,p3n)$	32	$^{25}Mg(p,^{4}He)$	3.2
		Al	SCR, GCR	$^{27}Al(n,2p4n)$	53	$^{27}Al(p,3p3n)$	56.5
				or $(n,\alpha 2n)$	23.4	or $(p,3d)$	45.7
		Si	SCR, GCR	$^{28}Si(n,3p4n)$	65	$^{28}Si(p,4p3n)$	68.7
				or $(n,^{7}Li)$	24	or $(p,^{7}Be)$	27.7
		Na	SCR, GCR	$^{23}Na(n,2n)$	13	$^{23}Na(p,pn)$	16.0
^{26}Al	0.72×10^{6}	Mg	SCR	-	-	$^{26}Mg(p,n)$	7.8
		Al	SCR, GCR	$^{27}Al(n,2n)$	13.1	$^{27}Al(p,pn)$	7.7
						or (p,d)	5.0
		Si	SCR, GCR	$^{28}Si(n,p2n)$	16.3	$^{28}Si(p,2pn)$	20.0
				or $(n,^{3}H)$	16.1	or $(p,^{3}He)$	16.0
^{53}Mn	3.7×10^{6}	Mn	SCR, GCR	$^{55}Mn(n,3n)$	19.5	$^{55}Mn(p,p2n)$	25.0
						or $(p,^{3}H)$	16.0
		Fe	SCR, GCR	$^{56}Fe(n,p3n)$	30.0	$^{56}Fe(p,2p2n)$	36.0
						or $(p,p\alpha)$	6.8
^{60}Co	5.26	Co	GCR	$^{59}Co(n,\gamma)$	0.025-1.00	-	-
		Ni	GCR	$^{60}Ni(n,p)$	5	-	-

(i) Passage of the sun through arm-interarm regions of our spiral galaxy,

(ii) cosmic ray gradient perpendicular to galactic plane upto galactic latitudes covered by the inclined solar orbit about the galactic center, and

(iii) frequency of stellar explosions (e.g. Supernova) in the solar vicinity.

From ($^{39}Ar/^{36}Ar$) activity ratios measured in then recently fallen meteorites Schaeffer and Heymann (1965) found that GCR intensity averaged over last 400 years (mean-life of ^{39}Ar) is within 10% of the GCR intensity averaged over last 0.40 Myrs (mean-life of ^{36}Cl), indicating that supernova associated with Crab-nebula (1054 A.D.) did not change GCR intensity by more than 10%. Voshage and Hintenberger (1963) found that ^{40}K-^{41}K exposure age of meteorites were systematically 50% higher than ^{36}Cl-^{36}Ar ages indicating that GCR intensity averaged over the last 0.4 Myr was higher by about 50% compared to that averaged over exposure ages of iron meteorites ($\sim$600-900 Myr). These age discrepancies cannot be accounted for by space erosion of meteorites or by any other mechanisms except GCR intensity change in the past. According to Schaeffer (1975), this exposure age discrepancy can be understood if there is latitudinal (Z) gradient of GCR intensity in our galaxy given by

$$I_Z = I_o \exp(-Z/Z_c) \qquad .....(I.6)$$

where Z_c is the characteristic scale height ($\sim$ 200 parsecs).

(iv). The SCR Intensity in the past:

The sunspot activity undergoes cyclic variation with average periodicity of 11 years, known as solar cycle. The solar magnetic polarity is reversed every 22 years. With increasing sunspots the frequency of flare occurrence increases and many sunspots are destroyed through flares during falling part of sunspot cycle, although even during sunspot minimum period solar flares are known to occur. Sunspot observations have been made from time to time since Galileo first saw sunspots through his telescope and these records are traceable. Recently, Eddy (1976) has gone through these records and those of aurorae and eclipse observations and has shown that our Sun has undergone two prolonged sunspot minima in recent times, known as the Sporer minimum (1460-1550 A.D.) and Maunder minimum (1645-1715 A.D.) which were preceeded by Grand Maximum (1100-1250 A.D.).

Also recent developments in solar neutrino astronomy are quite interesting in this connection. According to the standard stellar models (Schwarzchild 1958, Cox and Giuli 1968), if the energy generation in the solar core is due to continuous burning of hydrogen through PP I and PP II or PP III nuclear reaction chains, depending upon their relative probabilities of occurrences, the most energetic neutrinos emitted in radioactive beta decay of $^{8}B \rightarrow {}^{8}Be + \beta^{+} + \nu$ (14.06 MeV) should be detectable (Bahcall 1979). But, the observed low solar neutrino capture rate of 2.2 SNU compared to the expected 7.7

SNU has raised doubts regarding the standard stellar models (Rowlay et al 1980). It is not known, today, whether the fault lies with standard solar model or with the physics of neutrino propagation. The general consensus is that the observation of ^{8}B decay neutrinos can best serve as a test of details of nuclear reaction chains rather than the test for occurrence of nuclear reactions themselves. The objective can best be achieved by detecting neutrinos emitted in $P+P \rightarrow {}^{2}H + \beta^{+} + \nu(0.420\ MeV)$ using detectors such as ^{71}Ga, ^{87}Rb, ^{115}In or ^{205}Tl which are sensitive to the low energy neutrinos (Bachcall 1979).

Non-standard solar models have been advanced by Ezer and Cameron (1972), according to which a relatively low central temperature is caused by mixing of material between the core and non-nuclear buring zones leading to variation in solar luminosity. Fowler (1972) suggested that low neutrino flux observed today is due to sudden changes in solar structure in the past a few million years. However there has not been any convincing argument for such an unstable sun.

The studies of nuclear particle tracks due to VH nuclei which are cumulative over the entire exposure time have revealed information on chemical composition and energy spectrum of cosmic rays. This fossil track method has been applied for evaluating cosmic ray characteristics in meteorites(Schaeffer 1975, Bhandari et al 1971, Fleischer et al 1967) and moon rocks (Lal 1969, Crozaz et al 1970, Fleischer et al 1971 and Bhandari et al 1971), the results of which generally agree but they differ in details.

If the observations of sunspot activity variations (Eddy 1976) and the low solar neutrino flux are related, then the solar flare activity, which is expected to vary with sunspots, and solar luminosity should also show variation (Intrigillator 1975). Thus, it is interesting to look for solar flare activity in the past.

(D) Scope of the Thesis:

The objective of the Thesis is to define the dependence of production rates of some cosmogenic stable and radioactive nuclides in meteorites and lunar samples on size, depth and target element composition and then, to obtain long-term characteristics of solar and galactic cosmic rays. This information is used to understand some of the physical processes occurring in the interplanetary space, like erosion, collisional fragmentation, and ablation occurring in the earth's atmosphere.

The approach has been to select documented samples of known exposure history, shielding depth and irradiation geometry so that the cosmic ray effects can be correlated with these parameters. The experimental techniques include radiochemical determination of radioisotopes ^{26}Al, ^{10}Be, ^{22}Na and ^{60}Co in selected meteorite and lunar samples. Five meteorites of preatmospheric sizes (R_E) ranging from 6.5 cm to $\sim$ 100 cm are chosen. Four radioisotopes viz $^{10}Be(t_{\frac{1}{2}} = 1.6$ Myr), a high energy ($E \gtrsim 100$ MeV) product, $^{26}Al(0.72$ Myr), $^{22}Na(2.60$ yr) produced mainly by 10-100 MeV particles and $^{60}Co(5.26$ yr)

an epithermal neutron (0.5-300 eV) capture product are measured. The counting systems used include $\beta^{\pm}\gamma$ coincidence spectrometer for ^{26}Al, ^{22}Na and ^{60}Co and $\beta\bar{G}$ anticoincidence detector system for ^{10}Be counting. This experimental study has been supplemented by model calculations of nuclide production in cosmic ray interaction, ablation of meteorites in atmosphere of the earth, fragmentation and multiple exposure in interplanetary space. The changes in nuclide production due to solar modulation of GCR during solar cycle 20 are evaluated based on recent flux measurements.

(i) Radionuclides in meteorites:

Experimental depth profiles of ^{26}Al, ^{10}Be, ^{22}Na and ^{60}Co are determined in a Dhajala chondrite ($R_E \sim$ 50 cm). Using the ^{26}Al depth profile and the Reedy-Arnold model as applicable to meteorites, the spectral shape parameter α as a function of depth are obtained. Using the deduced α values, the expected depth profiles of some other radionuclides are calculated and compared with the experimental depth profiles. The observed discrepancy between these two profiles are discussed in view of the limitations of Reedy-Arnold model calculations. The solar modulation of GCR and its effect on short-lived radionuclides are investigated. The experimental ^{60}Co depth profile is obtained and compared with the theoretical profiles given by Eberhardt et al. (1963). The slowing down density of neutrons are calculated.

Three radioisotopes (^{26}Al, ^{10}Be, ^{60}Co) in Kirin ($R_E \sim 100$ cm) chondrite are measured. Based on comparison of relative concentrations of ^{10}Be, ^{53}Mn and ^{26}Al with those in Dhajala chondrite, an estimate of exposure age of Kirin chondrite is obtained. Using this exposure age, the depth dependent production rates of various nuclides are obtained.

The ^{26}Al production levels are measured in small chondrites ($R_E \leq 15$ cm) and are compared with production rates calculated for these size meteorites.

(ii) ^{26}Al depth profile in Lunar Samples :

One lunar rock 61016 and two rock chips (69935 and 69955) which were taken from a same parent boulder have been analysed for ^{26}Al depth profile. The suntan exposure ages of these are well known from the depth profile of track density measurements (Bhandari et al 1975). The measured ^{26}Al depth profiles in these rocks are used to deduce the best fit SCR spectral parameters and compared with those deduced from ^{26}Al depth profiles in some lunar drill-cores and soils. The nature of ancient solar flare activity is discussed in light of results obtained.

(iii) Multiple exposure of meteorites:

The depth and size dependence of ^{21}Ne production rates and $(^{22}Ne/^{21}Ne)_{sp}$ for various size meteorites (bigger than 6 cm) are calculated. A criterian based on track production rates and $(^{22}Ne/^{21}Ne)_{sp}$ for identifying meteorites with complex exposure history has been established. Some meteorites with complex exposure history have been identified.

(iv) Meteorite Ablation in the Earth's Atmosphere:

Following Baldwin-Sheaffer model (Baldwin and Sheaffer 1971), a computer code has been developed to calculate the trajectory and ablation of meteorites with known entry conditions. The general applicability of the model are discuesed and improvement of it is suggested to match the calculated ablation for meteorites with the limited observations available. The preatmospheric velocities of several meteorites with known preatmospheric size and ablation are deduced.

CHAPTER-II

EXPERIMENTAL TECHNIQUES

Several chondrites and lunar samples have been analysed in this work. These samples have been selected on the basis of their suitability for studying the cosmic ray produced radionuclides. A brief description of the meteorites and lunar samples studied and the experimental techniques followed are given in this chapter.

(A) Sample Description:

1. Dhajala Meteorite:

This meteorite fell in Gujarat (India) on 28th January 1976 at 2040 hrs IST at Dhajala. According to Bhandari et al. (1976a) and Noon et al. (1976) this meteorite belongs to the H-group, probably H3 class of Van Schmus and Wood classification. The total recovered mass of the meteoroid is $\sim$ 65 kg. More than 500 fragments weighing between 250 g to 12 kg were recovered from $\sim$ 50 km^2 strewnfield. A few fragments were studied for cosmogenic radioactivity within a few days of the meteorite fall enabling measurement of very short-lived (5 days) radioisotopes in a few fragments (Bhandari et al 1978). ^{21}Ne and ^{38}Ar cosmic ray exposure age of Dhajala is 6.3 ± 1.0 Myr (Gopalan et al. 1977). More than 250 fragments were analysed for cosmogenic particle tracks and based on observed minimum track density in sample T-9 Bagolia et al. (1977) estimated the preatmospheric size of $\sim$ 40 cm. Finding of another Dhajala sample with still lower track density (DH-9) has yielded preatmospheric size of $\sim$ 50 cm. From the visual observations

of the Dhajala luminous trajectory the most probable heliocentric orbit has been calculated by Ballabh et al. (1978) assuming preatmospheric velocity of 21.5 km/sec determined from the mass ablation of 94% deduced from particle track and rare gas studies. This orbit had relatively high angle of inclination to the ecliptic plane of 27°.

Bulk samples weighing between 40 to 55 g of different fragments were dissolved for radiochemical separation and purification of elements of interest viz. Al, Be, Co and Na. The radiochemically purified samples were counted for ^{26}Al, ^{10}Be, ^{60}Co and ^{22}Na isotopes.

2. Bansur, Udaipur, Madhipura and Kirin Chondrites :

Bansur meteorite fell in Rajasthan (India) in 1892. This belongs to L group of chondrites. The recovered single piece of this meteorite weighes ~ 15 kg. The preatmospheric mass is estimated to be ~ 50 kg (R_E ~ 15 cm). The meteorite has been extensively studied for cosmogenic rare gases (Gopalan and Rao 1976) and particle tracks (Bhattacharya et al. 1980). Particle track study shows asymmetric ablation. The ^{21}Ne exposure age of this meteorite is 15 Myr.

Udaipur is also an Indian meteorite which fell near Udaipur (Rajasthan). The mass of this single piece is ~ 1.2 kg. This belongs to H group of chondrites. The preatmospheric mass of this meteoroid is estimated to be ~ 14 kg(R_E=g cm), and the ^{21}Ne exposure age is 22 Myr (Gopalan and Rao 1976).

Meteorite Madhipura, another Indian meteorite fell on 23 May 1950 in India. This belongs to L group of the chondrites. The recovered mass is ∿ 1 kg corresponding to effective recovered radius of 4 cm. The extensive particle track density measurements have yielded preatmosphere size R_E=6.5 cm (Bhandari et al.1980). The cosmic ray exposure is 15 Myr (Gopalan and Rao 1976). The ablation deduced from rare gas and track studies is relatively uniform around 2.5 cm.

Spot samples from surfaces were studied for tracks to acertain the sides which were least ablated and almost radial cores were taken through above meteorites for measurement of ^{53}Mn depth profile (Bhattacharya et al.1980). The directions of maximum track density gradient were determined and the cores were taken by an electromechanical water cooled diamond drill corer.

The Al containing fractions of the core samples (after extracting Mn, Fe, Co) from various depths of Madhipura meteorite core were mixed and processed for ^{26}Al radiochemistry. Cutting powders of Bansur and Udaipur meteorites weighing between 3-3.5 g were processed.

Kirin Chondrite:

On March 8,1976 this largest stony meteorite fell in Kirin Province in China. The total recovered mass of the meteorite was about 4000 kg with the largest fragment weighing about 1770 kg. The dimensions of this piece are 117 cm x 93 cm x 84 cm. The next largest fragment weighs∿ 70 kg. It has been possible

to put together the recovered fragments and reconstruct its prefragmentation size and shape (Co-operation Group, China 1977). Thus reconstructed body is almost spherical in shape with effective recovered radius of ~65 cm. The meteorite has been classified as H5 according to the scheme of Van Schmus and Wood (1967).

3. Lunar Rock 61016:

The selection of this lunar rock and many others for non-destructive $\beta^{+}\gamma$ coincidence measurement of ^{26}Al by our group previously, was based on some important criteria, viz. (i) concordance of both the rare gas and track exposure ages, (ii) high Al contents, (iii) low concentration of U, Th etc. to minimise their interference in measurement of β^{+} activity, (iv) having well preserved top surface, (v) relatively large size of the rocks to minimise geometry effect in whole rock counting, and (vi) known exposure geometry.

A vertical slice from 11.7 kg Apollo-16 anorthositic clast rich breccia 61016 which was collected from the Cayley plain, Station 1, near the eastern rim of Plum crater was considered to be a good sample meeting the above criteria. This piece 61016, 287 (Parent No.40) weighed 35.04 g and had well preserved 3.3 cm^2 top surface. The sample is from ~ 30° zenith angle location on the parent rock (Apollo-16 Preliminary Science Report).

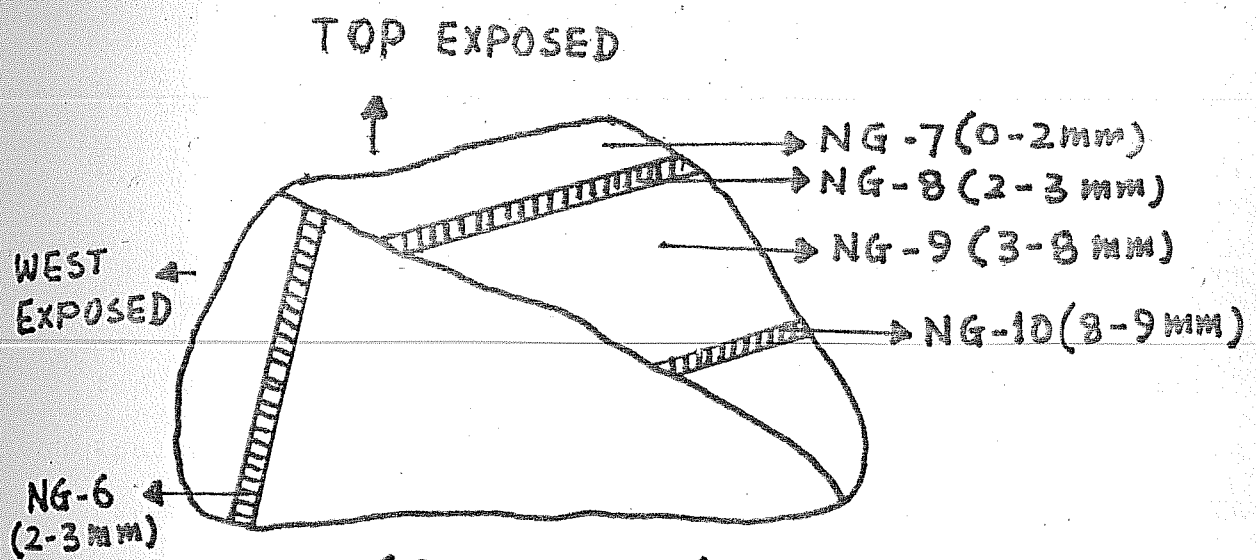

69935,14 (NG)

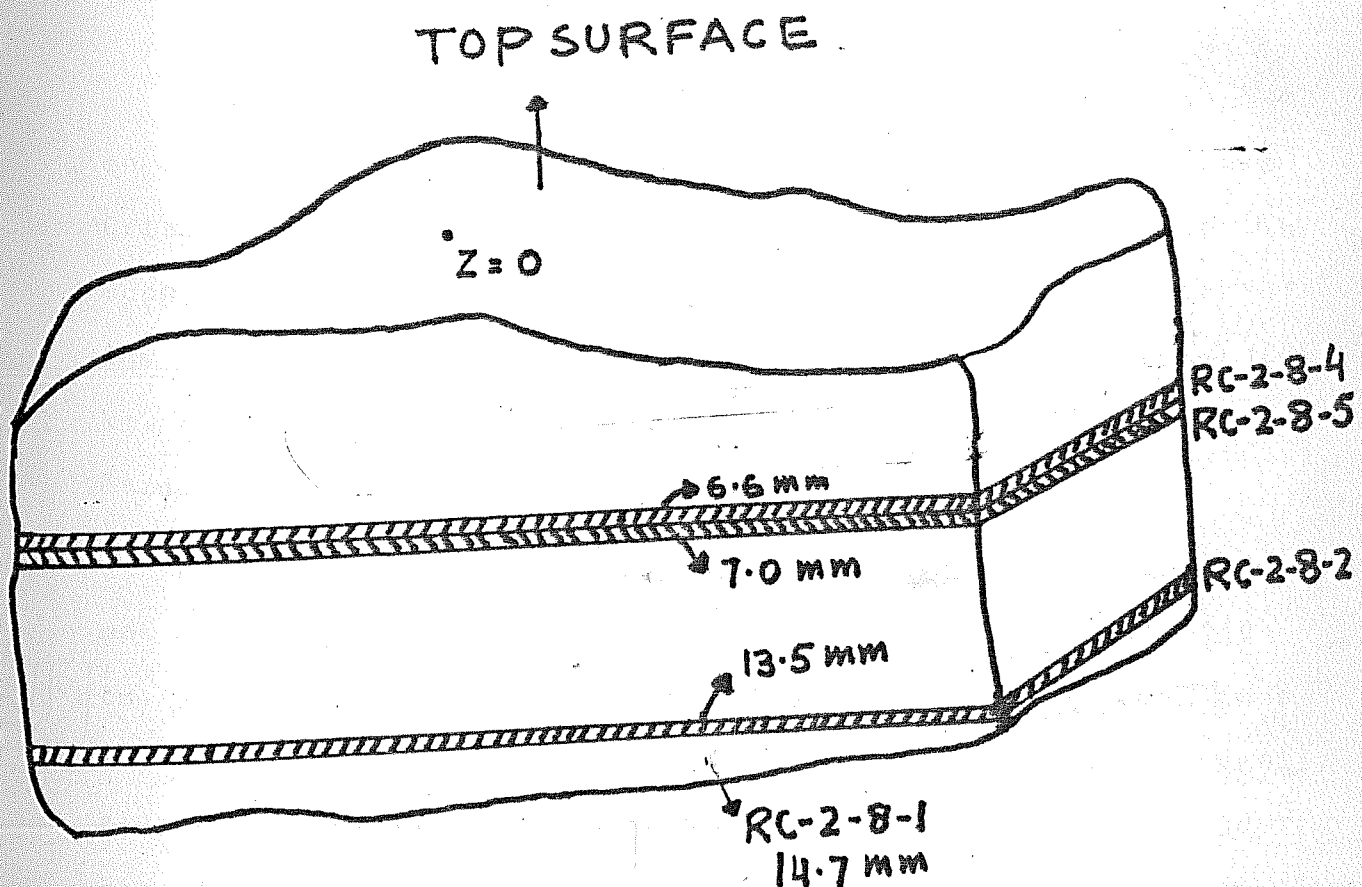

61016,287 (RC)

Fig.II.1 Schematic cutting diagram and sample locations in lunar rocks 61016,287 and 69935,14.

In Fig.II.1 the schematic diagram of sample locations in the rock 61016,287 is given. Four samples from depths of 6.6, 7, 13.5 and 14.7 mm were cut and chemically processed.

4. Boulder Chips 69935 and 69955 :

Two boulder chips 69935 and 69955 were removed from top and bottom of a same parent boulder of ~60 cm in size by Apollo astronauts. The parent boulder was located at Station 9. (Apollo-16 Preliminary Science Report). The schematic diagram of sample locations in 69935 is given in Fig.II.1.

5. Lunar Soils :

Core Soil 24087 and Scoop Soil 67481 :

An automatic Russian space craft Luna-24 landed on Moon on 18th August 1976, just outside the inner ring of the Mare Crisium. Mare Crisium is amongst the oldest formations on the moon and has an unique multiringed structure. The diameter of the inner ring is ~ 500 km and that of the outer ring is ~ 1000 km. About 1200 km from the landing site and away from the Mare Crisium is a young crater Bruno.

Although the penetration depth of the Luna-24 drill core was ~ 210 cm, the length of the recovered core was only 140 cm. The diameter of the core was 8 mm and the total soil mass was 170 g. The tube was empty upto 47 cm depth and was scantily filled upto 58 cm. From 58 to 73 cm the core tube contained only the coarse grains (Barsukov et al.1977). Because of the difficulty in remote operation of the corer, some loss of soil

is possible. About 250 mg of soil strata removed from 86-87 cm geometrical depth along the core is counted for total positron activity by non-destructive $\beta\pm\gamma$ coincidence technique.

Apollo-16 scoop soil (67481) was also counted for the total positron activity. The U, Th content of this soil being quite low ($\sim$1 ppm), the interference of ^{232}Th in positron channel is expected to be minimum.

(B) Experimental Techniques :

The experimental techniques adopted are divided into two parts, viz. (i) the radiochemical separation and purification of elements, and (ii) measurement of concentration of radioactive isotopes by suitable radiation detectors.

Among the chosen radioisotopes the ^{22}Na and ^{26}Al decay by positron emission to the excited states of ^{22}Ne and ^{26}Mg. These nuclides de-excite to their ground states by emission of their characteristic gamma rays. The positrons ultimately capture electrons from the ambient medium and annihilate into two 0.511 MeV gamma quanta moving in opposite directions. The most specific scheme for their unambiguous identification is to count the 0.511 MeV quanta and the other characteristic gamma quanta in coincidence with the β^+ precursor and this is achieved by a $\beta\pm\gamma$ coincidence spectrometer as described in Fig.II.2. The radionuclide ^{60}Co decays by $\beta^-\gamma$ coincidence mode. The characteristic gamma quanta of 1.173 MeV and 1.333 MeV are emitted in coincidence with β particle. ^{10}Be decays by β^- emission and is not accompanied by any gamma rays. Hence, ^{10}Be is counted on $\beta\bar{\gamma}$ anticoincidence system.

I. CHEMICAL SEPARATION OF MAJOR ELEMENTS

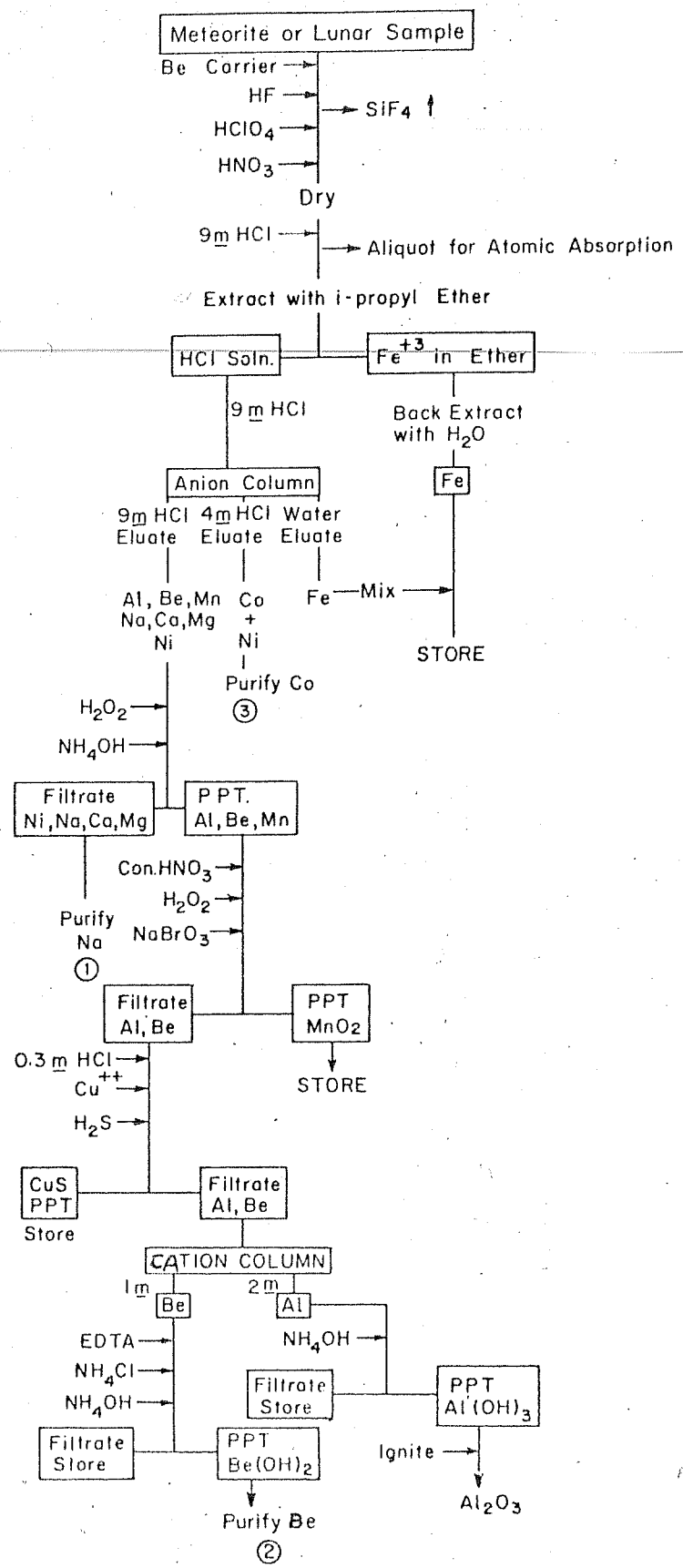

Fig.II.2 Flow chart of radiochemical procedure.

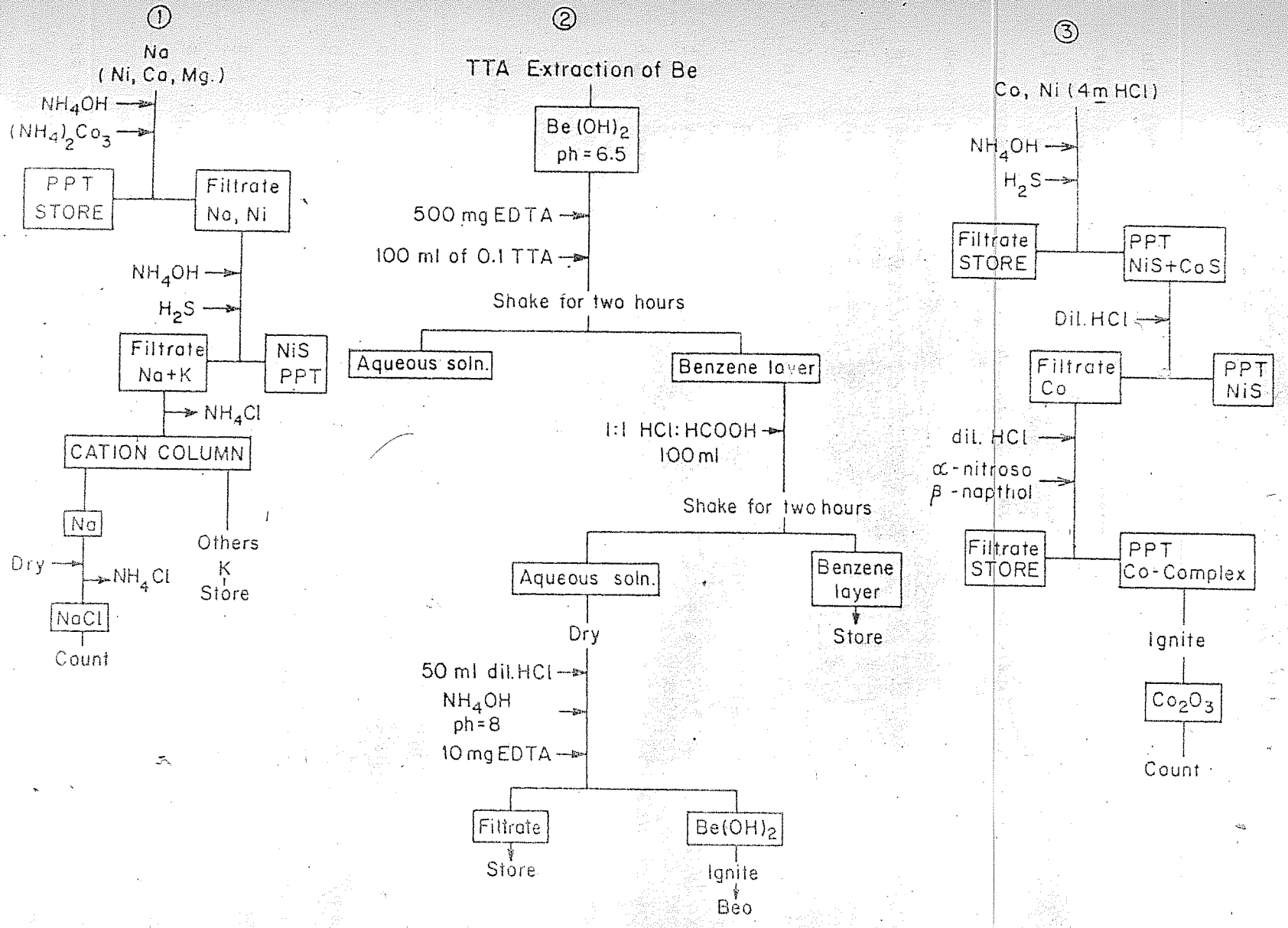

Fig.II.2 Flow chart of radiochemical procedure (contd.)

Radiochemical Methods:

Radiochemical methods of separation and purification of elements is necessary in both the β^- and β-γ coincidence techniques to discriminate isotopes of interest from other interfering isotopes and to achieve higher signal to background ratios. The radiochemical method employed in this work is similar to the methods of Shedlovsky et al. (1970) and Marti et al. (1969) which which were later improved upon by Finkel (1972) and Kohl (1975).

(a) Chemical Separation:

Fig. II.2 gives the flow chart of the main chemical steps involved. The chemical procedures consists of the following important steps (for a typical sample of 50 g of meteorite). In case of small amount of meteorite samples and lunar samples, the procedure was modified depending upon their chemical composition.

(i) Crushed and sieved bulk samples ($\sim$ 2.5-50 g of meteorite samples and 0.4-1.5 g of moon rock samples) were dissolved in 48% Hydrofluric Acid (HF). After treatment with perchloric acid ($HClO_4$), nitric acid (HNO_3) and Sulphuric Acid (H_2SO_4) the dried residue was, finally, dissolved in 9 m HCl.

After the solution became clear 1% by volume aliquot was taken for atomic absorption spectrophotometric (AAS) determination of abundances of several elements.

(iii) Iron was extracted by complexing with ice-cooled di-isopropyl ether saturated with conc.HCl from 9 m HCl solution.

(iii) Cobalt was separated on a 150 cc anion exchange column (Dowex-1,x 8 , 50-100 mesh) conditioned and eluted with 9 m HCl. The Co green band from the column was eluted with 4 m HCl.

(iv) Four column volumes of 9 m HCl elute from anion exchange column containing Al+Be+Mn+Ni+Na+Ca+Mg+... was boiled down to ~ 100 ml and Al, Be, Mn were precipitated as hydroxides by NH_4OH(pH=8) in presence of dilute hydrogen peroxide (H_2O_2), and it was allowed to stand for 3-4 hrs to blacken due to formation of Mn-oxi-hydroxide $MnO(OH)_2$. The precipitate was filtered through Whatman 42 filter paper. The well washed black precipitate was dissolved in conc.HNO_3. The bluish coloured filterate contained Na.

(v) The conc.HNO_3 fraction from step (iv) above was dried and repeatedly treated with conc.HNO_3 to drive off NH_4Cl. The final solution in conc.HNO_3 was cooled to ~ 50°C and Mn was precipitated as MnO_2 by adding sodium bromate ($NaBrO_3$) in presence of dil.H_2O_2. The precipitate was centrifuged.

(vi) The centrifugate from step (v) above was diluted to ~ 300 ml. Al and Be were precipitated as hydroxides and it was separated on a centrifuge. The precipitate was dissolved in ~ 30 ml of dil.(2 m) HCl. By adding pure NaOH pallets the hydroxides were precipitated at pH=7. $Al(OH)_3$ and $Be(OH)_2$ were preferentially dissolved in equal volume of 4 m NaOH solution.

The solution was vigorously boiled for 10 minutes. The luke-warm solution was then centrifuged. The precipitate was again mixed with ~ 300 ml of 4 m NaOH and above procedure was repeated for 2 to 3 times. The final combined centrifugate was acidified (pH=5) with conc.HCl. Al and Be were precipitated as hydroxides at pH=8 by adding NH_4OH solution. The precipitate was filtered through Whatman 42 filter paper and it was repeatedly cleaned to remove NaCl completely. The precipitate was then dissolved in 0.3 m HCl solution.

About 10 mg Cu carrier was added to the above solution. CuS scavenge was precipitated by passing H_2S and the precipitate was filtered.

(vii) The filtrate from step (vi) was dried and residue was dissolved in 40 ml of 1 m HCl.

(viii) The filtrate from step (iv) containing Na+Ni+Ca+Mg+.. was processed further for Na chemistry. Ni was precipitated as NiS at pH=8 by passing H_2S. The step was repeated until NiS precipitation was complete.

(ix) Mg and Ca were precipitated quantitatively as Mg-and Ca-orthophosphates at pH=8 by $(NH_4)_2HPO_4$. The step was repeated until the phosphate precipitation was complete.

(x) The filtrate was boiled down and treated with conc.HNO_3 to expel bulk quantity of ammonium chloride salt formed in the above step (ix).

(b) Radiochemical Purification :

(i) Purification of Co :

The 4 m HCl elute from anion exchange column was dried and taken in 50 ml of 0.3 m HCl. About 10 mg of Cu carrier was added and CuS scavenge was precipitated by passing H_2S. At pH=8, NiS was precipitated by passing H_2S. The filtrate was dried and NH_4Cl was driven off by treating with conc.HNO_3. The dried residue was dissolved in dil.HCl (1 m).

The α -nitroso-β -napthol reagent was prepared by dissolving 4 g of the salt in 100 ml of glacial acetic acid and 100 ml of warm water. Filtered cool solution was used within about two hours. About 0.25 g of α -nitroso- β -napthol is required for complexing 10 mg of Co. Co was then complexed with α -nitroso- β -napthol. The red-blood coloured precipitate was warmed to coagulate and the cooled solution was filtered through Whatman 42 filter paper. The precipitate was dried in an oven at a temperature of 100°C for about 6 hrs and then it was ignited in a furnace at 850°C for 2-3 hrs. The cobalt-oxide (Co_2O_3) formed was then deposited on perspex source holder for β-γ coincidence measurement of ^{60}Co. In some cases the recovered Co_2O_3 was dissolved in dil.HCl and then cobalt was electroplated on a copper planchet. The electroplating procedure is described later.

(ii) Separation and Purification of Al and Be :

The 40 ml of 1 m HCl solution from step (vii) above contained both Al and Be. This solution was charged on a 150 ml

calibrated cation exchange column (Dowex-50, X8, 100-200 mesh) conditioned and eluted with 1 m HCl. The 5th, 6th and 7th column volumes of 1 m HCl elute contained Be. After passing additional 10 column volumes of 1 m HCl, the 16th, 17th and 18th column volumes of 4 m HCl elute was collected which contained Al.

The Be fraction was boiled down to $\sim$10 ml and then diluted to 50 ml with water. By adding dilute ammonia solution the pH was controlled at 7. A drop of dil.HCl was added to dissolve the white turbidity. About 10 mg of EDTA-Na_2 salt was added. Then at higher pH.(=9) $Be(OH)_2$ was precipitated by dil.NH_4OH solution. The precipitate was filtered on an ashless filter paper and ignited. The BeO recovered was deposited on Cu-holder.

The Al fraction was boiled down to $\sim$ 20 ml and diluted with $\sim$ 100 ml of water. $Al(OH)_3$ was precipitated with dil.NH_4OH solution at pH=8. The filtered and well washed precipitate was ignited to Al_2O_3.

(iii) Purification of Na :

The Na fraction from step a(x) was dried and dissolved in 20 ml of 1 m HCl solution. It was charged on a pre-calibrated cation exchange column (conditioned and eluted with 1 m HCl). The 3rd, 4th and 5th column volumes of 1 m HCl elute contained Na fraction. In this process, Na is well separated from potassium and trace quantities of other interfering elements. The Na was allowed to crystalise as NaCl.

(iv) Purification of Be :

In case of pure beta counting, it is essential to assure that the sample is pure, because there is no selection available in counting. Since Be is a reactive element, the problem is very severe. After first counting, the Be sample was purified by extracting with Theonyl-Trifluoro-Acetone (TTA). This purification was repeated until constant ^{10}Be specific activity was obtained.

TTA Extraction of Be :

It consists of following steps:

1. 2.22 g of TTA was dissolved in 100 ml of analytical grade Benzene to prepare 0.1 m TTA solution.

2. About 50 ml of dil.HCl solution containing $BeCl_2$ was neutralised with dil.NH_4OH solution. About 500 mg of EDTA-Na_2 salt was added. Using Harleco pH standards (pH=4 and 8), the pH of the solution was controlled at 6.5. At this pH white turbidity due to formation of $Be(OH)_2$ appears.

3. This solution was mixed with TTA solution in a tightly stoppered shaking flask, and shaked vigorously for about 2 to 3 hrs on a flask shaking machine until white turbidity in lower solution disappeared.

4. The Benzene layer was separated from the aqueous layer. The Benzene solution which contained Be-TTA complex was mixed with 1:1 (by vol.) of conc.HCl and Formic acid

(85%) (HCOOH) in a stoppered flask and shaked vigorously for 2-3 hrs.

5. The aqueous layer was separated and evaporated to dryness under infrared lamp. The residue was dissolved in 50 ml dil.HCl (∿1 m HCl) and $Be(OH)_2$ was precipitated at pH=8 to 9 in presence of 10 mg EDTA-Na_2 salt. This $Be(OH)_2$ precipitate was dried and ignited to BeO.

(v) Electroplating of Cobalt :

For electroplating of Cobalt, the Co_2O_3 obtained in step b(i) above was dissolved in ∿ 50 ml of dil.HCl. The following plating bath was used for∿ 30 mg Co. A mixture of 4 g of ammonium sulphate, 1.2 g of tartaric acid and 1.5 g of hydrazine sulphate was dissolved in about 50 ml of Co-solution. Sufficient conc. ammonia solution was added to adjust pH=8 (Finkel 1972). The solution was then made to 80 ml by adding distilled water. Copper planchet cleaned in dil.HCl and in chromic acid cleaning solution was kept at a negative bias. Spiral platinum anode wire was kept hanging over the Cu-planchet.

The electroplating was carried out at constant current of 200 mA at 1.5 - 4 volts. Throughout the plating process, it was necessary to control the pH at∿ 8 by adding dil.NH_4OH solution. As far as possible plating bath was kept covered with a perforated perspex sheet to allow the liberated gas at the anode wire to escape. The plating normally took∿ 8 hrs and the plating efficiency was normally greater than 90%.

(c) Radioactivity Measurements :

For the measurement of radioactive isotopes in extra-terrestrial samples, the selective and specific low level counting techniques are adopted for the following reasons :

(i) Small quantities of samples available due to their precious nature,

(ii) the unusually low specific activities of cosmogenic radionuclides and

(iii) high backgrounds due to environmental radioactivity and penetrating components (γ -rays, μ -mesons) produced in nuclear cascades generated by high energy cosmic ray particles in their interaction with the earth's atmospheric constituents.

In low level radioactivity measurement techniques it is necessary to reduce the background and increase the counting efficiency as far as possible. Significant reduction in background is obtained by adopting specific counting techniques, such as dual coincidence $\beta^{\pm}\gamma$, $X-\gamma$, $\gamma-\gamma$. (Bhandari 1969). Because of the specificity in detection techniques, tremendous reduction in backgrounds ($\sim 10^3$ to 10^4) is achieved without loosing much in detection efficiency. Because of the specific detection mode ($\beta^{\pm}\gamma$ coincidence) adopted, the interference in positron channels due to any other impurity is neglegible.

Detector system performance is evaluated in terms of minimum combined counting time T that must be spent in counting source and background to obtain a certain precision in the net

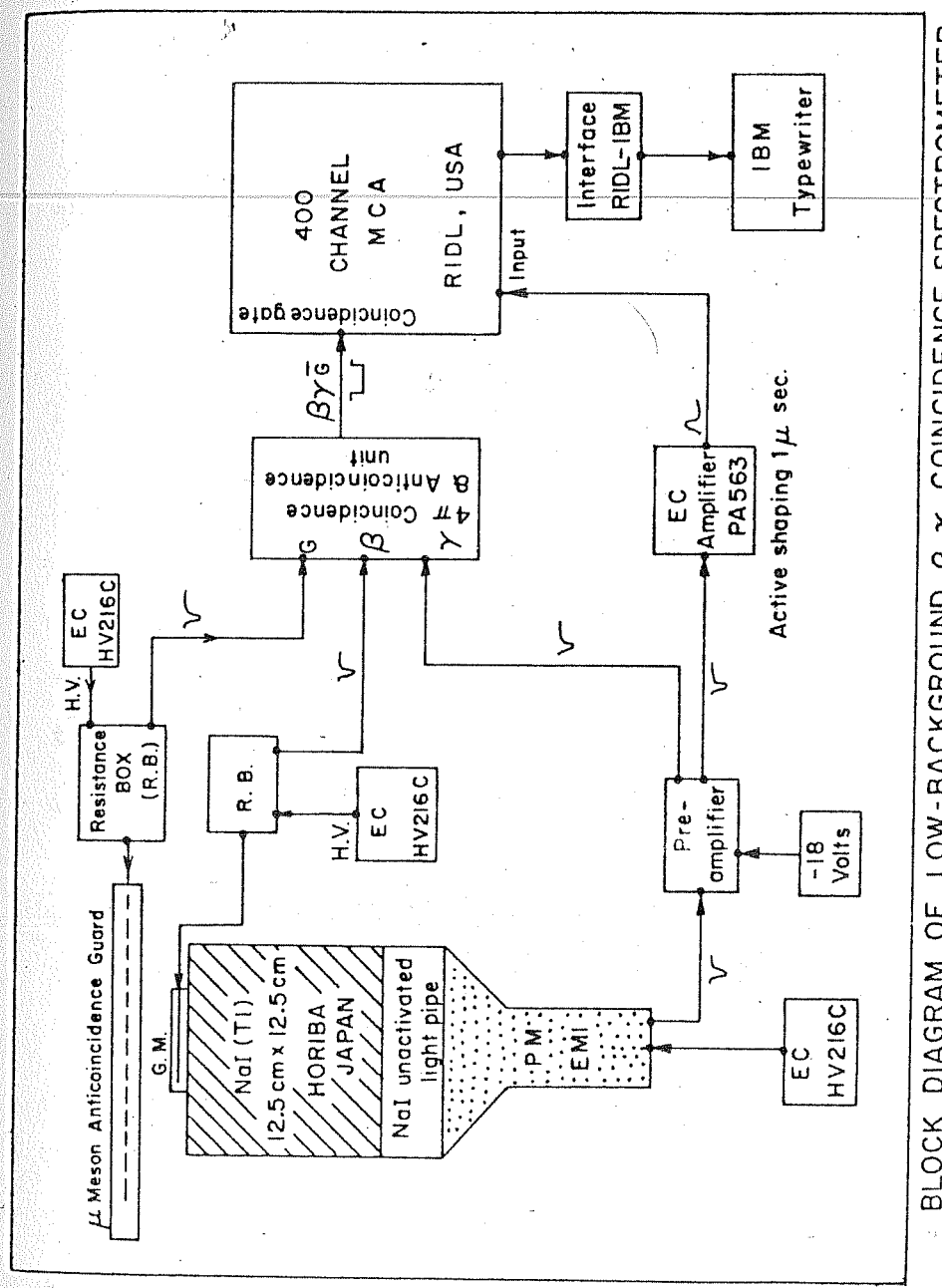

BLOCK DIAGRAM OF LOW-BACKGROUND β-γ COINCIDENCE SPECTROMETER

Fig. II. 3

counting rate. The FIGURE OF MERIT (FOM) of a counting system is then defined as $\frac{1}{T}$ and is given by (Oeshger and Wahlen 1976),

$$FOM = \frac{1}{T} = \frac{\varepsilon^2 S^2}{4B} \left\{ \frac{2}{(1 + \frac{S}{B})^{1/2} + 1} \right\}^2 \quad \ldots\ldots(II.1)$$

where S = net counting rate

B = Background rate

$\varepsilon = \frac{\sigma_S}{S}$ i.e. relative standard deviation in S.

In low level counting techniques, $S \approx B$ and we can write

$$FOM \propto \frac{S^2}{B} \propto \frac{\eta^2}{B}$$ where η = counting efficiency for a standard.

In beta-gamma spectrometric technique adopted in this work the system having maximum value of $\left(\frac{\eta}{B}^2\right)$ and the energy interval over which $\frac{\eta^2}{B}$ is maximum is chosen.

1. Beta-Gamma Coincidence Spectrometer:

Schematic diagram of $\beta^{\pm}$-γ coincidence spectrometric system is shown in Fig.II.3. A thin window Geiger-Muller (GM) counter is kept in flush on top or in well of 12.5 cm x 12.5 cm NaI (Tl) scientillator recording γ-rays following the design of Bhandari (1969). Anticoincidence guard counter is positioned just above the GM Beta Counter. The entire detector system is housed in a 10 cm thick lead shield.

The detector system stability was checked by running standard and background periodically. The detector system

TABLE II.1

Detector System Configurations

Properties of Detector Systems	β-γ coincidence spectrometer System-I	System-II	System-III	Beta Counting System System-IV
1. Crystal size (dia x thickness)	12.5 cmx12.5 cm	12.5x12.5 cm	12.5x12.5 cm	12.5x12.5 cm
2. GM(β) counter geometry	Flush on top of the crystal	Flush on top of the crystal	Inside well	Inside well
3. Active Area of counter	3.63 cm^2	9.6 cm^2	1.2 cm^2	4.0 cm^2
4. Area of the Anticoincidence Guard	100 cm^2	100 cm^2	-	-
5. Sample Holder	Porspex	Porspex	Copper	Copper
6. β efficiency(%)	35 (^{26}Al)	40 (^{26}Al)	45 (^{26}Al)	40 (^{10}Be)

TABLE II.2

Characteristics of Counting System

Detector Systems	Efficiency(%)			Background Rate(cpt)*			(Figure of Merit)$^{-1}$,(Th.mts.)**					
	0.511± 0.046 MeV	1.173+ 1.333 MeV	0.511+ 1.022+ 2.32 MeV	0.511+ 0.045 MeV	1.173+ 1.333 MeV	0.511+ 1.022+ 2.32 MeV	ϵ=0.1, S=8			ϵ=0.1, S=38		
	(1)	(2)	(3)	(1)	(2)	(3)	(1)	(2)	(3)	(1)	(2)	(3)
I. $\beta^{\pm}\gamma$ Coincidence spectrometer												
System-I	12	2.4	–	2.9	5.8	–	216	100	–	111	17	–
System-II	9	–	–	5.8	–	–	100	–	–	17	–	–
System-III	9.9	–	13.5	0.6	–	3.3	970	–	177	167	–	30

II. Beta Counting	(^{10}Be) Beta Efficiency (%)	Background(cph)***	FOM^{-1}(hrs) (ϵ=0.1, S=8)	FOM^{-1}(hrs) (ϵ=0.1, S=38)
System-IV	40	2.45±0.11	238	41

* cpt = counts per thousand minutes

** Th.Mts = thousand minutes

*** cph = counts per hour (hr)

resolution was (FWHM) 8.5% at 662 KeV ^{137}Cs peak.

2. Beta Counting System :

For beta counting of ^{10}Be a well GM counter in anti-coincidence with NaI(Tl) detector was used. BeO was deposited on Cu-holder.

The details of different detector configuration and system performance are given in Tables II.1 and II.2.

(D) Determination of Radionuclide Concentrations :

The specific activity, expressed in "distintegrations per minute per kg of bulk sample (dpm/kg)", is calculated using the following formula:

$$\text{Specific Activity(dpm/kg)} = \frac{\text{Net signal(cpm)} \times 10^3}{F_c \times F_{SA} \times F_d \times F_{ch} \times W \times BR} \quad \ldots\ldots(II.2)$$

where F_c = ideal detection efficiency

F_{SA} = β-particle self-absorption factor

F_d = decay correction factor

F_{ch} = chemical yield

W = weight of bulk sample processed for chemistry, g

BR = Branching ratio of mode of decay under detection

cpm = Net count rate per minute

The self-absorption factor is related to the absorption coefficient μ of the deta particles and the thickness, t, of the deposited salt, by

TABLE-II.3

Decay Characteristics of Radionuclides Investigated

S.No.	Properties	Radionuclides			
		^{10}Be	^{22}Na	^{26}Al	^{60}Co
1.	Decay Mode	β^-	$\beta^+ - \gamma$	$\beta^+ - \gamma$	$\beta^- - \gamma$
2.	Branching Ratio(BR)*	1.0	0.9057	0.821	1.00
3.	Half-life, $t_{1/2}$ (yr)*	1.6×10^6	2.60	0.72×10^6	5.26
4.	Maximum Beta Energy, E_{max}(MeV)*	0.555	0.545	1.17	0.318
5.	Absorption coefficient μ (cm^2/mg) & Medium	0.0356 (BeO)	0.0441 (NaCl)	0.01155 (Al_2O_3)	0.10 (Co_2O_3)
6.	Gamma Energies* (MeV)	-	0.511, 1.275	0.511, 1.809	1.173, 1.333

* Le derer and Shirley (1978)

$$F_{SA} = \frac{1-e^{-\mu t}}{\mu t} \qquad \ldots (II.3)$$

The absorption coefficient μ is given by

$$\mu = \frac{0.693}{\tau_{\frac{1}{2}}} \qquad \ldots (II.4)$$

where $\tau_{\frac{1}{2}}$ is the absorption half-thickness of beta particles.

The absorption coefficient μ were obtained experimentally by measuring absorption half-thickness $\tau_{\frac{1}{2}}$ of the $\beta^{\pm}$-particles in appropriate medium. The decay characteristics, mode of decay and absorption coefficients of the radionuclides studied are given in Table II.3.

(1) Determination of ^{10}Be

The specific activity of ^{10}Be was determined in several Dhajala fragments and in a Kirin sample.

A ^{10}Be standard was procured from Dr.McCorkell (Smithsonian Astrophysical Observatory. The standard was deposited on two source holders to determine detection efficiency. The idel detection efficiency was 27% for standard deposited on perspex holder and 40% for standard deposited on copper holder.

Although, the maximum energy E_{max} of β^--particles of ^{22}Na and ^{10}Be is similar, their detection efficiencies are quite different. While, the ideal detection efficiency of ^{22}Na β^+particles is 35%, that of ^{10}Be β^--particles is 27%.

TABLE-II.4

Radiochemical details of ^{10}Be Measurements in Dhajala Samples

Sample Code & wt.(g)	Chemical form	Carrier added (mg)	Amount counted (mg)	Detection mode	Ideal detection efficiency (%)	Background (cph)*	Signal (cph)	Specific Activity (dpm/kg)	Average Specific Activity (dpm/kg)
DH-9 (39)	BeO	65.20	28.2	β^-	40	3.25±0.18	4.96±0.20	18.2±0.74	18±0.7
T-92 (40)	BeO	65.20	27.2	β^-	40	2.45±0.11	5.89±0.23	17.3±0.67	17±0.7
T-272 (42.34)	BeO	65.20	15.2	β^-	40	2.45±0.11	4.18±0.30	19.2±1.3	19±0.8
	BeO	65.20	9.0	β^-	40	2.45±0.11	2.54±0.18	18.9±1.4	
T-273 (52.32)	BeO	73.22	24.9	β^-	40	3.25±0.21	8.90±0.42	21.6±1.0	20.8±0.8
	BeO	73.22	24.9	β^-	40	2.45±0.11	6.88±0.26	20.0±0.8	
T-9-1 (52.64)	BeO	109.88	27.0	β^-	28.70	9.34±0.37	3.85±0.61	19.4±3.0	21.8±1.5
	BeO	109.88	27.0	β^-	41.1	10.5± 0.63	6.00±0.84	21.2±3.0	
	BeO	109.88	25.0	β^-	40	2.45±0.11	6.12±0.30	24.7±1.2	
T-11 (326)	BeO	110.00	50.0	β^-	24	1.98±0.16	4.20±1.01	17.3±4.3	17.3±4.3
T-68 (30.0)	BeO	73.22	22.8	β^-	40	4.45±0.11	4.22±0.52	21.5±0.2	21.5±0.2

* cph = counts per hour.

The radiochemical and counting details of ^{10}Be measurements in Dhajala samples and in Kirin sample are given in Table II.4 and II.8, respectively.

(2) Determination of ^{22}Na :

The specific activity of ^{22}Na was measured in four Dhajala samples. In case of all the four samples, sodium content in aliquot which was taken just after dissolution of bulk sample was found to be higher than that expected from the normal H chondritic abundance. After realising the Na excess in case of first two samples analysed, precautionary measures were taken to check the source of contamination. The chemicals used, (viz. HCl, HNO_3, HF, $HClO_4$ and Boric acid powder) were tested for Na-content. The amounts found were too small to account for the excess Na. In order to check the excess sodium comming from leaching of glass wares by possibly untreaded HF, in subsequent samples the dried cake obtained after HF treatment was crushed by a teflon rod, and repeatedly treated with conc.H_2SO_4 and boric acid in a platinum dish and fumed to drive off HF completely. Inspite of the above pracautionary measures, it was found that some excess Na was always present.

The effeet of Na contamination was merely to dilute the ^{22}Na activity. In determining chemical yield, the excess sodium was taken into account. The efficiency of sodium was calculated by using the aliquot value of sodium, representing the initial value. Radiochemical and counting details are given in Table II.5.

TABLE-II.5

Radiochemical Details of ^{22}Na Measurements in Dhajala Samples

Sample Code & wt.(g)	Date counted	Chemical form	Amount expected (mg)	Amount counted (mg)	Detection Mode	Background (cpt)	Signal (cpt)	Ideal Positron detection efficiency (%)	Specific Activity (dpm/kg)	Average Sp.Activity (dpm/kg)
DH-9 (39)	22.11.1979	NaCl	933	420	$\beta^+-\gamma$	0.03±0.93	12.92±1.25	9.74	115±11	-
T-272 (42.34)	5.11.1980	NaCl	1590	220	$\beta^+-\gamma$	7.69±0.51	10.2±0.98	12.0	135±13	-
T-273 (52.32)	15.01.1980	NaCl	1373	302	$\beta^+-\gamma$	7.69±0.51	11.8±1.10	12.0	105±15	-
T-9-1 (52.64)	28.09.1978	NaCl	1297	112	$\beta^+-\gamma$	5.66±0.66	7.64±1.69	9.80	71±16	73±11
	28.01.1979	NaCl	1297	112	$\beta^+-\gamma$	5.66±0.66	8.00±1.75	10.80	75±16	

(3) Determination of ^{26}Al :

The specific activity of ^{26}Al is determined in several Dhajala samples and in a Kirin sample. The level of ^{26}Al activity in Madhipura, Bansur, and Udaipur chondrites are also determined. Depth profile of ^{26}Al in well documented lunar rock sample 61016,287 and in boulder Chip 69935,14 were determined. Also, ^{26}Al activity in deep shielded sample 69955 was also measured.

The radiochemical details of ^{26}Al determination in Dhajala samples are given in Table II.6. In Table II.7, the radiochemical and counting details of ^{26}Al determination in Madhipura, Udaipur, Bansur chondrites are given. The details of ^{26}Al measurement in Kirin are given in Table II.8. The atomic absorption spectrophotometric measurement of some major target element abundances in various depth samples of rocks 61016, 69935 and in sample 69955, along with the adopted chemical composition of two lunar soils 67481 and 24087 are given in the Table II.9. The radiochemical and counting details of ^{26}Al measurements in various depth samples of rocks 61016, 69935 and in sample 69955 are given in Table II.10.

The radiochemically recovered Al_2O_3 from Dhajala and Kirin samples were deposited on 3.63 cm^2 perspex holders and counted on system I and in some cases the salts were redeposited on 9.6 cm^2 perspex holder and counted on System-II.

TABLE-II.6

Radiochemical details of ^{26}Al measurements in Dhajala samples

Sample Code & wt(g)	Chemical form	Amount expected(mg)	Amount counted(mg)	Detection mode	Ideal positron detection efficiency (%)	Background (cpt)*	Signal (cpt)	Specific Activity (dpm/kg)	Average Specific Activity (dpm/kg)
DH-9 (39)	Al_2O_3	847.2	562.4	$\beta^+-\gamma$	9.00	7.65±1.75	71.2±3.5	51±2.5	51±2.5
T-92	Al_2O_3	388.9	396.7	$\beta^+-\gamma$	9.24	19.75±1.75	55.1±4.4	50±4	
(40)	Al_2O_3	868.9	396.7	$\beta^+-\gamma$	9.00	7.20±1.06	52.7±2.7	49±3	49.5±2.5
T-273	Al_2O_3	1136.5	296.1	$\beta^+-\gamma$	9.66	5.64±0.47	34.2±2.7	48.8±3.9	
(53.32)	Al_2O_3	1136.5	599.5	$\beta^+-\gamma$	9.24	10.70±1.20	72.8±2.8	48.8±1.9	49±2
T-9-1 (3.08)	Al_2O_3	66.9	30.6	$\beta^+-\gamma$	13.5	3.33±0.20	5.25±0.53	46±4	45±4
T-68 (30)	Al_2O_3	652.5	237.2	$\beta^+-\gamma$	9.24	5.84±0.75	30.0±2.3	53.9±3.2	54±3
T-11 (326)	Al_2O_3	7081	326.0	$\beta^+-\gamma$	9.24	19.35±1.75	59.2±3.6	55.9±3.4	56±3.4

* cpt = Counts per thousand minites.

TABLE-II.7

Radiochemical details of ^{26}Al measurements in some chondrites

Meteorite	Sample Wt. (g)	Al_2O_3 expected (mg)	Al_2O_3 counted (mg)	Detection mode	Ideal detection efficiency (%)	Background (cpt)*	Signal (cpt)	Specific Activity (dpm/kg)
Madhipura(L)	3.08	56.80	37.60	$\beta^+-\gamma$	13.5	3.33 ± 0.20	6.04 ± 0.73	36 ± 4
Udaipur(H)	3.05	58.19	40.00	$\beta^+-\gamma$	13.5	3.33 ± 0.20	5.89 ± 0.93	38 ± 6
Bansur(L)	3.53	73.25	55.30	$\beta^+-\gamma$	13.5	3.33 ± 0.20	11.15 ± 1.28	48 ± 5

*Cpt = counts per thousand minutes.

TABLE-II.8

Radiochemical details of Radioisotope Measurements in Kirin Chondrite

(Sample weight : 25 g)

Isotope	Date counted	Chemical form	Amount expected(mg)	Amount counted (mg)	Detection mode	Ideal detection efficiency (%)	Background (cpt)*	Signal (cpt)	Specific Activity (dpm/kg)
^{10}Be	10.5.1980	BeO	65.20	24.7	β^-	40	2.45 ± 0.11	2.48 ± 0.15	$12.9 \pm .8$
^{26}Al	20.3.1980	Al_2O_3	540	170.0	$\beta^+\gamma$	9.82	5.64 ± 0.47	13.18 ± 1.20	27 ± 2
^{60}Co	26.12.1979	Co_2O_3	29.54	22.8	$\beta^-\gamma$	2.30	7.73 ± 0.51	20.45 ± 1.07	103 ± 5

* Cpt = counts per thousand minutes

TABLE-II.9

Description and Chemical Composition of Lunar Samples

Sample Code	Depth (mm)	wt.of sample (g)	Chemical Composition(% by wt) Na	Mg	Al	Si	Ca	Fe	Mn
Rock 61016,267 (Anorthosite)									
RC-2-3	4.25±25	0.727	0.35	0.12	17.48	20.5(a)	11.78	0.34	0.0085
RC-2-8-4	6.6±0.25	0.686	0.48	0.11	18.44	20.5	11.84	0.36	0.0091
RC-2-8-5	7.0±0.25	0.793	0.28	0.13	17.28	20.5	12.99	0.20	0.0125
RC-2-8-2	13.5±0.25	0.848	0.60	0.19	16.41	20.5	13.00	0.18	0.0069
RC-2-8-1	14.7±0.25	0.901	0.47	0.11	17.72	20.5	11.09	0.40	0.0008
Boulder Chip 69935,14 (Breccia)									
NG-7	1±1	0.398	0.36	2.33	17.23	20.8(b)	11.89	3.36	0.0503
NG-9	5.5±2.5	0.769	0.71	2.41	16.00	20.8	10.53	3.65	0.0540
Boulder Chip 69955 (Anorthosite)									
NI-3	600	1.159	0.24	0.56	17.53	20.5(a)	11.95	0.80	0.0170
Apollo-16 Scoop Soil(c) 67481,7	scoop	0.228	0.32	3.90	13.90	21.20	-	-	-
Luna-24 Core Soil(d) 24087,1	860-870	0.162	0.22	5.82	6 .24	21.37	-	-	-

a) Average composition of Anorthosite rocks.
b) Average composition of Brecciated rocks.
c) Wanke (1974)
d) Blanchard et al (1977), Murali et al (1979)

TABLE-II.10

Radiochemical details of ^{26}Al measurements in Lunar Rocks

Sample Code	Sample wt.(g)	Chemical form	Amount expected(mg)	Amount counted(mg)	Detection mode	Ideal detection efficiency (%)	Background (cpt)*	Signal (cpt)	Specific Activity (dpm/kg)
61016,287(RC)									
RC-2-8-1	0.901	Al_2O_3	301.75	297.5	$\beta^+\gamma$	12.0	2.88±0.32	6.65±1.15	117±20
RC-2-8-2	0.848	Al_2O_3	265.12	217.0	$\beta^+\gamma$	12.0	2.88±0.32	6.21±0.69	125±14
RC-2-8-4	0.666	Al_2O_3	238.99	179.2	$\beta^+\gamma$	12.0	2.86±0.32	6.44±0.78	195±24
RC-2-8-5	0.793	Al_2O_3	260.56	202.0	$\beta^+\gamma$	12.0	2.88±0.32	8.36±0.84	198±20
69935,14(NG)									
NG-7	0.398	Al_2O_3	129.52	100.0	$\beta^+\gamma$	13.5	3.33±0.20	7.09±0.60	270±23
NG-9	0.769	Al_2O_3	232.54	191.4	$\beta^+\gamma$	12.0	2.88±0.32	5.05±0.90	108±17
69955(NI)									
NI-3	1.159	Al_2O_3	383.93	178.0	$\beta^+\gamma$	14.0	2.88±0.32	2.86±0.87	68±21

* cpt = counts per thousand minutes

Bulk samples of three meteorites (Madhipura, Udaipur, Bansur) weighing ~3 to 3.5 g were chemically processed and the extracted Al_2O_3 were deposited on 1.05 cm^2 cu-holders and counted on System-IV.

The ^{26}Al activity in ~ 3 to 3.5 g samples of Madhipura, Udaipur, Bansur and of some Dhajala samples were detected in 0.511 MeV positron annihilation peak, 1.022 MeV sum peak and the intermediate energy channels and 2.32 MeV sum peak (1.809+0.511) were detected. The ideal detection efficiency of 13.5% in the above energyy regions and background as low as 3.3×10^{-3} cpm were achieved. The typical counting times varied between 15 to 20 days.

(d) Determination of ^{60}Co :

The ^{60}Co activity was determined in several Dhajala samples and in a Kirin sample. The radiochemical and counting details of ^{60}Co measurements in Dhajala and Kirin samples are given in Tables II.11 and II.8, respectively.

The two closely spaced γ-peaks (E=1.173 MeV and 1.333 MeV) of ^{60}Co are separated on the β-γ spectrometer with the tails of the peaks slightly overlapping. So, the channels in the energy range 1.08 MeV to 1.44 MeV were chosen. The detection efficiency was ~2.4% for Co-samples deposited over perspex holders and was ~ 4% when Co was plated on copper planchets.

The chemical yield of Co in Kirin sample was 77% and for Dhajala samples varied between 67% and 98%. The Co abundance in all Dhajala samples was uniform at a value of

TABLE-II.11

Radiochemical and counting details of ^{60}Co measurements in Dhajala samples

Sample code & wt (g)	Date counted	Chemical form	Amount expected (mg)	Amount counted (mg)	Detection mode	Ideal detection efficiency (%)	Background (cpt)*	Signal (cpt)	Specific Activity (dpm/kg)	Average Specific Activity (dpm/kg)
DH-9	15.10.1979	Co_2O_3	43.0	42.0	$\beta^-\gamma$	2.54	11.01±1.30	30.3±2.2	81±6	83±5
(39)	28. 2.1980	Co	29.9	24.7	$\beta^-\gamma$	4.20	11.01±1.30	45.6±3.5	85±7	
T-92 (40)	15.12.1979	Co_2O_3	40.0	38.2	$\beta^-\gamma$	4.20	7.73±0.51	7.5±1.5	58±3.5	58±3.5
T-273	27. 8.1978	Co_2O_3	53.7	36.0	$\beta^-\gamma$	2.43	5.79±0.50	7.5±1.5	19.6±3.9	19±2.3
(52.32)	20. 5.1979	Co_2O_3	54.5	36.8	$\beta^-\gamma$	2.38	5.79±0.50	6.9±2.3	18.4±2.3	
T-272 (42.34)	10. 3.1979	Co_2O_3	43.5	36.8	$\beta^-\gamma$	2.38	5.79±0.50	9.0±1.0	25.0±2.7	25±3
T-9-1 (52.64)	20. 9.1978	Co_2O_3	54.0	52.2	$\beta^-\gamma$	2.27	4.80±0.51	2.9±1.0	6.6±2.3	6.6±2.3

* cpt = counts per thousand minutes

730 ppm, as determined by AAS in different aliquots. The Co-content in Kirin was 840 ppm.

(E) Determination of positron activity in Apollo-16 and Luna-24 Soils:

The positron activity in 228 mg of Apollo-16 scoop soil (67481) and in 162 mg of Luna-24 core soil (24087) were measured by non-destructive $\beta^{+}\gamma$ coincidence technique. The soil samples were spread uniformly on a thin mylar film of 2 cm^2 area and counted on System-I. The signal in 0.511 ± 0.045 MeV and 0.580 ± 0.050 MeV energy channels were detected. The counting details are given in Table II.12.

In case of non-destructive counting a significant contribution to positron channels arises from compton scattered gamma rays from 0.580 MeV peak of ^{208}Tl, a daughter product of ^{232}Th. The relative contribution due to ^{208}Tl was determined by Bhattacharya (1979) and Bhandari et al*(1976) by counting terrestrial basalts and granites containing known concentration of ^{232}Th on the same counting system. Following Bhattacharya (1979), a relative contribution factor of 1.137 is used. To obtain net positron signal, the contribution due to the net count rate in 0.580 ± 0.050 MeV channels in positron channels wwere substracted. The errors are large because of the interference correction and small sample available as shown in the table. The positron signal in case of Apollo-16 soil was due to only ^{26}Al while in case of Luna-24 soil, the signal was due to both ^{26}Al and ^{22}Na as it was counted soon after it was collected from the Lunar surface.

TABLE-II.12

Details of non-destructive β-γ measurements of Lunar soils

Soil	Sample wt. (g)	Deposited area (cm^2)	Total counting time (min)	Gross count rate in (511 ± 45) kev channels (cpt)*	Count rate in (580 ± 50) kev channels (cpt)	Net count rate** (cpt)	Specific Activity ($^{22}Na + ^{26}Al$) (dpm/kg)
24087,1	0.162	2.35	30056	4.3 ± 0.4	2.1 ± 0.3	0.59 ± 0.48	57 ± 45
67481,7	0.228	2.35	8870	6.2 ± 0.8	1.6 ± 0.4	3.10 ± 0.95	245 ± 75
Background	-	5.25***	15840	2.3 ± 0.3	0.7 ± 0.2	-	-

* cpt = counts per thousand minutes.

** Mean date of counting : 15th May, 1977.

*** Beta counter area.

CHAPTER-III

RESULTS

The experimental techniques used for the measurement of ^{10}Be, ^{22}Na, ^{26}Al and ^{60}Co in several Dhajala fragments and ^{26}Al in Madhipura, Udaipur and Bansur chondrites and in some lunar rocks and soil samples have been described in Chapter-II. In the present chapter, the results are presented and the depth profiles of various radionuclides are constructed.

(A) Depth Profile and Radionuclides in Dhajala Chondrite:

(i) Shielding depth of Dhajala samples :

The Dhajala meteorite fragments resulted from multiple fragmentations producing a shower, of which more than 500 fragments could be recovered from about 50 km^2 of the strewn field. The largest fragment (T-92) weighs about 12 kg. Most of the fragments were subjected to cosmogenic particle track studies. A few selected fragments were studied extensively for tracks and their shielding depths are well determined.

In Table III.1, the ^{10}Be, ^{22}Na, ^{26}Al and ^{60}Co data in Dhajala fragments studied so far, their activity ratios and available track density in some samples are summarised. The shielding depths given in the table are for preatmospheric size $R_E \sim 50$ cm (Bhandari et al.1980) and the exposure age of 6.3 ± 1 Myr (Rao et al.1979). Only in case of samples T-67, T-11 and T-92, the track data are satistically good and reliable. Their deduced shielding depths are accurate within about ± 3 to ± 5 cm. In DH-9 sample, however, no cosmogenic tracks could be found giving lower limit to 40 cm on its

TABLE-III.1

Summary of cosmogenic radionuclide and particle track data in Dhajala samples

Radio-Nuclide/ Ratio	Specific Activity (dpm/kg meteorite)/Ratios									
	T-9-1	T-273	T-272	T-92	DH-9	T-11	T-68	T-67 (a)	T-72 (a)	DH-9 (b)
^{10}Be	21.8±1.5	20.8±0.8	19.0±0.8	17.0±0.7	18±0.7	17.3±4.3	21.5±0.24	-	-	-
^{22}Na	73±11	105±15	135±13	126±12 (c)	115±11	-	-	100±2	109±2	110±8
^{26}Al	45±4	49±2	-	49.5±2.5	51±2.5	56±3.4	54±3	48±1	-	48±6
^{60}Co	6.6±2.3	19.0±2.3	25±3	58±3.5	83±5	15±2	-	6±1	13±1	77±6
$\left[\frac{^{10}Be}{^{60}Co}\right]$	3.30±1.17	1.09±0.14	0.76±0.10	0.29±0.02	0.22±0.01	1.15±0.32	-	-	-	-
$\left[\frac{^{22}Na}{^{26}Al}\right]$	1.62±0.28	2.14±0.22	-	2.55±0.27	2.25±0.24	-	-	2.08±06	-	2.29±0.33
$\left[\frac{^{10}Be}{^{26}Al}\right]$	0.48±0.05	0.42±0.02	-	0.34±0.02	0.35±0.02	0.31±0.08	0.40±0.02	-	-	-
TPM ($cm^{-2}.Myr^{-1}$)	-	-	-	1.49×10^{2}	(d)	5.3×10^{3}	-	7.3×10^{4}	-	(d)
Shielding depth (cm)	-	-	-	$35^{+5}_{-2.5}$	40 (45±5)	15±1	-	6±2	-	40 (45±5)

(a) Rancetelli (Private communication), (b) G.Heusser (Private communication),
(c) Bhandari et al. (1978), (d) See text

shielding depth. The track data in samples T-272, T-273, T-68 and T-75 are not statistically good enough to deduce their shielding depths.

From the Table III.1, it is observed that the measured ^{60}Co is minimum in T-67(depth $\sim$ 6 cm) and maximum in DH-9 (shielding depth > 40 cm and is assumed to be 45 ± 5 cm in this discussion). The ^{10}Be activity in sample T-9-1 is 21.8 ± 1.5 dpm/kg and 18 ± 0.7 dpm/kg in DH-9. Since the activity of ^{60}Co is expected to increase with shielding depth in a 50 cm radius body(Eberhardt et al 1963) and the activity of high energy product, ^{10}Be, is expected to gradually decrease with shielding depth, it is expected that the activity ratio ($^{10}Be/^{60}Co$) should be a good indicator of the relative shielding depths in meteorites. In Fig.III.1, the observed ($^{10}Be/^{60}Co$) ratios in samples T-67, T-11, T-92 and DH-9 are plotted against their shielding depths. Unfortunately, reliable ^{10}Be data for sample T-67 does not exist. However since the ^{60}Co activity in T-9-1 and T-67 samples differ slightly, the ^{10}Be activity in T-67 can be assumed to be the same as that in T-9-1. The ($^{10}Be/^{60}Co$) ratio decreases from 3.7 at depth of 6 cm to 0.22 at depth of 45 cm. This depth calibration curve based on ($^{10}Be/^{60}Co$) ratio is used to deduce the shielding depths of other samples. In case of sample T-68 and T-75, the ^{10}Be data does not exist. Their shielding depths are deduced from the ^{60}Co profile constructed based on other samples (Fig.III.2).

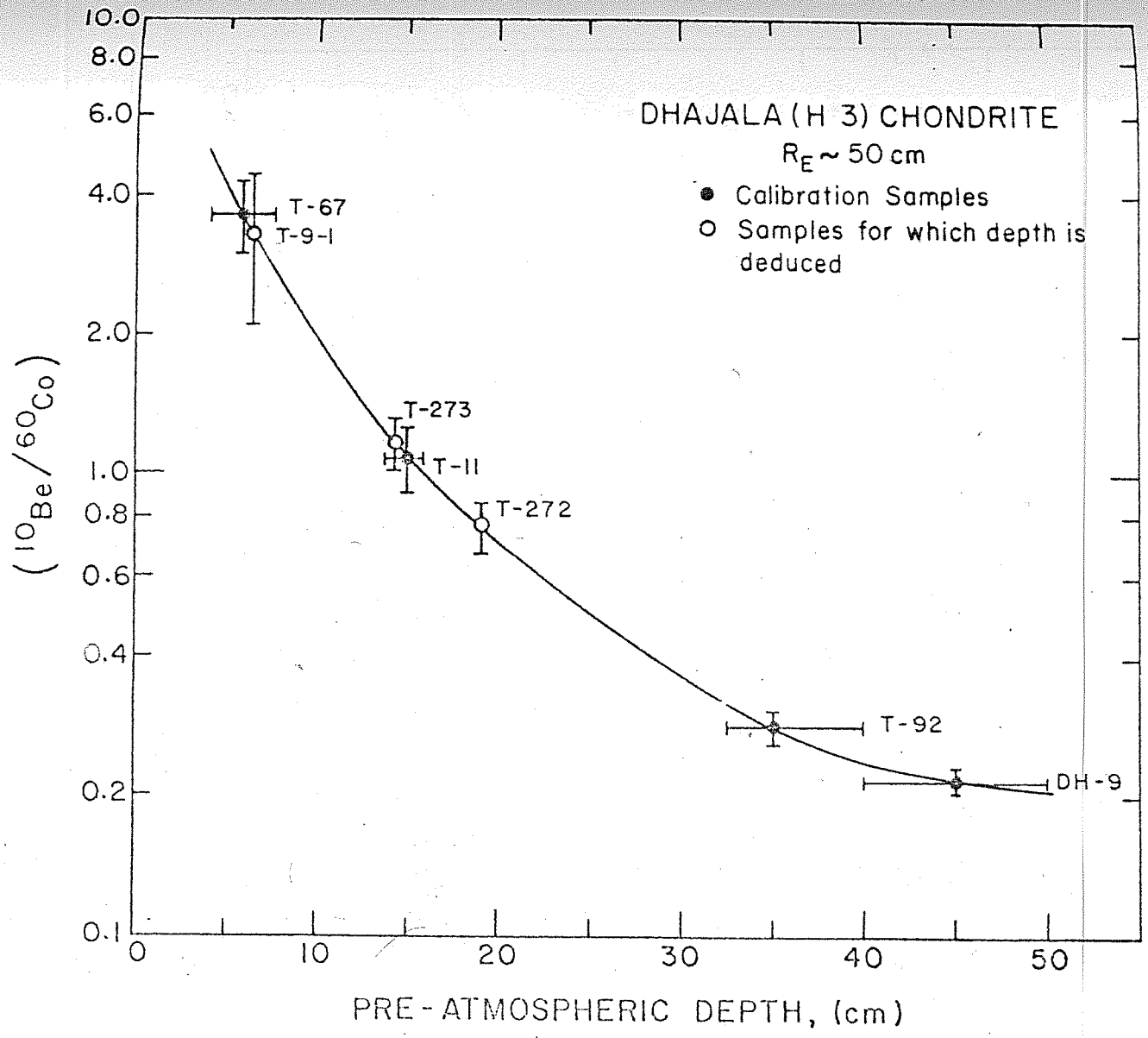

Fig.III.1 $(^{10}Be/^{60}Co)$ vs. depth calibration curve.

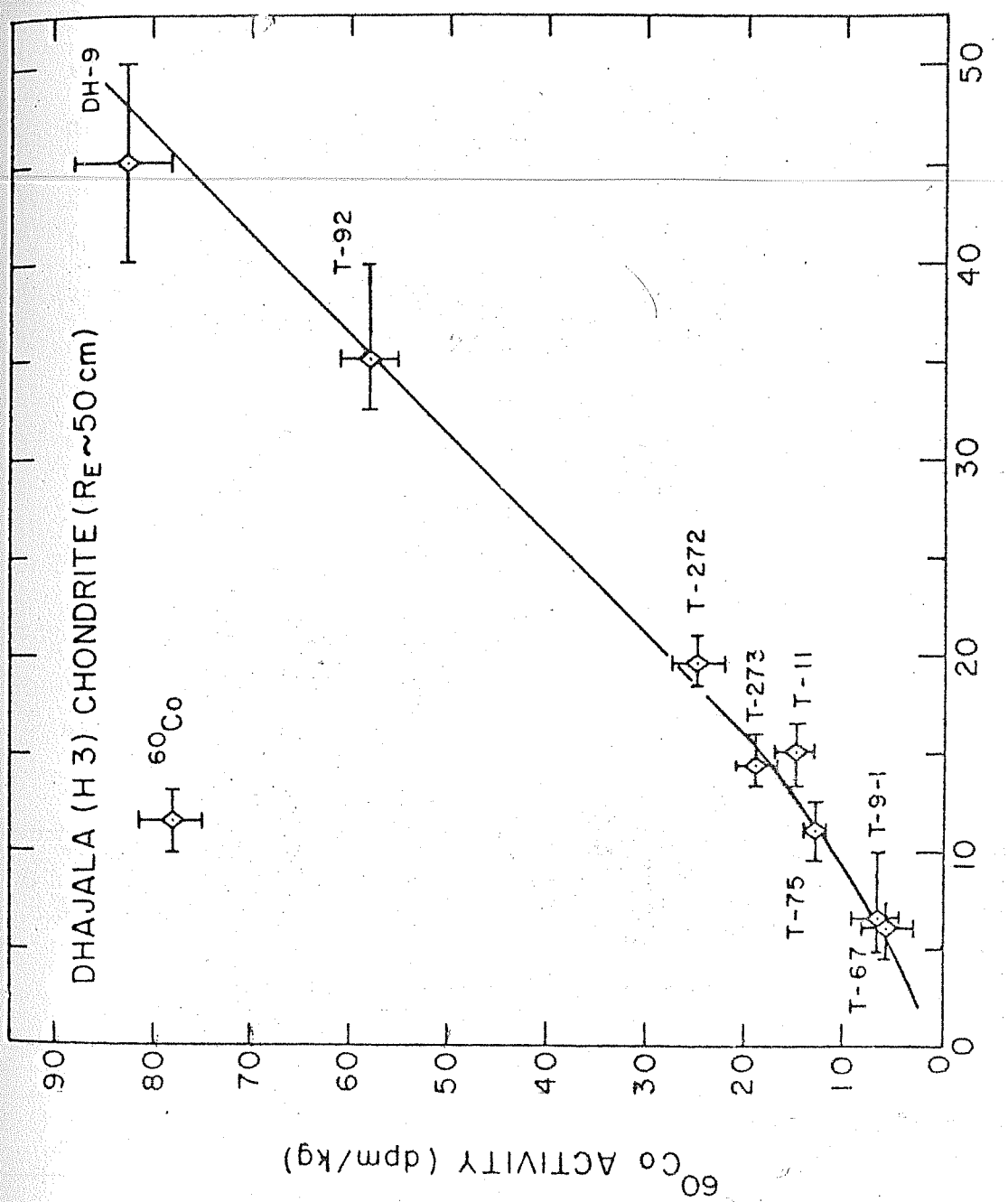

Fig. III.2 Depth profile of ^{60}Co in Dhajala chondrite.

(ii) Depth profile of ^{60}Co :

This radioisotope shows maximum depth variation. Its production rate varies by a factor of ∿ 13 over a depth interval of 6 to 45 cm (Fig.III.2). Being an epithermal neutron capture product, its production is directly related to flux of 132 eV neutrons. The depth variation shows that the neutron flux increases with shielding depth.

(iii) Depth profile of ^{26}Al :

The depth profile of ^{26}Al is plotted in Fig.III.3 and the best fit curve is drawn to show its depth variation. The ^{26}Al production rate is 48 dpm/kg at depth of 6 cm, it increases to 54 dpm/kg at depth of ∿ 15-20 cm and falls down to 50 dpm/kg at depth of 35 cm. Thereafter it remains nearly constant with depth. Since shallow depth samples are not available the entire depth profile is assumed to be due to GCR particles and is used to deduce the depth profile of the spectral shape parameter in a body of 50 cm radius, as discussed in Chapter-IV.

(iv) Depth profile of ^{22}Na :

The ^{22}Na depth variation is similar to that of ^{26}Al. The production rate increases from 100 dpm/kg at a depth of 6 cm to 126 dpm/kg at depth of ∿ 15 cm, and decreases to 110 dpm/kg at depth of ∿ 35 cm. At larger shielding depths, the profile flattens out (Fig.III.4).

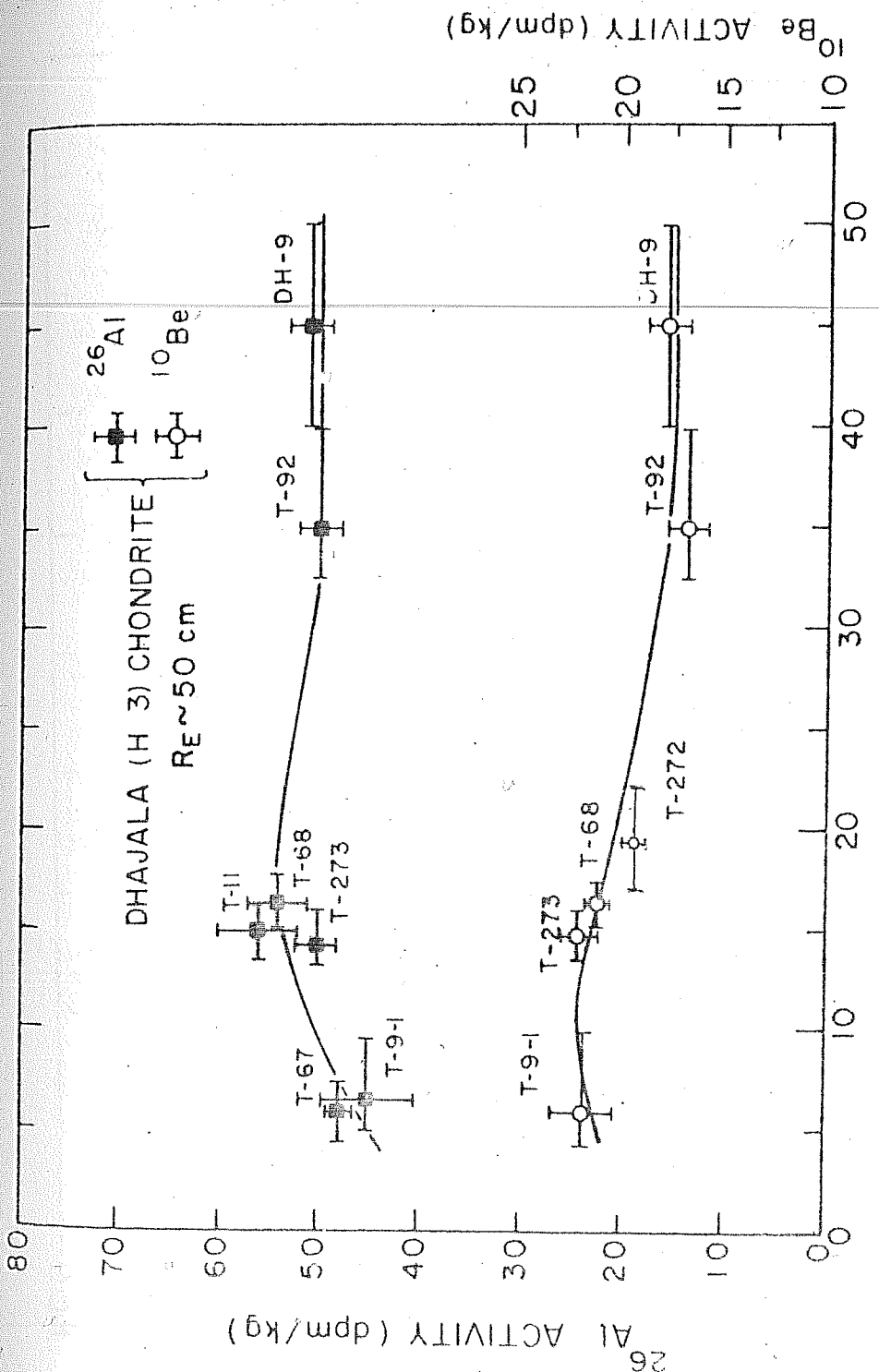

Fig.III.3 Depth profiles of ^{26}Al and ^{10}Be in Dhajala chondrite.

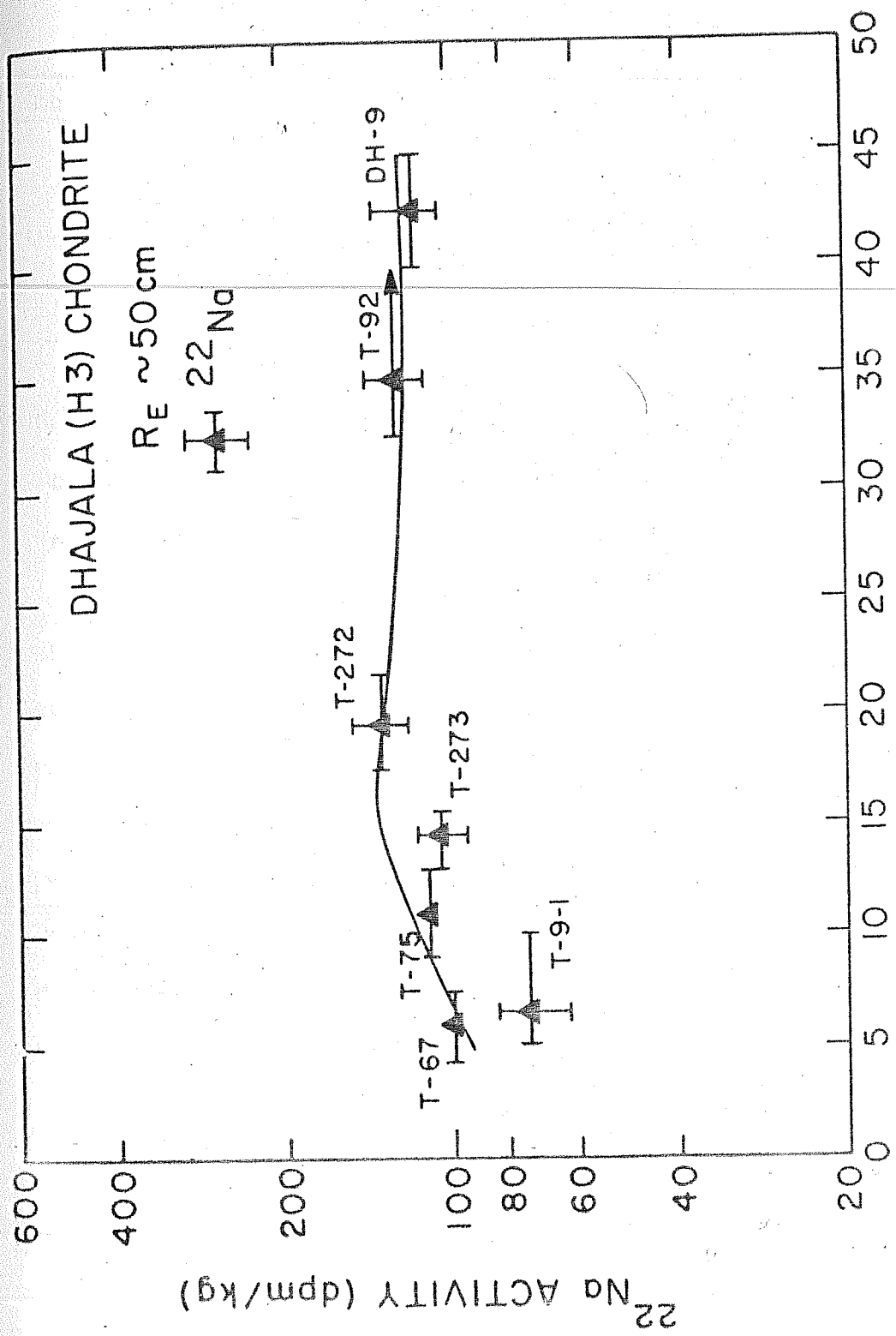

Fig.III.4 Depth profile of ^{22}Na in Dhajala chondrite.

(v) Depth profile of ^{10}Be :

The ^{10}Be profile shows least variation with depth. The ^{10}Be activity increases from about 21 dpm/kg at depth of 6 cm to 22.5 dpm/kg at 12 cm depth and then decreases to 17 dpm/kg at large shielding depths (Fig.III.3).

(B) Radionuclides in Meteorites :

(i) ^{26}Al in Madhipura, Udaipur and Bansur Chondrites :

The description of these meteorites is given in Chapter-II. The preatmospheric size of Madhipura, Udaipur and Bansur chondrites are 6.5, 9.0 and 15 cm, respectively. The depth profile of ^{53}Mn was measured in these meteorites by Bhattacharya et al (1980) and the profiles were found to be nearly flat. Being a low energy product like ^{53}Mn, the depth profiles of ^{26}Al is also expected to show similar depth variation. We have measured ^{26}Al activity in 3 to 3.5 g sample of each of these chondrites to determine the level of ^{26}Al production rate in these chondrites. In Table III.2, the measured ^{26}Al activity and other relevant data on these meteorites are summarised.

(ii) Radionuclides in Kirin chondrite :

We have measured ^{10}Be, ^{26}Al and ^{60}Co in a 25 g sample of Kirin chondrite and the results are already given in Table II.8. The detailed interpreation of these data will follow in Chapter-IV.

TABLE III.2

^{26}Al and other relevant data on Madhipura, Udaipur and Bansur Chondrites

Meteorite	Preatmospheric radius (cm) (a)	Recovered effective radius (cm)	Shielding depth of samples (cm) (b)	^{21}Ne exposure age (Myr) (c)	Specific activity of $(^{53}Mn)_{sat}$ (dpm/kg Fe) (b)	Specific activity of ^{26}Al (dpm/kg)
Madhipura(L)	6.5	4.7	2.5-6.5	15	306 (289-331)(d)	36 ± 3
Udaipur(H)	9.0	4.6	3.7-9.0	22	312 (301-322)	38 ± 6
Bansur(L)	15.0	10.0	2.5-15	15	377 (359-400)	48 ± 5

a) Bhandari et al. (1980)
b) Bhattacharya et al.(1980)
c) Gopalan and Rao (1976)
d) Range of ^{53}Mn activity

(C) Depth profile of ^{26}Al in Lunar rocks :

(i) Shielding depth of samples in Lunar rock 61016,287:

The details of this rock specimen are given in Chapter-II. The 35.04 g of the slice 61016,287 was saved from the 11.7 kg parent boulder. The surface of the slice was exposed at zenith angle of 30° on the parent boulder. The cutting diagram and sample locations are schematically shown in Fig.II.1 (Chapter-II). Five depth samples were cut using 0.5 mm thick diamond cutting wheel driven by an electromechanical motor. The samples shown by shaded region in the diagram are cutting powders. Although, the thickness of each powder sample is 0.5 mm, the depth of the entire sample has uncertainty of 2 mm which is due to the non-flat top surface of the slice. The depths of the samples measured along the edges of the slice are 2 mm less than the depths measured from a point on top of the surface (shown as Z = 0 in the diagram). Since most of the mass of each samples comes from interior regions (away from the edges), the effective depth of the sample is close to the depth measured from the point Z = 0. For sample with depth greater than 1 cm, the effect of this uncertainty on the effective depth is calculated to be insignificant.

Since the bottom of the rock slice was not parallel to the top surface and the bottom-most sample was sliced parallel to the top surface sample, RC-2-8-1 has largest uncertainty of 4 mm in its depth. Because it is from large shielding depth,

the error is not serious and we have adopted its depth to be equal to the mean depth measured from the point Z = 0. The summary of ^{26}Al data measured by radiochemical method is given in Table III.3.

^{26}Al depth profile :

The observed ^{26}Al activity is due to both the GCR and SCR contributions. Since the SCR contribution at large shielding depths (> 10 g.cm^{-2}) is negligible, the ^{26}Al activity at large shielding depth is entirely due to GCR particles. Towards shallower depths the SCR contribution dominates. The ^{26}Al activity in near surface sample of 61016 rock is highest and equal to 735±75 dpm/kg (Bhandari et al.1976). The activity decreases rapidly with depth reaching a value of ∿300 dpm/kg at depth of 1 g.cm^{-2}(ρ = 3 g.cm^{-3}) and ∿ 195 dpm/kg at depth of 2 g.cm^{-2}. Thereafter the activity decreases slowly with depth to a value of ∿ 150 dpm/kg at 4 g.cm^{-2}.(Table III.3).

(ii) Shielding depth of samples in 69935,14 [illegible] ^{26}Al

Two chips 69935 and 69955 were removed by Apollo-16 astronauts from top and bottom of a boulder located near South Ray crater. The description of the boulder chips is given in Chapter-II. The chip 69935 had two exposed surfaces (i) top exposed, slightly concave in shape and (ii) west side exposed, slightly convex in shape. In the present study we have limited our studies to the samples from top exposed portion. The schematic diagram of two portions of the chip

TABLE-III.3

Summary of ^{26}Al measurements in Lunar Rock samples

Rock	Type	Exposure age (Myr)	Sample code	Sample depth ($g.cm^{-2}$)	Specific activity of ^{26}Al (dpm/kg)
61016,287 (RC)	Anorthosite	1.5 (a)	RC-2-8-4	1.98 ± 0.15	195 ± 24
			RC-2-8-5	2.10 ± 0.15	198 ± 20
			RC-2-8-2	4.05 ± 0.15	175 ± 12
			RC-2-8-1	4.40 ± 1.20	117 ± 20
69935,14 (NG)	Breccia	0.4 (a)	NG-7	0.3 ± 0.3	269 ± 23
			NG-9	1.65 ± 0.75	108 ± 17
69955	Anorthosite	2.13 (b)	NI-3	~ 180	68 ± 21

a) Bhandari et al. (1976)

b) ^{21}Ne exposure age by Drozd et al. (1974)

and the sample locations are shown in Fig.II.1. The zenith angle of the chip on the parent boulder is ∿ 20°. Two samples NG-7 and NG-9 were processed for ^{26}Al radiochemistry. The depth of NG-7 is 0-2 mm and NG-9 is 3-8 mm.

The boulder chip 69955 (NI-3) which was removed from the bottom of the parent boulder is from effective shielding depth of 60 cm (∿ 180 $g.cm^{-2}$)

^{26}Al profile :

The summary of our measurements of ^{26}Al in NG-7, NG-9 and NI-3 is given in Table III.3. Although the data are limited, they compare well with the ^{26}Al profile in 61016 sample. The ^{26}Al activity in top 2 mm thick sample is 269±23 dpm/kg and in 3-8 mm depth sample the activity is 108±17 dpm/kg. The activity in NI-3, a deep shielding sample is 68±21 dpm/kg.

(D) Positron activity in Lunar soils (24087,1 and 67481,7):

The description of the two lunar soils is given in Chapter-II, and the details of measurement of the total activity by non-destructive $\beta\pm\gamma$ coincidence spectrometry are given in Table II.12. The results are discussed in the Chapter-IV.

CHAPTER-IV

DISCUSSIONS

(A) Radionuclides in Meteorites :

The production of cosmogenic nuclides depend sensitively on the size and shielding depth of meteorites. The production due to SCR protons is confined to first $\sim$ 20 $g.cm^{-2}$ of depth and in deeper regions GCR protonsand their secondaries (viz. neutrons, protons and charged π mesons etc.) dominate. Due to the atmospheric ablation suffered by meteorites, the layers containing SCR records are usually lost. Only in a few rare cases of ablation, near surface regions can survive the atmospheric transit.(Bhandari et al.1980).

The nuclide production rate at any depth depends on (i) the target element concentration, (ii) the reaction excitation functions, and (iii) the flux and energy spectrum of nuclear active particles. There are three main approaches of calculation of production rates : (i) thick target bombardment calculations (Kohman and Bender 1967, Trivedi and Goel 1973), (ii) Monte-carlo simulation of intranuclear evaporation-cascade in thick target irradiations (Armstrong and Alsmiller 1971,and Van Ginneken and Turkevich 1970), and (iii) analytical method using thin target excitation functions and flux and energy spectrum of primaries and secondaries. This last method has the advantage in that it allows for more and more refinement as and when improved and new cross-section data become available. An analytical method of calculating the spectra of primary and secondary

nucleonic flux was first attempted by Ebert and Wanke (1957) which was later improved by Lavrukhina et al. (1969). Reedy and Arnold (1972) developed an analytical model to calculate depth profiles of radionuclides in the Moon, based on an approach similar to that of Arnold et al. (1961). This model requires a priori knowledge of the flux and shape of the energy spectrum of the nuclear active particles and the reaction excitation functions. The production rate at depth X in a body of effective preatmospheric radius R_E is given by equation I.4 (Chapter-I). In Reedy-Arnold model the energy spectrum above E ~ 100 MeV is assumed to be of the form

$$\frac{dJ}{dE}(X, R_E) = K \{\alpha + E\}^{-2.5} \quad \ldots(IV.1)$$

and in the energy range of $2.5 \leq E \leq 100$ MeV,

$$\frac{dJ}{dE}(X, R_E) = K\{\alpha + 100\}^{-2.5} \{M(E) - (\alpha - 50)\delta(E)\} \quad \ldots(IV.2)$$

where $M(E) = 94E^{-1} + 603\ E^{-2} - 300\ E^{-3}$

and $\delta(E) = 0.3\ E^{-1.26} - 0.00091$. $\ldots(IV.3)$

In $0.5 \leq E \leq 2.5$ MeV, the spectrum is assumed to be

$$\frac{dJ}{dE}(X, R_E) = K(\alpha + 100)^{-2.5} \{115 - (\alpha - 50) \times 0.094\}$$
$$\times \{1.3175 + 0.5E - 0.25E^2\} \quad \ldots(IV.4)$$

In above equations, J, K and α are functions of X and R_E In general Reedy-Arnold model predicts the depth variation in agreement with the measured depth profiles of some isotopes in the Moon (Kohl 1975, Finkel 1972), but there are disagreements between the measured and calculated production rates for other isotopes. This discrepancy may be due to inaccurate and scanty cross-section data available.

If F_o is the integral proton flux above 1 GeV in free space and F_G is the integral nucleonic flux (> 1 GeV) at geometrical depth X in a meteoroid body of effective radius R_E, then we have

$$F_G(X,R_E) = \int_0^{2\pi} d\Phi \int_0^{\pi} \left[\{ F_o \exp(-\frac{r}{\lambda_p}) + a F_o \exp(-\frac{r}{\lambda_\alpha}) \} + b \frac{F_o}{d} \{ \exp(-\frac{r}{\lambda_p}) - \exp(-\frac{r}{d}) \} / (\frac{1}{d} - \frac{1}{\lambda_p}) \right] \sin\theta \, d\theta$$

..... (IV.5)

where λ_p, λ_α, a, b and d are constants taken from Reedy and Arnold (1972),

θ is zenith angle,

Φ is azimuthal angle, and

$r(X,R_E,\theta)$ = distance along zenith angle θ of a point at geometrical depth X and is given by (Bhattacharya et al.1972),

$$r(X, R_E, \theta) = -(R_E - X)\cos\theta + \left[R_E^2 \cos^2\theta + 2R_E X \sin^2\theta - X^2 \sin^2\theta\right]^{1/2} \quad \ldots\ldots (IV.6)$$

The depth variation of the spectral shape parameter was obtained by Bhattacharya et al.(1980) from the experimental depth profiles of ^{53}Mn in meteorites of different sizes. Using the production excitation function of Gensho et al. (1978) for ^{53}Mn production from Fe, the free space GCR integral proton flux of 1.7 protons/(cm^2.sec.4 πsr) and absorption and interaction parameters of Reedy and Arnold (1972), they calculated the values of α for 6.5, 9, 15 and 25 cm size meteorites. For large meteorites this value is not available.

Here we derive the depth profile of spectral shape parameter from the measured ^{26}Al depth profile in a 50 cm radius meteoroid Dhajala. Using these deduced α values, the expected production depth profiles of other radionuclides viz. ^{10}Be and ^{22}Na are calculated and compared with experimental profiles.

(1) <u>The ^{26}Al depth profile and spectral shape parameters</u>:

The depth profile of ^{26}Al in Dhajala has been described in Chapter-III and is shown in Fig.III.3. The best fit depth profile is used to deduce the values of spectral shape paramter, α.

The ^{26}Al is mainly produced from target elements Al and Si due to GCR particles. The production reactions are (Table-I.1).

TABLE-IV.1

Calculated characteristics of the nucleonic spectra in a 50 cm body

Depth (cm)	Spectral shape parameter (MeV)	Normalising constant, K particles/ ($cm^2 . 4\pi$ sr. $MeV^{-3/2}$)	$J_G(>1$ GeV) particles/(cm^2.sec.4π sr)	$J_G(>10$ MeV)
5	372	87523	1.179	10.601
10	310	73095	1.057	12.114
15	272	63846	0.967	13.169
20	260	58310	0.895	12.953
25	252	54189	0.841	12.667
30	250	51333	0.793	12.156
35	247	49077	0.767	11.929
40	243	47519	0.744	11.781
50	240	46275	0.729	11.704

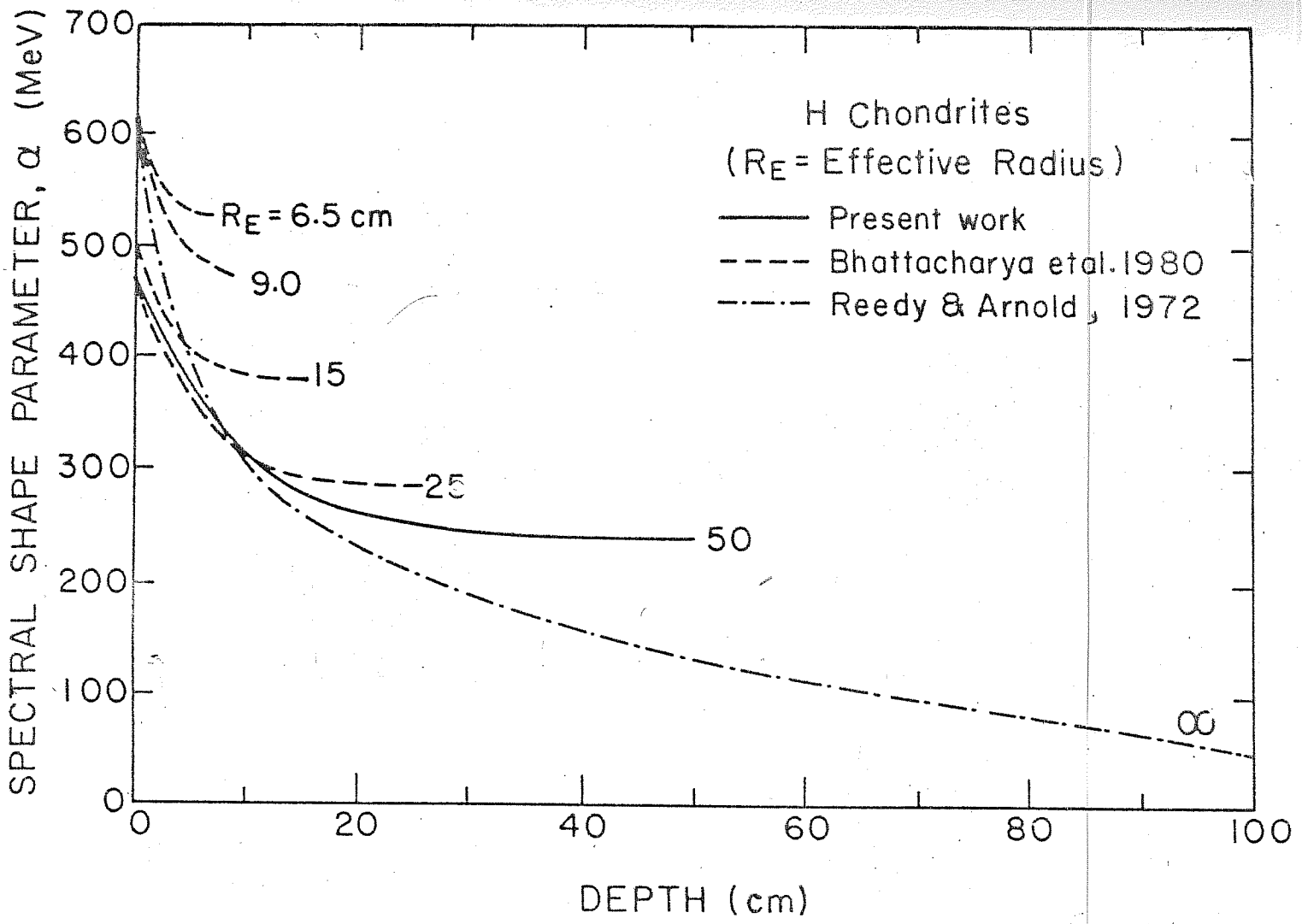

Fig.IV.1 Spectral shape parameter as a function of depth in 6.5, 9.0, 15.0, 25 cm (Bhattacharya et al. 1980), in 50 cm chondrites (present work) and in Moon (Reedy and Arnold, 1972).

$^{26}Mg(p,n)^{26}Al$,

$^{27}Al(p,pn)$ and $^{27}Al(n, 2n)$,

and, $^{28}Si(p,2p)$ and $^{28}Si(n, np)$.

Mg contribution is found to be negligible, and other target elements do not contribute more than 2%.

The reaction cross-sections of production are available for the energy range 25-52 MeV (Furukawa et al•1971) and at 600 MeV and 24 GeV (Regnier 1973). These cross-sections are known within ∿ 10% uncertainty. The contribution due to ^{26}Mg is very small and is neglected. The target element abundances are Al:1.15% and Si:17% by wt in Dhajala (H3) chondrite.

In Table-IV.1, the results of the calculations are presented. The best fit α values, deduced K values and flux above energy 1 GeV and 10 MeV are also tabulated. The exposure age of 6.3 Myr based on cosmogenic ^{21}Ne and ^{38}Ar was adopted for calculating the production rates (Gopalan et al.1978). The GCR flux above 1 GeV decreases with depth whereas the flux > 10 MeV first increases with depth upto ∿ 15 cm (due to secondary production) and then decreases.

The best fit α values deduced are shown in Fig.IV.1.for comparison, the α values for $R_E \leq$ 25 cm chondrites (Bhattacharya et al. 1980) and for Moon (Reedy and Arnold 1972) are also shown.

(2) ^{22}Na depth profile and GCR modulation during solar cycle 20 :

The experimental depth profile of ^{22}Na is described in Chapter-III and is shown in Fig.III.4. Whereas the shape of the profile is similar to the calculated profile, the absolute values are about 35% higher than the calculations. Since the calculated values are based on long-term average GCR flux of 1.7 protons/(cm^2.sec.4 π sr. > 1 GeV) and Dhajala fell at the time of solar minimum, the higher ^{22}Na activity may be due to higher GCR fluxes during the past decade before the fall. The excitation functions for ^{22}Na production from target elements Mg, Al, Si and Na are given in Fig.V.1(c).

This 2.56 .yr half-life ^{22}Na is produced mainly during the decade before the fall of the Dhajala chondrite in 1976, which covered the entire solar cycle 20 (1965-1976). The GCR flux in the interplanetary medium is modulated due to solar activity and before we calculate the effect of solar modulation, it is essential to know the GCR fluxes during the solar cycle 20.

GCR fluxes during Solar Cycle 20 :

For the calculation of modulation effect on ^{22}Na production the available measurements of GCR spectra (Bedijn et al.1973, McKibben 1977, Hsieh et al.(1971), Garcia-Munoz et al (1975a, b, c and 1977) over entire

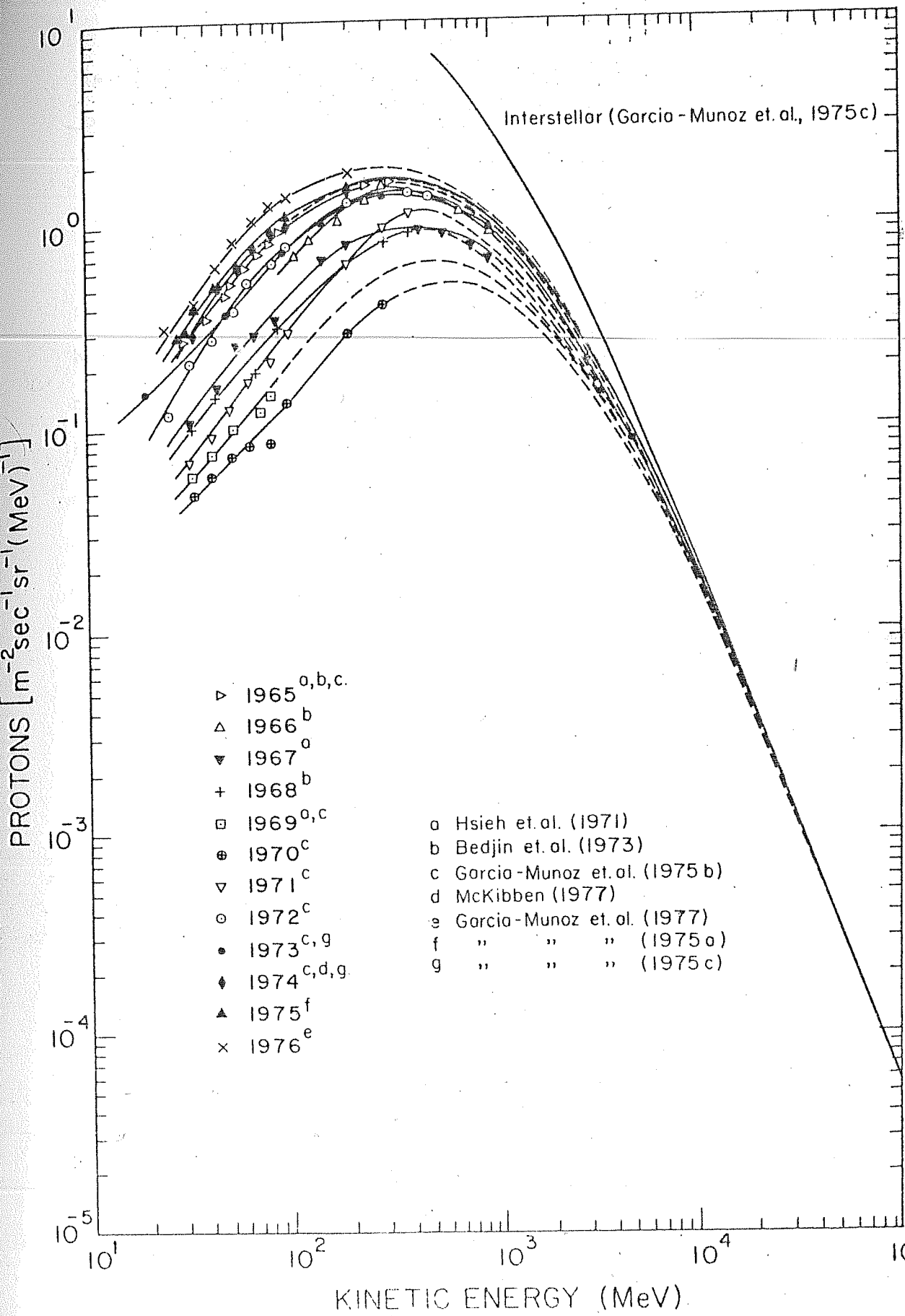

Fig.IV.2 Quiet time GCR spectra at 1 A.U. during Solar Cycle 20 and 1973 local interstellar GCR spectrum.

period of solar cycle 20 are used. The measurements at $\gtrsim$ 1 GeV are limited but there are good measurements available in $\sim$ 100 MeV to $\sim$ 1000 MeV region during solar quiet times for all the years covering solar cycle 20. These quiet time fluxes are taken to be the representative of the annual average GCR fluxes at 1 A.U. In view of the hysteresis effect observed at low energies, particularly during solar sunspot minimum (Van Hollebeke et al.1972, Burger and Swanenberg, 1973), only the high energy measurements are used for extrapolation to determine the GCR spectra at >1 GeV energies. This extrapolation is guided by the available high energy measurements, models of GCR modulation, the local GCR interstellar spectrum and the interplanetary spectrum of 1973 (Garcia-Munoz et al.1975). The available measurements of GCR spectra based on literature cited above are shown in Fig.IV.2. The spectrum beyond 20 GeV for all the years is assumed to have the spectral form given by (Wolfendale 1975):

$$\frac{dJ(E)}{dE} = K\, E^{-2.65} \qquad \ldots\ldots (IV.5)$$

The calculated integral proton flux above 1 GeV are given in Table-IV.2. The errors in the measured fluxes are of the order of 5 to 10% at 1 GeV, and since the integral proton flux depends mainly on GCR flux at 1 GeV the errors in the flux estimates are of the same order. The annual average GCR flux varied between 1.32 protons/ (cm^2.sec.4π sr. >1 GeV) in 1970 to 2.36 protons during 1976, with average of 1.9$\pm$0.1 protons/(cm^2.sec.4π sr. >1 GeV).

TABLE-IV.2

Computed GCR proton fluxes, $J_G(>1\ GeV)$ at 1 A.U. during Solar Cycle 20

Year	Annual mean 4π integral proton flux $J_G(>1\ GeV)$ (protons/cm^2.sec.)
1965 [a,b,c]	2.23
1966 [b]	1.97
1967 [a]	1.57
1968 [b]	1.62
1969 [a,c]	1.48
1970 [c]	1.32
1971 [c]	1.66
1972 [c]	2.04
1973 [c,d]	1.95
1974 [c,e]	2.06
1975 [f]	2.23
1976 [e]	2.36

Solar cycle 20 average proton flux $J_G(>1\ GeV) = 1.9 \pm 0.1$ Protons/(cm^2.sec.4 π sr)

a) Hsieh et al. (1971)
b) Bedijn et al. (1973)
c) Garcia-Munoz et al. (1975b)
d) McKibben (1977)
e) Garcia-Munoz et al. (1977)
f) Garcia-Munoz et al. (1975a)

TABLE-IV.2

Computed GCR proton fluxes, $J_G(>1\ GeV)$ at 1 A.U. during Solar Cycle 20

Year	Annual mean 4π integral proton flux $J_G(>1\ GeV)$ (protons/cm^2.sec.)
1965 [a,b,c]	2.23
1966 [b]	1.97
1967 [a]	1.57
1968 [b]	1.62
1969 [a,c]	1.48
1970 [c]	1.32
1971 [c]	1.66
1972 [c]	2.04
1973 [c,d]	1.95
1974 [c,e]	2.06
1975 [f]	2.23
1976 [e]	2.36

Solar cycle 20 average proton flux $J_G(>1\ GeV) = 1.9 \pm 0.1$ Protons/(cm^2.sec.4 π sr)

a) Hsieh et al. (1971)
b) Bedijn et al. (1973)
c) Garcia-Munoz et al. (1975b)
d) McKibben (1977)
e) Garcia-Munoz et al. (1977)
f) Garcia-Munoz et al. (1975a)

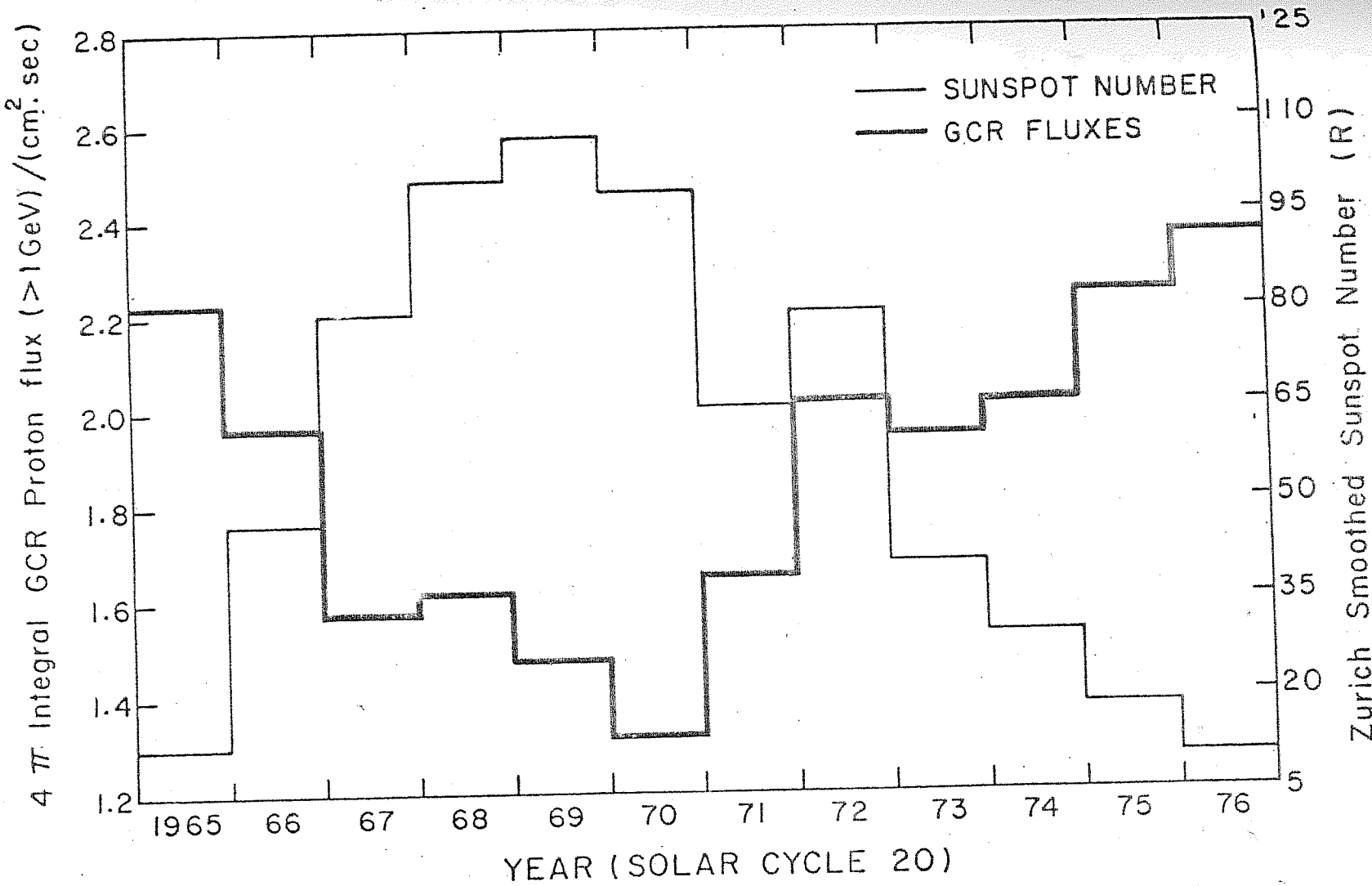

Fig.IV.3 Comparison of GCR fluxes and annual averaged Zürich smoothed sunspot numbers during Solar Cycle 20.

This value is higher than the long-term flux of 1.7 protons adopted by Reedy and Arnold (1972) and in this thesis. The flux of 1.7 protons is based on measurements during solar cycle 19 (Webber 1966). Since solar cycle 19 was the most active period of sunspot activity observed so far (i.e. since 1750), the above flux of 1.7 protons may not be representative of long-term (millions of years) average. In Fig.IV.3 the annual average GCR fluxes and the annual mean Zurich smoothed numbers (NOAA, Solar Geophysical Data No.397, 1977), R_Z for the entire solar cycle 20 are plotted. The GCR fluxes are seen to anticorrelate with the sunspot numbers with a phase lag of $\sim$ 1 year, as expected. The phase lag of one year is required for the sunspots to effect the change in the interplanetary magnetic field.

Based on the annual mean GCR fluxes given in Table-IV.2 the expected ^{22}Na activity at any time, t, during the solar cycle 20 is calculated by

$$A_{22}(t) = \sum_i P_{i,22} \{ 1-e^{-\lambda_{22} \Delta T} \} \times e^{-\lambda_{22}(t-t_i)} \quad \ldots(IV.6)$$

where $A_{22}(t)$ = ^{22}Na activity in a metorite fallen at epoch, t, during the solar cycle 20,

$P_{i,22}$ = Production rate of ^{22}Na during year indexed by i,

T = Period over which $P_{i,22}$ is constant, taken as 1 yr in the present case,

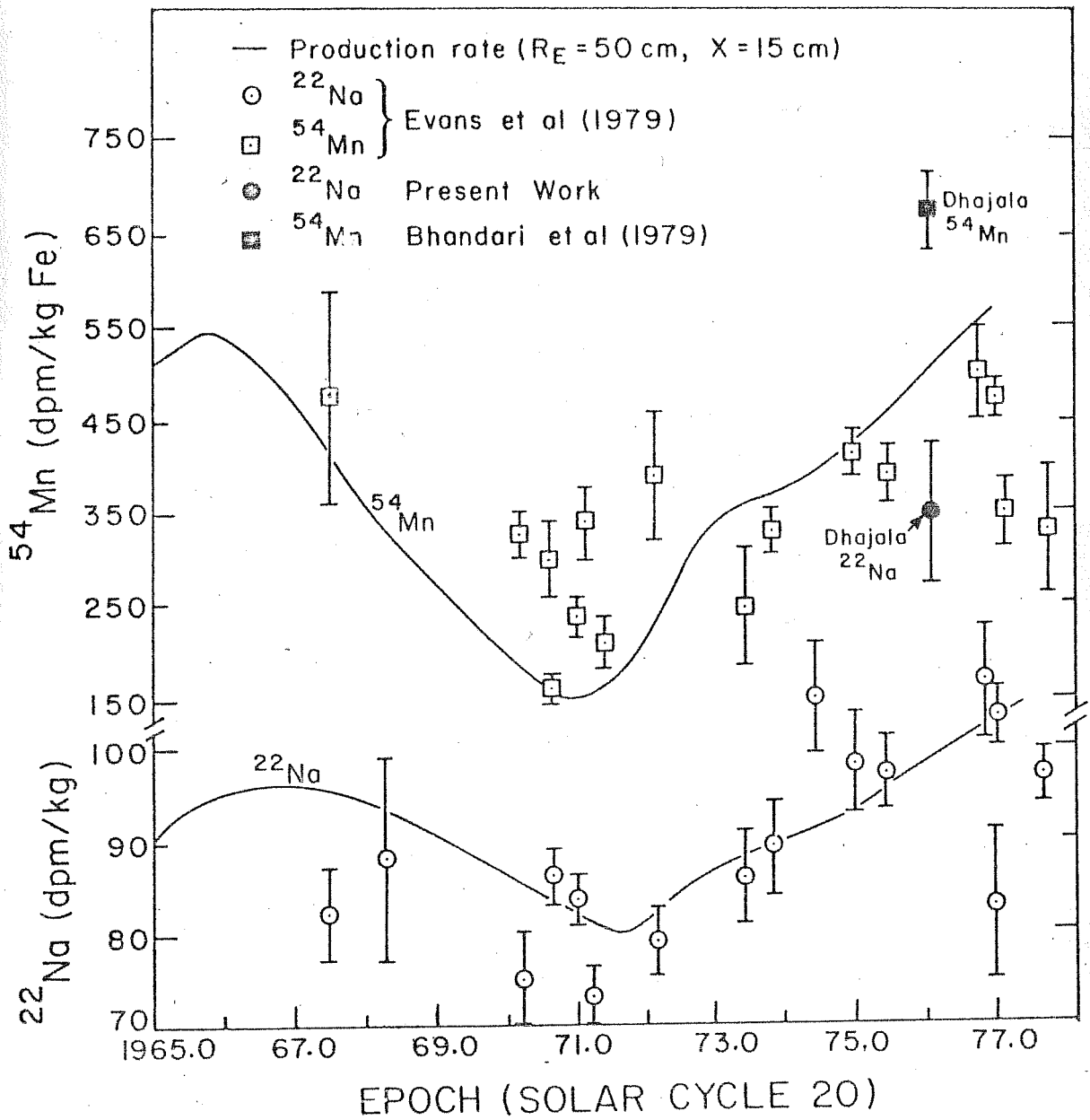

Fig.IV.4 GCR modulation of ^{22}Na and ^{54}Mn activities.

$t-t_i$ = time since the end of i^{th} year, and

$\lambda 22$ = decay constant of ^{22}Na, yr^{-1}

The results of the calculations are presented in Fig.IV.4 for production in a typical chondrite of 50 cm in radius and at typical depth of 15 cm. Similar calculations for ^{54}Mn are also shown in this figure. The ^{22}Na and ^{54}Mn measurements of Evans et al. (1979) in several chondrites which fell during 1968-1976 are plotted in Fig.IV.4 for comparison. Although the calculated curves agree with the general trend in the ^{22}Na and ^{54}Mn activities measured in meteorites. The departures from the expected activities are due to their different shielding depths, their different sizes and possibly due to different orbits of meteorites and chemical differences.

The ^{22}Na (present work) and ^{54}Mn (Bhandari et al.1978) activities at depth $\sim$ 15 cm in Dhajala ($R_E \sim$ 50 cm) plotted in the Fig.IV.4 show that the observed activities are higher than the calculated by 15% and 28%, respectively, over and above the +12 and +28% effect of solar cycle 20 modulation. This excess of 15% in ^{22}Na and 28% in ^{54}Mn activities have been attributed to the higher GCR fluxes (26% over the entire solar cycle 20) and 40% (over 3 to 4 yrs before 1976) at heliolatitudes $> 15^{\circ}$ by Bhandari et al. (1978), based on the calculated heliocentric orbit of Dhajala chondrite (Ballabh et al.1978). The ^{22}Na depth profile obtained in the present work supports the above conclusions of Bhandari et al. (1978).

(3) The ^{60}Co profile in Dhajala and Neutrons in Meteorites:

The experimental depth profile of ^{60}Co in Dhajala chondrite is shown in Fig.III.2.

The 5.26 - yr half-life ^{60}Co is produced in both the radiative thermal neutron capture by ^{59}Co reaction and the GCR induced spallation reaction on ^{60}Ni. As the GCR primaries traverse the matter they produce secondary evaporation neutrons of a few MeV energy. These fast neutrons are subsequently slowed down to epithermal (1 MeV-0.5 eV) to thermal (0.5-0.025 eV) energies in inelastic scattering with the nuclei of the medium, before they are captured or escape. If ξ is the logarithmic energy decrement and Σ_{tot} is the total macroscopic absorption cross section, then the slowing down length l of neturons in the medium under consideration is given by

$$l = \frac{1}{\overline{\xi\Sigma}_{tot}} \qquad \ldots\ldots\ldots(IV.7)$$

where $\overline{\xi\Sigma}_{tot}$ is known as the moderating power of the medium. The moderating power is given by

$$\overline{\xi\Sigma}_{tot} = \sum_{t} N_t \cdot \sigma_{a,t} \cdot \xi_t \qquad \ldots\ldots\ldots(IV.8)$$

where N_t is number concentration of scattering nuclei and $\sigma_{a,t}$ is the inelastic scattering cross section from scattering element, t.

If $q(E)$ is the slowing down density of neutrons and $\phi(E)$ is the flux of neturons, then we have

$$q(E) = \Phi(E) \cdot \overline{\xi\Sigma}_{tot} \cdot E \qquad .....(IV.9)$$

Eberhardt et al. (1963) calculated depth profile of several neutron capture nuclides viz. ^{36}Cl, ^{59}Ni and ^{60}Co, in spherical chondrites of various preatmospheric sizes. They used the cosmogenic ^{4}He depth profile measurements available in Iron meteorites to deduce the source function of fast neutrons. By adopting proper slowing down lengths for chondritic composition they evaluated the slowing down density and calculated the production profiles of the neutron capture nuclides. These production profiles have been used in literature to deduce the shielding depths of meteorite samples and preatmospheric sizes of meteorites. In Fig.IV.5, the theoretical production depth profiles of Eberhardt et al. (1963) for different size bodies and the experimental depth profiles in 50 cm radius Dhajala (H3) chondrite, about 100 cm radius Kirin (H5) chondrite and in about 100 cm size Allende (C3) carbonaceous chondrite are shown. It is seen that the Eberhardt et al. curves are in disagreement with the experimental profiles. The deduced ^{60}Co production rate of $\sim$ 100 dpm/kg at the centre of a 50 cm body is a factor of two smaller compared the Eberhardt et al production rates. In 50 cm body the

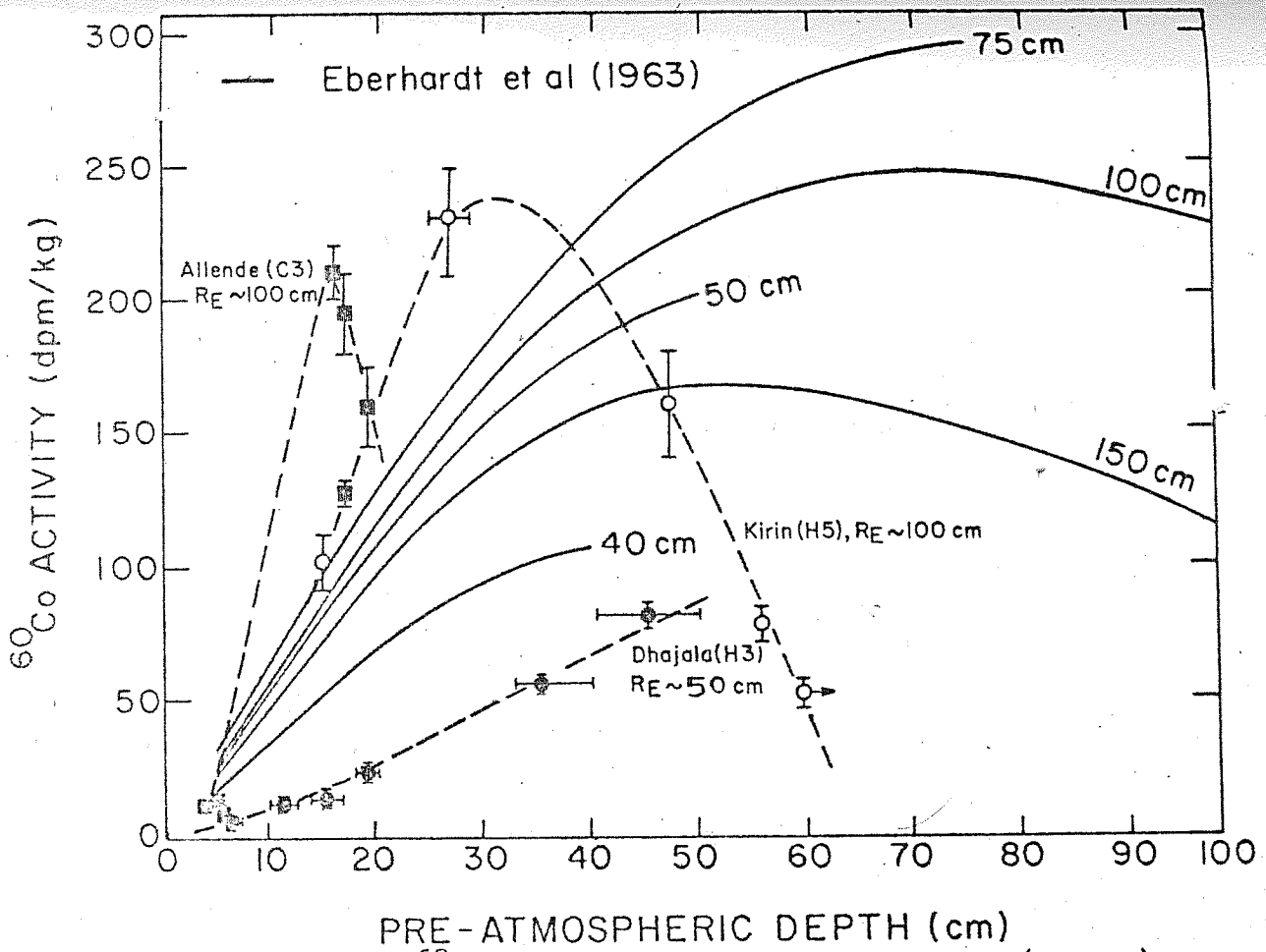

Fig.IV.5 Comparison of experimental ^{60}Co depth profiles in Dhajala (50 cm), Kirin (100 cm) chondrites and Allende (100) carbonaceous chondrite with the calculated profiles of Eberhardt et al. (1963). Track data in Allende are due to Bhandari, Goswami and Lal (private communication) and ^{60}Co data are from Cressy (1972), Hampel (1971), Rancetelli et al. (1969), Fireman (personal communication) and, Bhattacharya and Bhandari (1976). Track data in Kirin are due to Bourot-Denise and Pellas (1981) and for ^{60}Co data see Table-IV.3.

the production profile initially increases slowly with depth upto ∿ 20 cm and then increases rapidly with depth. In larger size bodies, the measurements indicate that the production increases with depth upto ∿ 30 cm where the ^{60}Co production goes through a broad maximum and then the production gradually decreases with depth. The observed maximum activity is ∿240 dpm/kg. In carbonaceous chondrite, Allende, the production peaks at shallower depth of ∿ 15 cm with maximum production of ∿ 210 dpm/kg. The slowing down length of evaporation neutrons in ordinary chondrites is ∿ 28 cm and in carbonaceous chondrites, it is calculated to be ∿ 16 cm. The recent improved calculations of neutron capture nuclide depth profiles of Spergel et al. (1981) have also yielded the production rates in disagreement with the measured depth profiles given here and the shapes of their calculated profiles are similar to those of Eberhardt et al. (1963).

There are several meteorites whose preatmospheric sizes are known from cosmogenic particle tracks and rare gas studies (Bhandari et al.1980) and the measurement of ^{60}Co in them are available. The ^{60}Co activity in Bruderheim (R_E = 37 cm), St.Severin (R_E = 25 cm), Ucera (R_E = 24 cm), Pribram (R_E = 24 cm), Harleton (R_E = 18 cm), Barwell (17 cm), Lost City (16 cm), Hamlet (15 cm), and San Juan Capistrano (8 cm) are, respectively, 8.5±1.1 dpm/kg (Fireman, 1966), 11±1 dpm/kg (Marti et al.1969), 10±2

dpm/kg (Bhattacharya and Bhandari, 1976), < 9 dpm/kg (Fireman, 1966), 14±1 dpm/kg (Cressy, 1964), 6±1 dpm/kg (Cressy, 1970), 5±4 dpm/kg (Cressy, 1971a), 6.5±2.4 (Fireman, 1966) and <2.9 dpm/kg (Finkel et al.1978). It is observed that the ^{60}Co activities in these meteorites except for San Juan Capistrano, is above the spallation ^{60}Co production level (which is $\sim$ 2 to 3 dpm/kg, calculated using the cross-section data for $^{60}Ni(n,p)$ reaction from Brookhaven National Laboratory Report No.325 and the spectral shape parameters given in Fig.IV.1). In San Juan Capistrano chondrite (R_E = 8 cm) the entire ^{60}Co production is due to spallation reaction, & in chondrites with R_E > 10 cm, the thermal neutron capture contribution is quite significant. Fireman (1966) measured ^{60}Co in several iron meteorites, and in some carbonaceous and ordinary chondrites and found that the Eberhardt et al. (1963) calculated production rates are higher than the observed production rates at the centre of a 40 cm size chondrites.

The Eberhardt et al. (1963) model calculations contain many uncertain parameters. The model is based on the fast neutron source function derived from the ^{4}He depth profiles in Grant Iron meteorite whose preatmospheric size was determined based on rare gases, while the depth and size dependent production rates from Fe target are still not very well known. The overestimation of the production rates

of neutron capture nuclides by Eberhardt et al. (1963) may be due to either :

(i) underestimation of (n, ^{4}He) cross-section and hence overestimation of neutron production rates, or

(ii) underestimation of the leakage of neutrons from meteorites during the slowing down process, or

(iii) overestimation of resonance escape probability.

From above discussion it is clear that further studies are required to settle the disagreement between the calculated and experimental depth profiles of ^{60}Co. However, it can be observed that the loss of evaporation neutrons from meteorites during slowing down process can be quite significant. This observation is supported by the slow increase in ^{60}Co production with depth in the near surface regions in Dhajala chondrite (Fig.III.2).

From the above discussion the following observations can be made :

1. The observed production depth profile are lower than the production rates given by Eberhardt et al.(1963).

2. In general, the Eberhardt et al. (1963) curves predict much higher production rates than observed in various size chondrites.

3. The maximum production of ^{60}Co occurs at depth of 30 cm in large ($\sim$ 100 cm) chondrites and at depth of 15 cm in large ($\sim$ 100 cm) carbonaceous chondrites.

These depths correspond to the slowing down lengths of evaporation neutrons in the appropriate media, and

4. The maximum production rate of ^{60}Co and hence the flux of thermal neutrons is approximately the same in carbonaceous chondrites as that in ordinary chondrites of the same preatmospheric size, although it occurs at different depths.

Slowing down density of neutrons in Dhajala :

The neutron capture cross-section of ^{59}Co varies from $\sim$ 37 barns at 0.025 eV to $\sim$ 8 barns at 0.5 eV. The cross-section shows $\frac{1}{\sqrt{E}}$ dependence in this thermal energy region. The cross-section decreases gradually from 8 barns at 0.5 eV to 5 barns at 100 eV. There is a very sharp resonance at 132 eV energy with peak cross-section of 10^4 barns and the FWHM of 30 eV. Most of the ^{60}Co is produced due to this resonance peak. The 0.5 eV-300 eV resonance integral cross section for ^{59}Co is 77 ± 4 barns (Fireman 1966).

If Φ_n is the flux of epithermal neutrons, then the production of ^{60}Co, P_{60}, is given by

$$P_{60} = \Phi_n \sigma_n v N_T f \quad \ldots\ldots (IV.10)$$

where σ_n is the resonance integrated cross-section, cm^2,

v is the velocity of epithermal (130 eV) neutrons, (cm/sec),

N_T is the concentration of target nuclide i.e. ^{59}Co atom/kg,

P_{60} is the production of ^{60}Co per kg per sec.

and f is the density of the medium, kg/cm^3.

The Co content of 0.073% by wt. and its atomic weight of 58.93 and Avogardo's number (6.023×10^{23} atoms/mole), give

$$N_T = 7 \times 10^{21} \text{ atoms of } ^{59}Co/kg.$$

The velocity of epithermal neutrons of energy 132 eV is 3.0×10^4 cm/sec and $f = 3.5 \times 10^{-3}$ for chondrites. We obtain

$$\bar{\Phi}_n = 1.4 \times 10^{-1} \, P_{60} \text{ neutrons}/(cm^2 . sec . 4\pi \, sr.)$$

and the slowing down density of neutrons integrated over the energy interval of 0.5 eV-300 eV is given by

$$q_n = \bar{\Phi}_n \cdot \xi \overline{\Sigma}_{tot} = 5 \times 10^{-2} \, P_{60} \text{(for chondrite)}$$

$$= 10^{-1} \, P_{60} \text{ (for carbonaceous chondrites)} \quad \ldots\ldots (IV.11)$$

At the center of Dhajala chondrite, the expected ^{60}Co production is 100 dpm/kg (i.e. 100 nuclides of ^{60}Co per kg per minute) giving the slowing down density of 0.084 (neutrons/(cm^3.sec.). This value is a factor of two lower than the slowing down density of Eberhardt et al.(1963). The slowing density of neutrons at depth of 30 cm in a 100 cm ordinary chondrite and at 15 cm depth in 100 cm carbonaceous chondrites are approximately $\sim$ 0.25 neutrons/(cm^3.sec) and $\sim$ 0.50 neutrons/(cm^3.sec), respectively. The measured

^{60}Co production of 11 dpm/kg (Co concentration = 430 ppm) (or production rate of 19 dpm/kg for Co concentration of 730 ppm) in St.Severin chondrite (Marti et al.1969) requires the slowing down density calculated from above equation IV.11 of 0.016 neutrons/(cm^3. sec) which agrees very well with the density calculated by Marti et al. (1969).

(4) <u>^{10}Be depth profile and energy spectrum of nucleons above 100 MeV</u>.

The experimental ^{10}Be production profile in Dhajala chondrite is described in Chapter-III and shown in Fig.III.3. The calculated depth profile of this radionuclide based on spectral shape parameters (given in Table.IV.1) deduced from ^{26}Al depth profile and the excitation functions described below is lower by a factor of 2.2 compared to the observed values. Thus, the Reedy-Arnold model underestimates ^{10}Be production by a factor of 2.2 and the calculated shape reproduces very well the observed depth variation of ^{10}Be.

The 1.6-Myr half-life ^{10}Be is produced in high energy spallation reactions of GCR protons and their secondaries (protons and neutrons) on target elements ^{16}O, ^{24}Mg, ^{28}Si, ^{56}Fe, ^{58}Ni and ^{60}Ni in the decreasing order of their importance. The main contribution to the total production comes from ^{16}O. The sources of reaction cross-sections used in the present calculations are : For ^{16}O target, Reedy and Arnold (1972); for ^{24}Mg at E < 1 GeV, Raisback and Yiou(1974)

and E > 1 GeV, Silberberg and Tsao (1973); for ^{28}Si target, Raisbeck and Yiou (1974) at E< 1 GeV and Silberberg and Tsao (1973) at E > 1 GeV. For ^{56}Fe at E ∿20 GeV and at 600 mev, Perron (1975) and for Ni, Raisbeck et al. (1975) at E ∿3 GeV. The excitation function for ^{10}Be production from ^{58}Ni + ^{60}Ni and ^{56}Fe are assumed to be identical. The relative contribution from the various target nuclides are as follows :

Target Nuclide	Calculated contribution(%)
^{16}O	82.2
^{24}Mg	8.5
^{28}Si	4.7
$^{56}Fe + ^{58}Ni + ^{60}Ni$	4.6

From the measured depth profile of ^{10}Be in lunar rocks and soil cores, Finkel (1972) and Kohl (1975) showed that the Reedy-Arnold production calculations are underestimated by a factor of about 3. This has been attributed to the uncertainty in the excitation functions (Reedy and Arnold 1972, Finkel 1971, Kohl 1975) of ^{10}Be production from ^{16}O. The fact that the ^{10}Be is produced by high energy ($\gtrsim$ 100 MeV) particles and its productions is underestimated, indicates that the Reedy-Arnold calculations have limitations in the calculations of the high energy products. The flux of 100-1000 MeV particles required is

about 2.5 times higher than the flux calculated in Reedy-Arnold model. The model assumes the spectral shape of particles above 100 MeV given by the equation IV.1 which is a decreasing function of E. This may not represent the true spectra of the nucleons in the free space and inside the meteorite bodies. The flux and spectrum of the particles may be different in this energy region (100 MeV-1 GeV).

(5) Summary:

The experimental production depth profiles of various radionuclides in a 50 cm body are determined. Based on ^{26}Al depth profile the deduced spectral shape parameters reproduces very well the depth variation of other radionuclides. The ^{22}Na production shows excess activity over that calculated and part of the excess is interpreted to be due to the modulation of the GCR fluxes in the interplanetary medium during solar cycle 20. For this purpose the annual GCR spectra have been constructed from the available measurements of GCR fluxes by satellites at $\sim$ 1 A.U. and the annual mean GCR fluxes are calculated. The effect of this solar modulations are estimated on various short lived nuclides. The solar cycle 20 average GCR flux of 1.9 ± 0.1 protons/(cm^2.sec.4 πsr) is obtained. The ^{60}Co depth profile in Dhajala ($R_E \sim$ 50 cm) is in disagreement with the production depth profile calculations of Eberhardt et al. (1963) and the possible cause of the discrepancy may be the loss of the neutrons from meteorites before they are moderated.

The thermal neutron fluxes peak at $\sim$30 cm depth in 100 cm radius chondrite and at $\sim$15 cm depth in 100 cm carbonaceous chondrite. The slowing down density of 0.5-300 eV epithermal neutrons in Dhajala vary from 0.005 neutrons/(cm^3.sec.) at depth of $\sim$ 6 cm to 0.084 neutrons at the center. The maximum slowing down density in $\sim$ 100 cm chondrite is 0.25 neutrons/(cm^3.sec.), and in $\sim$ 100 cm radius carbonaceous chondrite is 0.50 neutrons/(cm^3.sec.).

The ^{10}Be profile in 50 cm body agrees with the calculated profile if it is raised by a factor of 2.2. This may be due to underestimation of 100-1000 MeV nucleonic flux in Reedy-Arnold model calculations.

(B) The ^{26}Al Production rate in small ($\leq$15 cm) Chondrites:

From the experimental depth profile of ^{53}Mn, Bhattacharya et al. (1980) deduced the depth profile of spectral shape parameter in Madhipura (R_E = 6.5 cm). Udaipur (9), Bansur(15) and St.Severin (25) chondrites. These spectral shape parameters are shown in Fig.IV.1. Based on these α depth profiles and appropriate ^{26}Al production excitation functions, they calculated the ^{26}Al production profiles in the chondrites mentioned above and compared with measurements in several chondrites. Here, the ^{26}Al has been measured in Madhipura, Bansur and Udaipur meteorites. The comparison of the measured and calculated activities is given below:

Meteorite	Expected ^{26}Al(dpm/kg)	Measured ^{26}Al(dpm/kg)	$\frac{[^{26}Al]\text{measured}}{[^{26}Al]\text{expected}}$
Madhipura	44$\pm$2	36$\pm$3	0.82$\pm$0.08
Udaipur	44$\pm$2	38$\pm$6	0.86$\pm$0.14
Bansur	56$\pm$2	48$\pm$4	0.86$\pm$0.08

From the above table it is seen that the ^{26}Al production is $\sim$ 15% less than the calculated production rates. From the measured ^{26}Al depth profile in lunar core, Kohl (1975) showed that the Reedy-Arnold (1972) model calculations over predict the ^{26}Al production by $\sim$ 15%, which may be attributed to the uncertainties in the ^{26}Al production excitation functions. It can be concluded that, in general, the Reedy-Arnold production rate of ^{26}Al is overestimated by $\sim$ 15% for all size bodies by using the presently available excitation functions.

From the fact that the same set of α profiles based on 3.7 Myr-^{53}Mn reproduce the depth profile of 0.72 Myr-^{26}Al, it can be said that the GCR intensity averaged over last 15 Myr is same as the flux averaged over last 3 Myr, even though the presently accepted average flux of 1.7 protons may not represent the absolute average flux.

(C) Cosmogenic Radionuclides and rare gases in Kirin Chondrite :

Kirin is one of the largest chondrites with recovered mass of 4 tons. Several laboratories have studied Kirin samples for cosmogenic radionuclides, rare gases and particle tracks. However, the sample locations in the meteorite is not well documented making it difficult to relate the measured concentrations with depth. The concentration of some radionuclides and rare gases, viz. ^{21}Ne, ^{60}Co, ^{53}Mn, ^{3}He, measured in different samples show large variation. As they do not seem to follow the expected pattern, Honda et al. (1980) have considered the possibility of multiple exposure of this meteorite to explain these observation of cosmogenic nuclides. In their analysis they assumed that the depth variation of the production rates of ^{21}Ne, ^{22}Na, ^{26}Al, ^{53}Mn and ^{54}Mn are similar.

We have measured ^{26}Al, ^{60}Co and ^{10}Be in one 25 g Kirin sample. Its exact location on parent fragments is not available. In table IV.3 the available data on various radionuclides, rare gases and tracks in other samples are compiled, and tabulated in the decreasing order of ^{60}Co activity.

(i) Preatmospheric size of the Kirin chondrite:

The total recovered mass of this chondrite is 4000 kg, the largest fragment weighing ∿ 1700 kg. Because of the thick population in Kirin district and the bright fireball seen over a wide area, the recovery of the fragments is nearly complete. Although the preatmospheric velocity and angle of entry are not known, the estimate of limits and most probable value of preatmospheric size can be deduced from Fig.VI.3 (Chapter-VI), where preatmospheric mass as a function of surviving mass for various entry velocities is plotted. The minimum preatmospheric velocity of 11.0 km/sec gives the lower limit on the preatmospheric mass of 5000 kg, corresponding to the preatmospheric size of 75 cm. If we assume that the meteoriod had the most probable entry velocity of 16 km/sec (Chapter-VI), the preatmospheric mass would be 1.33×10^4 kg and the corresponding size would be 100 cm. For still higher velocity of ∿ 23 km/sec. the meteorite would have ∿ 99% of ablation putting upper limit on size of ∿ 200 cm. In the following discussion we adopt the most probable radius of 100 cm, although it is not critical for the arguments presented below.

(ii) Depth variation of cosmogenic nuclides :

The data on cosmogenic nuclides measured in different Kirin samples in various laboratories (Table IV.3) allow us to make the following observations:

TABLE-IV.3

Cosmogenic Radionuclides and Rare gases in Kirin Samples

Nuclide	Units	LABORATORY* (1)	(2)	(3)	(4)	(5)	(6)	(7)	(8)	(9)	(10)
^{10}Be	dpm/kg					12.8±1					
^{22}Na	"	107±8	70±9		145±5		122±14		104±14	97±9	
^{26}Al	"	24±1	19±7		25±1	27±2	20±9		23±8	26±4	
^{60}Co	"	55±2	53±7		77±3	103±5	160±20		230±20	237±11	
^{54}Mn	"		131±23		136±8		240±20		156±52	210±40	
^{53}Mn	dpm/kg(Fe+$\frac{1}{3}$Ni)	84±4		72±9		191±(10)**	108±5				168±11
^{3}He	10^{-8}cc STP/g	0.660	0.780	0.690	0.820		1.03	1.83	1.77		2.03
^{21}Ne	"	0.358	0.424	0.427	0.510		0.660	0.890	1.00		0.99
$\left[\frac{^{22}Ne}{^{21}Ne}\right]_{sp}$		1.073	1.085	1.07	1.07		1.085	1.081	1.07		
$\left[\frac{^{22}Na}{^{26}Al}\right]$	-	4.46 ±0.38	3.68 ±1.44		4.56 ±0.27		6.10 ±2.24	4.52 ±1.68	3.73 ±0.67		

*Laboratory (1) La Jolla, USA; Nishiizumi et al. 1980, (2) Heidelberg, Heusser et al 1979, (3) Battelle Memorial Lab., Private Communication (1979) from Evans & Rancetelli, (4) Smithsonian Institution, Bogard et al.1980, (5) Ahmedabad PRL, Present work, (6) Tokyo, Honda et al.1980, (7) Private communication from Crabb and Anders 1980, (8) Heidelberg, Heusser et al.1979, (9) Kanazawa University, Japan from Honda et al.1980 (10) Mainz, Begemann et al.1979.

** Assumed $\sim$ 5.0% error in ^{53}Mn activity.

(1) The particle track density (Bourot-Denise and Pellas, 1981) correlate directly with ^{60}Co activity. Since the track density decreases with increasing shielding depth, it is clear that the ^{60}Co decreases with shielding depth. In a large ($\sim$ 100 cm) size body, the ^{60}Co production is expected to increase initially (from nearly zero at the surface) with shielding depth upto 30-40 cm and then decrease with depth (Lingenfelter let al. 1972, Woolum et al. 1975). From this observation it is clear that the Kirin samples analysed so far except our sample as will be discussed later, are from large ($\gtrsim$ 20 cm) shielding depths, and certainly not from the region where ^{60}Co increases with depth.

(2) The concentration of ^{21}Ne is directly correlated with ^{60}Co and decreases with the shielding depth. Since most of ^{21}Ne is produced from ^{24}Mg in (n, ^{4}He) reaction (E_T=2.8 MeV) and ^{60}Co is produced in $^{59}Co(n, \gamma)$ reaction in 132 eV reasonance peak (Table I.1), the production of ^{60}Co and ^{21}Ne can be expected to be correlated in presence of higher fast and thermal neutron fluxes at large shielding depths as expected in a big body. This is further supported by the observation that ^{21}Ne varies by a factor of 3(=1.0/0.34) similar to that for ^{60}Co which varies by factor of 4.3(=230/53).

The measured $(^{22}Ne/^{21}Ne)_{sp}$ values in Kirin range between 1.06 and 1.085. Since these measured ratios are accurate to $\sim$ 1%(1 σ error), we can say that the $(^{22}Ne/^{21}Ne)_{sp}$ ratio is nearly constant with depth. The average value of neon ratio is 1.07. Such a value of Ne-ratio indicates exposure at 20-60 cm of shielding depths in large body and rules out the possibility of much deeper exposure (for significant fraction of its total exposure period) on a parent body (Chapter-V).

(3) The activity of radionuclides and the concentration of rare gases (listed in table IV.3) decrease with shielding depth, except for ^{22}Na, ^{26}Al and ^{54}Mn which remain relatively constant. The production depth profiles of cosmogenic nuclides in a 100 cm body are not known independently and unfortunately there is no ordinary chondrite of this size with which we can compare the productions observed in Kirin samples. Although Allende meteoroite had almost similar preatmospheric size as that of Kirin, because of its carbonaceous nature the production of fast neutrons and moderating power are high due to higher carbon and water content than those of ordinary chondrites and it is not suited for comparison. In the absence of a better case for comparison, we compare the productions in Kirin meteorite with those in Dhajala (H) chondrite which has the preatmospheric radius of 50 cm and the highest ^{60}Co activity measured is 83

dpm/kg and the depth profiles of various radionuclides (^{22}Na, ^{10}Be, ^{26}Al, ^{60}Co) are measured (Present chapter). This comparison leads to the following observations.

The ^{22}Na and ^{54}Mn production levels in Kirin are similar to those in Dhajala chondrite but the ^{26}Al activity is much lower than that is Dhajala. From the measured depth profiles of ^{26}Al and ^{22}Na in Dhajala, it is found that the production profiles of these low energy ($E_T \sim$ a few MeV) products flatten beyond 20 cm of depth. The Kirin data suggests that a similar behaviour is expected in a 100 cm size body at 20 cm shielding depths. Both these meteorites fell during solar minimum in 1976 separated in time by about one month. So, the solar modulation effect in Dhajala and Kirin should be about the same. The solar minimum effects on ^{22}Na and ^{54}Mn are calculated to be 12% and 28% respectively (Potdar and Bhandari 1979) and the residual excess of 15% and 28% in Dhajala ^{22}Na and ^{54}Mn activities have been attributed to productions due to about 26% and 40% higher GCR fluxes (above agerage GCR flux in ecliptic plane) at heliolatitudes $>15°$ during 1975-76 and the preceeding 10 years, respectively (Bhandari et al. 1979). Since the heliocentric orbit of Kirin is not known, the effects of these higher fluxes cannot be calculated. The solar minimum effect on Kirin may be quite high. The $(^{22}Na/^{26}Al)$ ratio is roughly constant with depth. The average value is 4.1 and the range

being 3.7 to 6.1 (with large error bars). The ($^{22}Na/^{26}Al$) value in Dhajala at large shielding depths is 2.4, much lower than that in Kirin.

(4) The ^{53}Mn activity varies by a factor of 1.6. The ^{53}Mn activity in our sample has the highest value of 191 dpm/kg (Fe + $\frac{1}{3}$ Ni) (Honda, personal communication), while ^{60}Co activity is 103 ± 5 dpm/kg. The shielding depth of our sample is not known in the absence of track density measurements. However, from ^{53}Mn and ^{60}Co data, a reasonable estimate of shielding depth can be made. In a large body, ^{53}Mn production is expected to peak around 15 cm of shielding depth and since the ^{53}Mn production is highest in our sample, the shielding depth of 15 cm is estimated for our sample.

(5) The measured ($^{26}Al/^{53}Mn$) ratio in various amples range between 0.20 to 0.28 and the average ratio is 0.24. The $(^{26}Al/^{53}Mn)_{sat}$ ratio in Dhajala at large shielding depths is similar and equal to 0.20. If we assume that relative production rates of ^{53}Mn and ^{26}Al are the same as those in Dhajala chondrite, an upper limit on exposure age of 6.3 Myr will be obtained, which is equal to the exposure age of Dhajala Meteorite.

(6) The ^{10}Be data in our sample having shielding depth $\sim$ 15 cm, as discussed above, is crucial since it is produced by high energy nucleons ($E_T \gtrsim 60$ MeV). The ($^{10}Be/^{26}Al$) activity ratio in Kirin is 0.47 ± 0.06 and the measured activity ratio

TABLE-IV.4

Calculation of shielding depths of Kirin Samples

(Exposure age = 6.3 Myr)

Sample	$(^{21}Ne)_m$	Track density $t cm^{-2}$	Cosmogenic component in track density ($t\ cm^{-2}$)	Track production rate TPM ($t\ cm^{-2}\ Myr^{-1}$)	Shielding depth cm (R_E = 100 cm)
(a)	(b)	(a)			
Mainz-A	0.43	37 ± 16	0 (see Text)	0	> 50
Mainz-F	0.72	131 ± 41	94 ± 44	43 ± 20	37^{+7}_{-2}
Mainz-B	0.99	156 ± 39	119 ± 42	53 ± 19	34^{+1}_{-2}
Heidel.1-2	0.88	243 ± 73	206 ± 75	92 ± 33	32 ± 2
VI-42-04	1.01	577 ± 182	540 ± 182	241 ± 81	27 ± 2

(a) Bourot-Denise and Pellas (1981)

(b) See Table IV-5

in low shielded Dhajala samples is 0.40 ± 0.06. If we assume the production ratio in Dhajala and Kirin to be the same, then the exposure age of Kirin would be about the same as that of Dhajala chondrite. We adopt Kirin exposure age to be about 6.3 Myr. Exposure ages varying from 2.2 Myr to 2.8 Myr have been obtained from ^{21}Ne contents, but since ^{21}Ne production rate is not reliable, such estimates are fallacious. Honda et al. (1980) give 0.5 and 10 Myr exposure ages based on their multiple exposure model.

(iii) Shielding Depths of Kirin Samples:

The lowest track density measured in Kirin olivines (Bourot-Denise and Pellas 1981) is 37 ± 16 tracks/cm^2. Assuming that the ^{244}Pu and ^{238}U fission contribution is comparable to this lowest observed track density, the cosmogenic contribution to the track density in other samples can be evaluated. Adopting an exposure age of 6.3 Myr the shielding depths of Kirin samples are deduced (Table IV.4) using theoretical track production profiles of Bhattacharya et al. (1973) and $\rho_{pyroxine}/\rho_{olivine} = 2.9$.(*). The depth profile of ^{21}Ne is plotted in Fig.IV.6. From ^{21}Ne and track data in various samples, the depth profiles of ^{60}Co, ^{53}Mn, ^{26}Al, ^{22}Na and ^{54}Mn are reconstructed and they are shown in Fig.IV.6. The ^{60}Co and ^{53}Mn depth profiles below 20 cm are extrapolated to include our sample whose deduced depth is $\sim$15 cm. It should be noted that the deduced depths are not very sensitive to the exposure age adopted here.

*Bagolia et al.(1980)

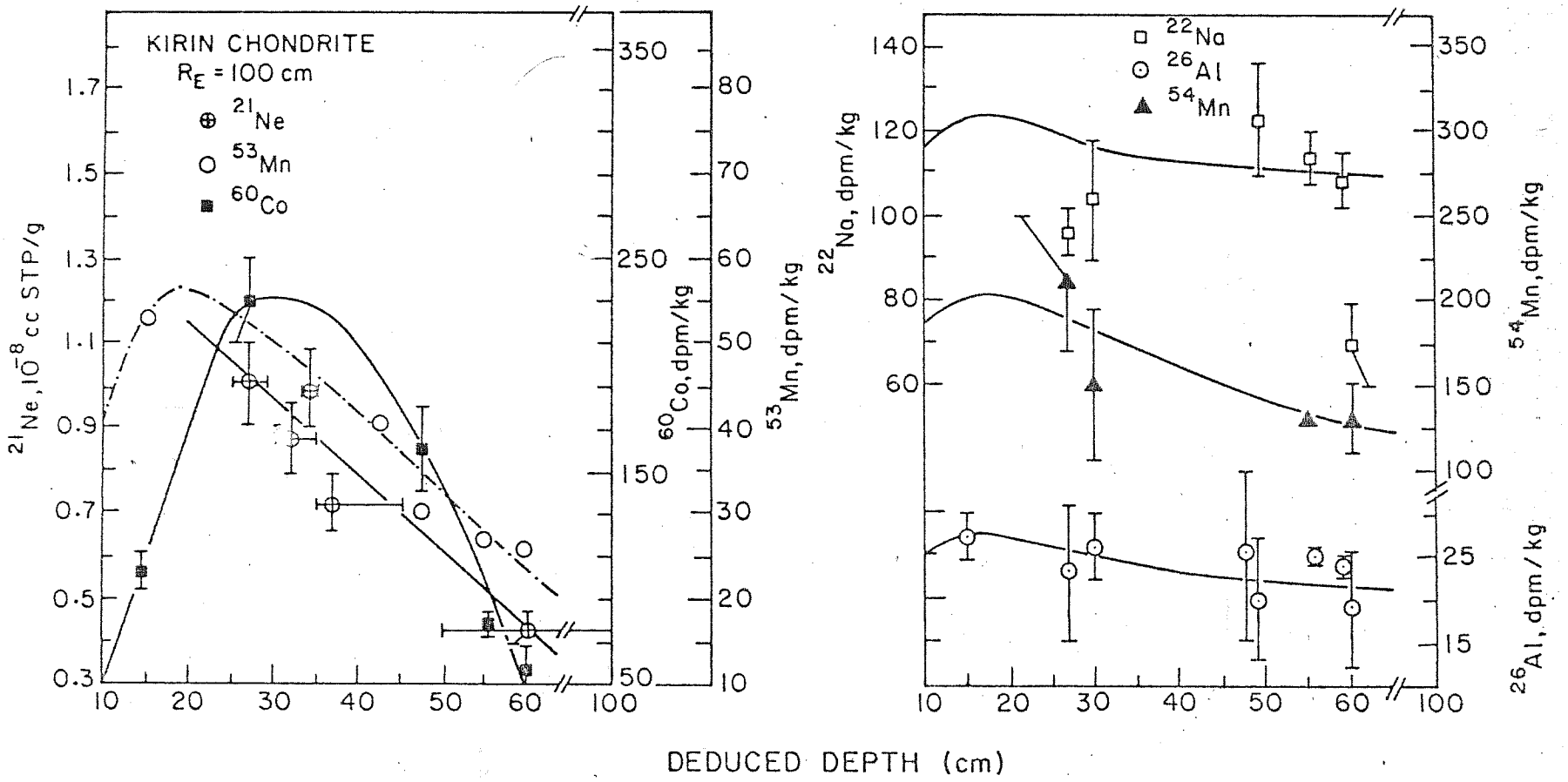

Fig.IV.6 Depth profile of various radionuclides and rare gases in Kirin chondrite ($R_E \sim 100$ cm).

(iv) Average production rates at large shielding depths:

Based on the depth profiles of various cosmogenic nuclides, their average production rates at large shielding depths in a 100 cm meteorite can be calculated. The average production rates of some nuclides are given below:

Nuclide	Production Rate
^{10}Be	14 dpm/kg
^{21}Ne	0.12×10^{-8} ccSTP/g/Myr
^{26}Al	24 dpm/kg
^{53}Mn	145 dpm/kg(Fe+$\frac{1}{3}$ Ni)

(v) Summary:

The available data indicate that the Kirin meteorite had preatmospheric size of approximately 100 cm and exposure age of about 6.3 Myr. Neutron effects on productions of various cosmogenic nuclides are quite clearly seen. The systematics of production of various nuclides have been determined.

(D) ^{26}Al depth profile in Lunar Rocks and Ancient Solar Flare Activity :

(A) Introduction:

The energy spectrum of SCR protons at 1 A.U. is best described by a power law in rigidity and is given by

$$Js(>R) = J_o \, Exp\,(-R/Ro) \qquad \ldots\ldots (IV.12)$$

where $Js(>R)$ is the integral SCR proton flux with rigidity > R MV,

Ro is the characteristic rigidity of the spectrum and J_o is the normalising constant.

$Js(>R)$ is expressed in units of protons/(cm^2.sec.4 Π sr) and Ro is mega-volts (MV). $Js(>137$ MV) i.e. Js(>10 MeV) and Ro are used to describe the SCR spectra.

Although the energy spectrum of SCR particles of an individual flare follows the form of equation IV.12 in rigidity, the flux and characteristic rigidity (Ro) vary from flare to flare (Freier and Webber 1963). Flares of high rigidity and high time integrated flux (fluence) are very infrequent and also no flares with fluence greater than $\sim 2\times10^{10}$ Protons/(cm^2.4 Π sr) have been observed so far (Reedy 1977) and there seems to be cut off at this value of fluence (Lingenfelter and Hudson 1980). The time averaged SCR flux is directly related to the sunspot activity and hence to solar mechanism of energy and magnetic field generation.

TABLE-IV.5

Estimated SCR spectral Parameters in past

Authors	Isotope	Half-life (yrs)	Samples studied	Exposure Age (Myr)	Erosion rate (mm/Myr)	Time averaged SCR parameters (Js, Ro)	Remarks
Finkel et al. (1971)	^{56}Co	77 days	12002	10(a)	0.5	(100,80)	^{81}Kr-^{83}Kr exposure age may not represent the suntan exposure age.
	^{54}Mn	303 "					
	^{22}Na	2.56					
	^{26}Al	0.72×10^{6}					
	^{53}Mn	3.70×10^{6}					
Bostrom et al. (1967-1973)	SPME(c)	-	-	(1967-1973)	-	(90,85)	Covers only the peak sunspot activity period of solar cycle-20.
D'Amico et al. (1971)	^{3}H	12.5	12002	10	-	(150, -)	
Niederer et al. (1975)	^{3}H	12.5	15058	-	-	(150,90) or (100,150)	No implanted ^{3}H found.
Boekl et al. (1972)	^{14}C	5730	12002	10	-	(200,100)	No implanted ^{14}C found. Possibly covered by lunar regolith (Reedy,1980).
Begeman et al. (1972)	^{14}C	5730	12053	-	-	(300,100)	Implanted ^{14}C found.
Marti & Lugmair (1973)	^{81}Kr	2.1×10^{5}	12002	10	-	(140,100)	Production cross-section not known exactly.
Bhandari et al. (1976)	^{26}Al	0.72×10^{6}	61016	1.5(b)	0.5	(140,150)	Based on total β^{+} counting.
Kohl et al. (1978)	^{26}Al	0.72×10^{6}	12002	10	0.5	(70,100)	Variable erosion rates used are untenable.
	^{53}Mn	3.70×10^{6}	14321	27(a)	2.2		
			68815	20(a)	1.3		
Venkatesan et al.(1980)	^{3}He	Stable	61016	1.5(b)	-	(70,100)	Possible loss of He during exposure period (Yaniv & Marti, 1981).
			64435	0.5(b)			

(a) ^{81}Kr-^{83}Kr age, (b) GCR tracks plateau age, (c) SPME: Solar proton monitor experiment.

(B) Estimated SCR fluxes in past :

There have been several attempts to measure experimentally the SCR fluxes both by direct and indirect methods. A brief summary of the results are given in Table-IV.5. The direct measurement on Solar Proton Monitor Experiment(SPME) of Bostrom et al. (1967-1973) on IMP satellites covered the period of solar cycle 20 peak sunspot activity. Among the indirect methods, there are several attempts to deduce the SCR fluxes by measuring the depth profiles of various radionuclides and rare gases in lunar rocks and soil columns. Radionuclides with half-lives varying from 77 days (^{56}Co) to 3.7×10^6 yrs (^{53}Mn) have been used to obtain the SCR spectral parameters averaged over either the exposure age of rocks or the three to five mean lives of the radionuclides.

From the table it is observed that the estimated SCR spectral parameters Js(>137 MV) and Ro averaged over different time spans show wide range of variation from (Js,Ro) = (70,100) to (300,100) through (140,150) and that, there is no systematic relation between the flux and the time span of averaging. While the millions of years time averaged parameters (70,100) of Finkel et al.(1971), Kohl et al.(1978) and Venkatesan et al. (1980) seems to be similar to the present day fluxes given by(90,85) based on SPME data (Bostrom et al.1967-1973), the flux derived from ^{3}H, ^{14}C, ^{81}Kr and ^{26}Al (D'Amico et al.1971, Boekl et al. 1972, Begemann et al. 1970, Marti and Lugmair 1975,

Bhandari et al. 1976) are higher by a factor of 2 to 3 with $R_o > 100$ MV.

The SCR spectral parameter deduced from depth profiles of various cosmogenic nuclides have inherent uncertainty due to uncertainties in (i) exposure age to SCR particles, known as "Suntan" exposure age or "insolation" age, (ii) production excitation functions, and (iii) erosion rates. The non-concordance of SCR fluxes derived so far may be attributed to the uncertainties in erosion rates, wrong exposure ages and erroneous production rates. From the table it is seen that only the rock 12002 has been studied extensively for various radionuclide depth profiles and the next well studied rocks being 14321, 68815 and 61016. The ^{14}C depth profile measurement of Boekl et al. (1972) in 12002 does not show the solar wind implanted ^{14}C in depth regions < 4 mm while in rock 12053, Begemann et al. (1972) could clearly see the implanted ^{14}C. However, the depth profiles in deeper regions of the both the rocks agreed with SCR parameters of (200,100). The subsequent measurement of surface correlated ^{14}C in lunar soils by Fireman et al. (1975) established the existence of solar wind implanted ^{14}C. The most probable explanation for absence of implanted ^{14}C in 12002 may be that the upper millimeter layer of this rock was lost during handling or the rock was covered by a few mm thick layer of lunar regolith during the last $\sim 10^4$ yrs at least (Reedy, 1980). If this is true,

TABLE-IV.6

Exposure ages of Boulders (Myr)

Rock	^{81}Kr-^{83}Kr Age	^{21}Ne Age	Track Age	Crater Age	Reference
15205	169 ± 7	-	0.07	0.1	1,2,3
61016,287	-	< 7	1.5	1.4	4,2
64435,95	-	0.6 ± 0.3	0.5	0.2-2	5,2
66095,146	-	1.1 ± 0.5	1.0	0.2	6,2
69935,14	1.99 ± 0.37	1.40 ± 0.33	0.5	-	7,2
69955	4.23 ± 0.41	2.13 ± 0.50	-	-	7

1. Drozd et al. (1976)
2. Bhandari et al. (1977)
3. Horz et al. (1975)
4. Stetler et al. (1973)
5. Bogard and and Gibson (1975)
6. Heymann and Hubner (1974)
7. Drozd et al. (1974)

then the SCR fluxes deduced based on depth profiles in this rock are the lower limits on the actual fluxes.

The ^{81}Kr-^{83}Kr ages of the rock 12002, 14321 and 68815 may not represent their suntan exposure ages, since a substantial fraction of the stable Krypton (^{83}Kr) is produced in their previous irradiations in different shielding conditions before the last excavation event in which these rocks were brought to the lunar surface, or because of chipping of surface fragments ($\lesssim$1 cm in size due to meteorite impacts) exposing underlying new surfaces. In Table IV.6, we have tabulated various exposure ages of some lunar rocks. The ^{81}Kr-^{83}Kr ages of the boulders are higher than ^{21}Ne ages, which in turn are higher than track ages. Generally track and crater ages are concordant. From the non-concordance of different exposure ages, it is observed that the boulders show multiple exposures within the top a few meters of lunar regolith. In case of the parent boulder of rock chips 69935 and 69955, at least four events at approximately 4, 2, 1.5 and 0.5 Myr period must have taken place, as indicated by various exposure ages given in Table-IV.6 (Bhandari et al.1981a). From the observed ^{60}Co production of 80 dpm/kg.Co at depth of $\sim$350 g.cm^{-2} which is comparable to the 100 dpm/kg.Co at $\sim$100 g.cm^{-2} measured by Wahlen et al. (1973) in lunar soil cores, the neutron profile is flat with depth and this can produce quite significant amount of Kr even at these large depths. The GCR track exposure ages deduced from GCR VH nuclei track

densities in 1-2 cm depth regions of rocks (Bhandari et al.1975) represent very well the Suntan exposure ages, because, due to the characteristic steep depth gradient of track production rate, the tracks accumulated during previous irradiations are negligible. Bhattacharya and Bhandari (1975) measured the track density profiles in 0-2 cm regions of several rocks and showed that rocks 61016, 64435 and 69955 had well defined plateau ages (GCR ages) whereas rocks 12002 and 14321 did not have good plateaus indicating that those rocks had multiple exposures at subdesimeter shielding depths. The energy spectrum of VH nuclei in energy region of 50 to 500 MeV/amu deduced by Bhandari et al. (1971) agrees fairly with those of Crozaz and Walker (1971) and Hutcheon et al. (1974). At lower energy ($<$50 MeV/amu), there are disagreements, because of erosion effects. The energy spectrum below 50 MeV/amu of Hutcheon et al. (1974) is based on track profiles in surveyor glass and in rock 72315 with a short exposure age. At lower energy, the spectrum of Hutcheon et al. and at higher energy the spectrum of Bhandari et al. and Crozaz and Walker should represent the VH nuclei spectrum in the interplanetary space at 1 A.U. The erosion rate deduced by Bhandari et al. (1975) of $\sim$0.5 mm/Myr based on SCR VH nuclei fluxes in 50-500 MeV region of Bhandari et al. (1971) and in $<$ 50 MeV of Hutcheon et al. (1974), and the observed track production depth profile in 61016,287 is in agreement

with 0.4-1 mm/Myr rates deduced for lunar rocks by Crozaz et al. (1970), Price et al. (1967) and Lal et al.(1969).

The micrometeorite erosion rate is a dominant process. Fireman and DeFelice (1961) tried to explain the low exposure ages of chondrites compared to Iron Meteorites by introducing effects of space erosion due to micrometeorite impacts which is dependent on the crushing strength of meteorites. Geiss and Oeshger (1960) put forward the argument that erosion due to micron size dust particles does not depend on crushing strengths which was subsequently supported by Heymann (1964) showing that in ion bombardment experiments both stone and iron meteorites showed same erosion rates. Price et al. (1967) deduced erosion rate of $\leq$ 1 mm/Myr based on track data in Patwar meteorite, which is consistent with that deduced by Lal et al. (1969). If the erosion rates of lunar rocks is assumed to be independent of crushing strength and similar to that of meteorites (< 1 mm/Myr), then the agreement of depth profiles of ^{26}Al and ^{53}Mn in 12002, 14321 and 68815 (Kohl et al.1978) by introducing variable erosion rates of 0.5, 2.2 and 1.1 mm/Myr, respectively seems to be an artifact.

(C) (i) <u>^{26}Al depth profile in 61016 and 69935 and long-term averaged SCR parameters</u> :

The radionuclide ^{26}Al is best suited for SCR studies because its half-life (0.72 Myr) is of the order of exposure ages (Suntan) of lunar rocks and hence the preirradiation

effects are negligible. The energy threshold for production is ($\sim$10 MeV), thus being sensitive to large fraction of SCR particles. Besides, it is produced abundantly in (p,pn) reaction of ^{27}Al which is quite abundant (5 - 18% by wt.) in lunar samples. The excitation functions of ^{26}Al production reactions from target elements Mg, Al and Si are very well known.

Bhandari et al. (1976) measured ^{26}Al depth profile with high depth resolution by non-destructive β^{+}-γ coincidence spectrometry in 61016 and several other rocks. Based on suntan exposure ages derived from GCR track densities in 1-2 cm depths from surface of rocks and the erosion rates derived from solar VH nuclei track density profiles in 0-1 cm regions they deduced 1.5 Myr averaged SCR parameters of (140 ± 20, 150 ± 20). In the present study we have carried out radiochemical measurement of ^{26}Al depth profile in rocks 61016 and in 69935 with better precision. Based on the combined radiochemical and non-destructive measurement of ^{26}Al we have attempted to derive the best fit SCR parameters. These SCR parameters are used to calculate the expected depth profiles in rock 69935, and in lunar soil cores 15010/11 and 60009/10 and compared with the present measurements in 69935 and those of Fruchter et al. (1981) and Fruchter et al. (1976).

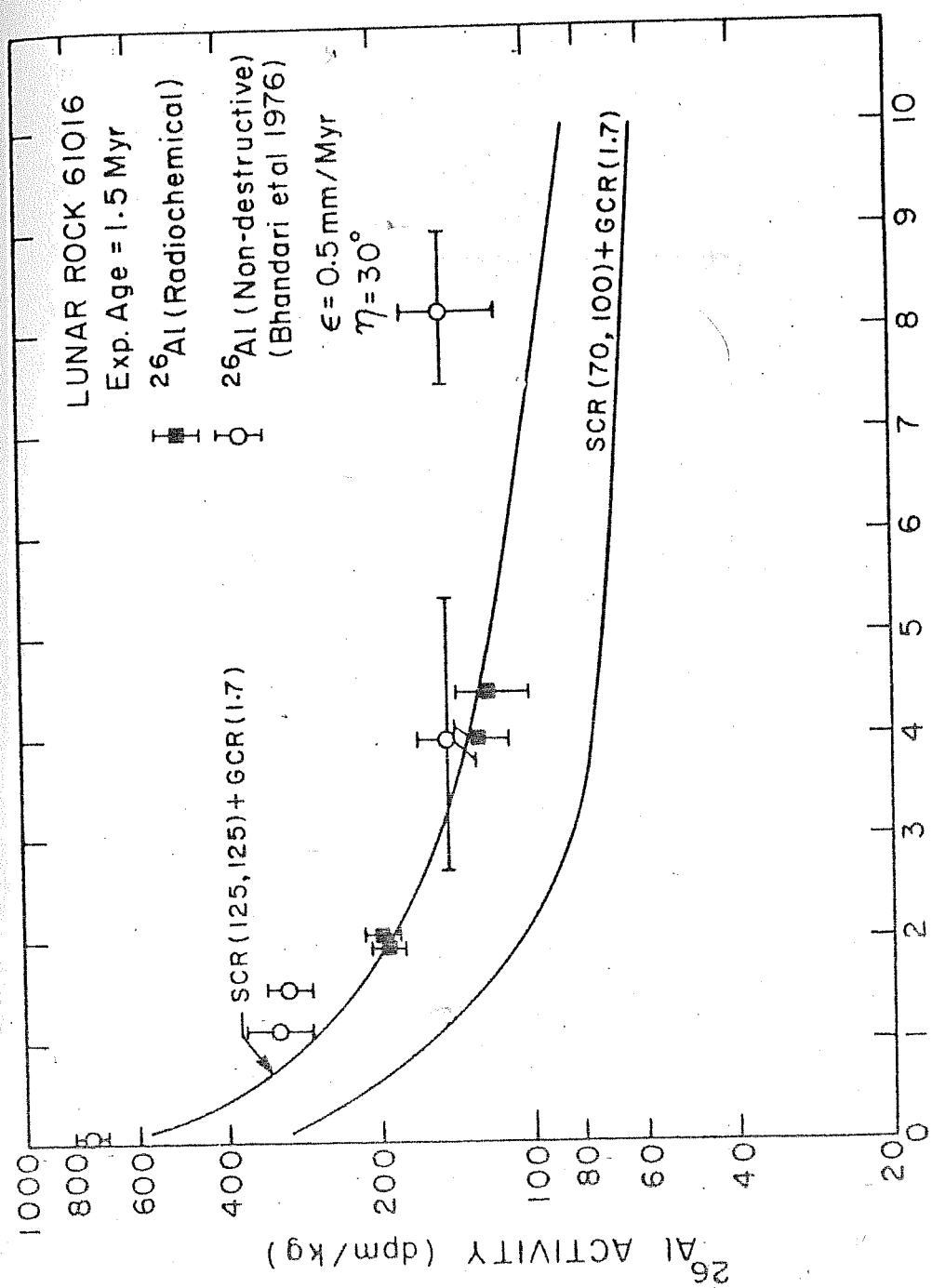

Fig. IV.7 Depth profile of ^{26}Al in 61016, 287 rock profiles based on SCR flux given by (Js, Ro) = (125, 125) and (70, 100) and GCR flux of 1.7 proton/(cm^2 · sec · 4π sr. > 1 GeV).

In Fig.IV.7, we have plotted both the radiochemically determined and non-destructive $\beta\pm\gamma$ measurement of ^{26}Al in 61016. The calculated total (SCR + GCR) ^{26}Al production depth profiles based on SCR flux of (125,125) and (70,100) and GCR flux of 1.7 proton/(cm^2.sec.4 Π sr.>1 GeV) and Reedy-Arnold spectral shape parameters are plotted. The average chemical composition of various samples (Table-II.9) are used in these calculations. The calculated production rates are corrected for the erosion rate of 0.5 mm/Myr, suntan exposure age of 1.5 Myr and for exposure geometry (zenith angle $\eta = 30°$) following the work of Bhattacharya et al. (1972). In deducing best fit SCR parameters, higher weightage is given to the radiochemically measured ^{26}Al data points. The effect of erosion is calculated using the equation.

$$P_{26}(X) = \int_0^T P^1_{26}(X + \epsilon t)e^{-\lambda_{26} t}\, dt \qquad \ldots(IV.13)$$

where $P^1_{26}(X)$ is the production depth profile in absence of erosion at depth X, mm

$P_{26}(X)$ is the production depth profile corrected for erosion

ϵ is the erosion rate, mm/Myr

T is the suntan exposure age, Myr

and, λ_{26} is the decay constant of ^{26}Al, Myr^{-1}.

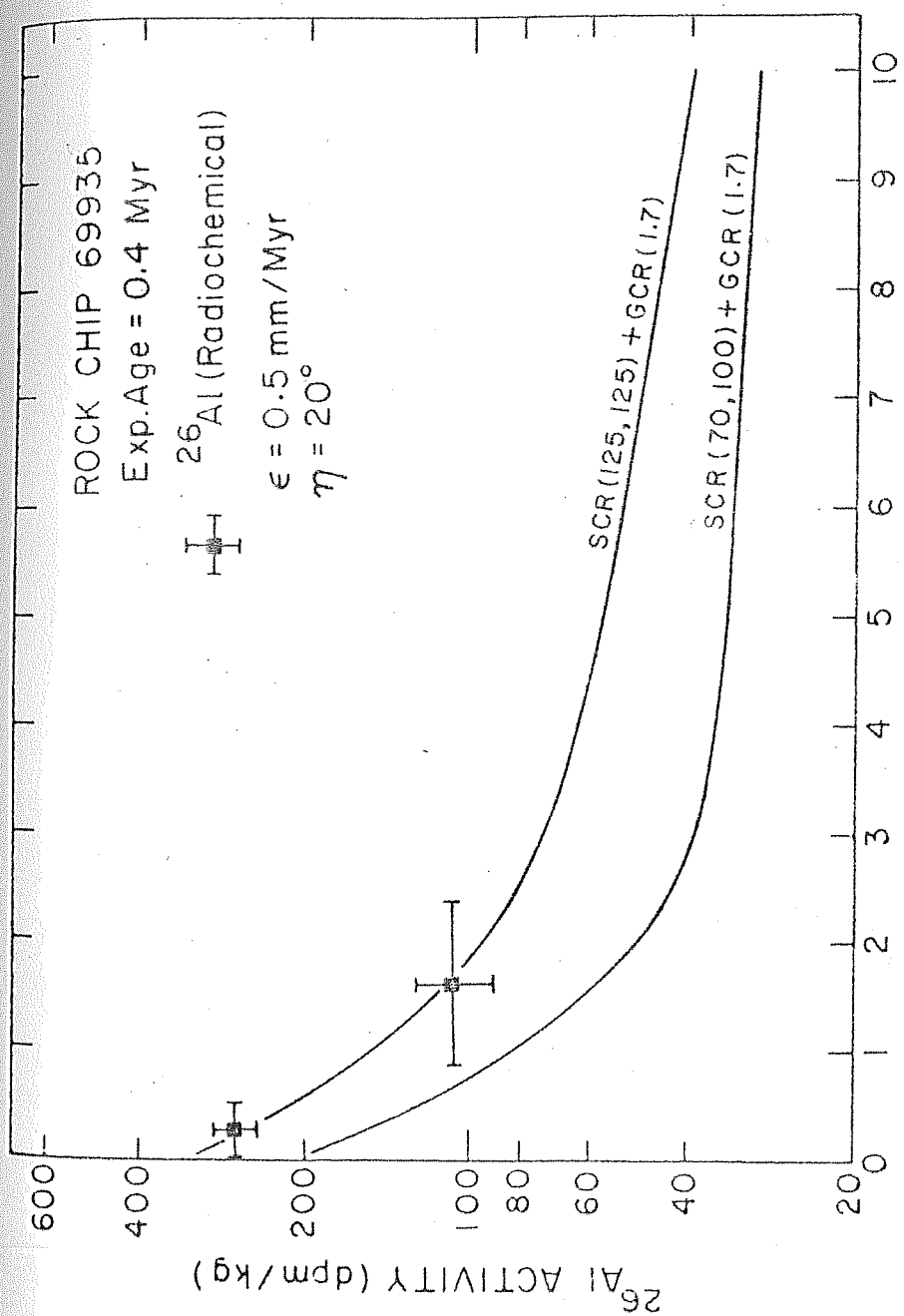

Fig.IV.8 Depth profile of ^{26}Al in 69935,14 rock and comparison with calculated depth profiles based on SCR flux of (Js,Ro)=(125,125) and (70,100) and GCR flux of 1.7 protons/(cm^2.sec. 4π sr. >1 GeV).

The erosion correction is about 5% at surface and reduces to zero below 5 $g.cm^{-2}$ depth. The zenith angle correction is $\sim$5% on the total (SCR + GCR) production profile. The best fit SCR flux given by (Js, Ro) = (125, 125) agrees with ^{26}Al data based on non-destructive $\beta\gamma$ counting within the errors of measurement. It is to be noted that different combinations of (Js, Ro) viz. (80,150) and (190,100) can also fit the measured profile using variable erosion rates. However, we adopt a flux given by (125, 125) which is based on an appropriate erosion rate of 0.5 mm/Myr. The flux combination of (Js, Ro) = (70,100) does not fit with the ^{26}Al profiles in this rock and other rocks and lunar soil columns as discussed below.

(ii) ^{26}Al depth profile in 69935:

In Fig.IV.8, we have plotted radiochemical data on two depth (viz. 1 ± 1 and 5.5 ± 2.5 mm) samples of rock chip 69935 (from top exposed portion). The calculated depth profiles based on mean chemical composition (Table-II.9) and SCR parameters (70,100) and (125,125) are plotted for comparison. The correction for 0.5 mm/Myr erosion rate and 0.4 Myr suntan exposure age (Bhandari et al. 1975) and exposure geometry (zenith angle $\eta=20^{\circ}$) are incorporated in the calculated depth profiles. The flux combination of (Js, Ro) = (125,125) fits the data very well while (70,100) is much lower than the observed values. The ^{81}Kr-^{83}Kr and

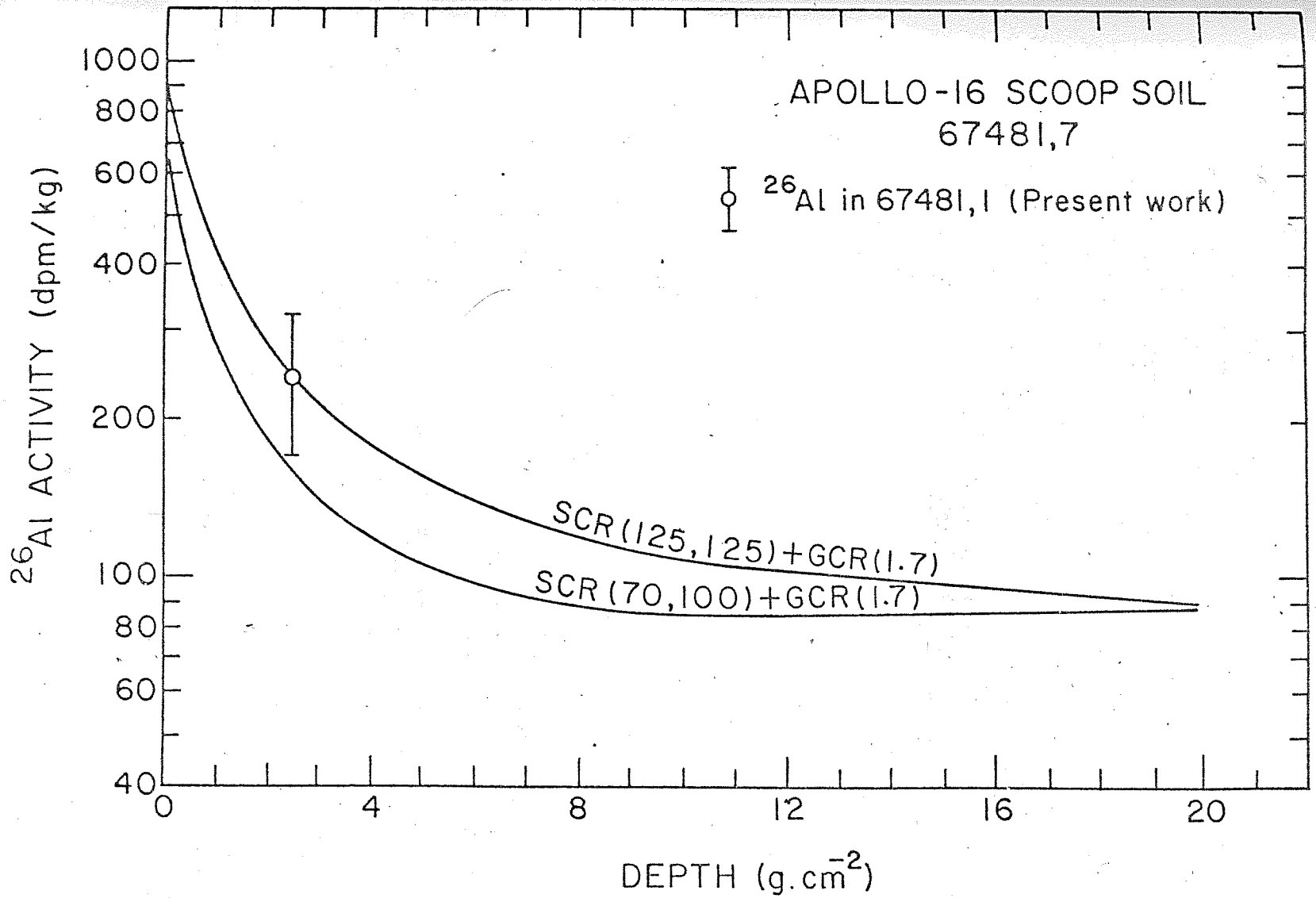

Fig.IV.9 ^{26}Al in Apollo-16 scoop soil (67481,7) and the depth profile of ^{26}Al in Lunar soil core based on (Js,Ro)=(125,125) and (70,100) and GCR flux of 1.7 protons/(cm^2. sec.4 π sr. >1 GeV).

^{21}Ne ages of this rock are 2 ± 0.16 and 2.13 ± 0.51 Myr respectively (Peppin et al.1974) whereas the GCR track exposure age is only 0.4 Myr which represents the suntan exposure age. This age discrepancy may be attributed to an event in which the surface chipping (thickness $\sim$ a few cms) occurred about 0.4 Myr ago exposing the present surface to SCR.

(iii) ^{26}Al in Apollo-16 Scoop Soil 67487,7 :

In Fig.IV.9, the non-destructive measurement of ^{26}Al in the Apollo-16 scoop soil for average shielding depth of ~ 2.5 g.cm^{-2} is plotted along with the expected depth profile of ^{26}Al in Moon based on the adopted chemical composition of the soil (Table-II.9) and the SCR flux given by (125,125). It is seen that the agreement between the expected activity and the measured activity is quite good supporting our above conclusion that the long-term ($\sim$ 3 Myr) averaged SCR flux is best represented by (125,125). At least during last three million years, there has been no regolith turn over upto a depth of 5 g.cm^{-2} due to micrometeorite impacts.

In Fig.IV.10, we have compared the depth profile of ^{26}Al in a long soil column 15010/11 measured by Fruchter et al. (1981) with the calculated profile based on the SCR parameters (125,125). The measured profile is best

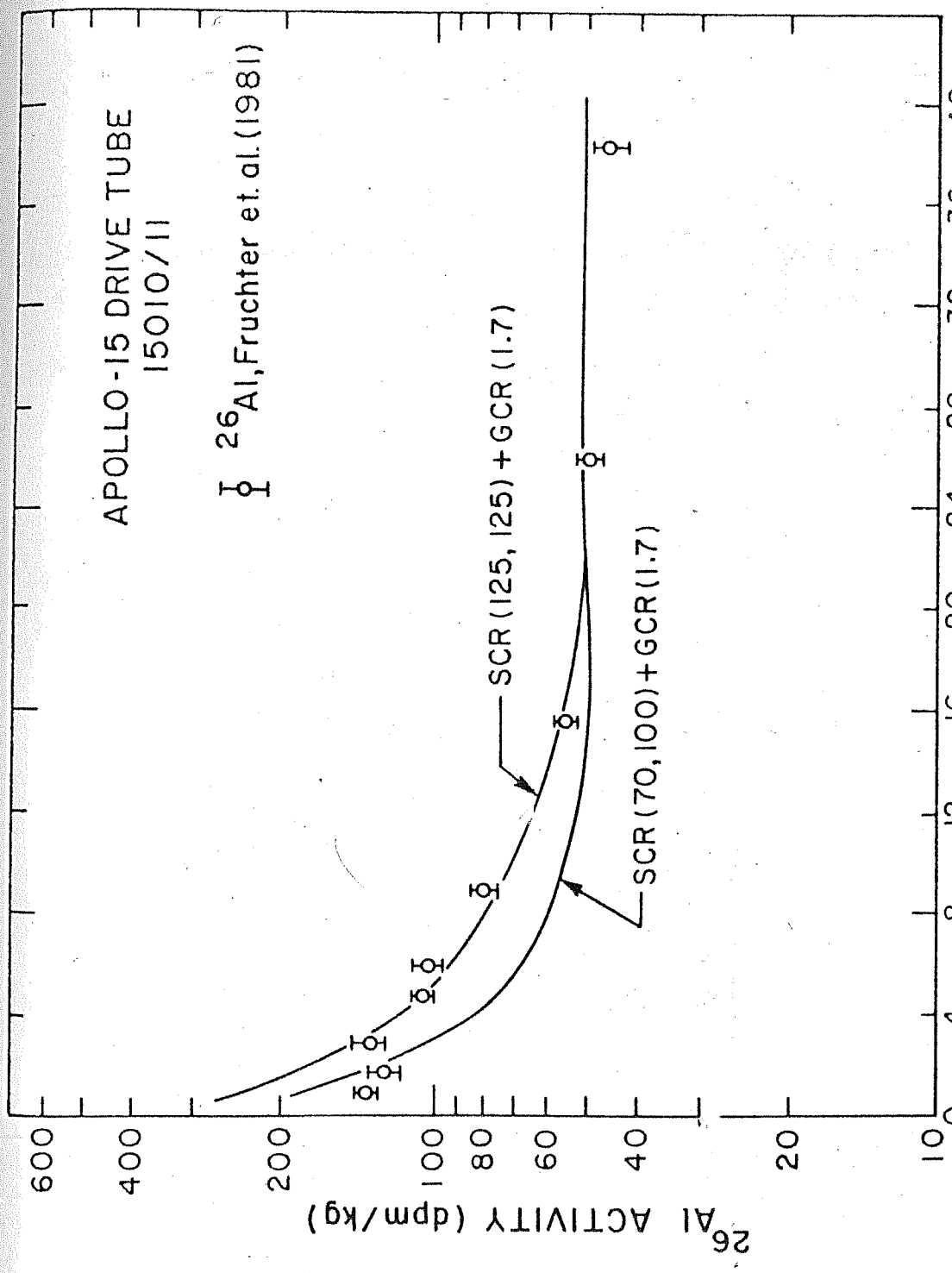

Fig.IV.10 Depth profiles of ^{26}Al in soil core 15010/11 (Fruchter et al.1981) and comparison with the calculated profile based on (Js,Ro)=(125,125) and GCR flux of 1.7 proton/(cm2.sec.4π sr. >1 GeV).

represented by (125,125) rather than (70,100). Fruchter et al. (1981) have argued that the observed 63% excess ^{26}Al activity in 0-16 $g.cm^{-2}$ depth of this core over expected activity based on (70,100) is due to slumping of soil from Hadle Rille. Similar arguments like accretion of surface material during lunar regolith gardening are advanced by Nishiizumi and Arnold (1981) to explain their observed excess ^{53}Mn activity in 0-10 $g.cm^{-2}$ of core 60010 over the expected activity based on (70,100). Soil slumping rate of 7 $g/(cm^2.Myr)$ and acretion rate of 0.5 $g/(cm^2.Myr)$ are required for 15010 and 60010 cores. The calculated ^{26}Al depth profile based on (125,125) when compared with the ^{26}Al depth profile in 60010 measured by Fruchter et al. (1976) show a good agreement with calculated profile given by (Js, Ro) = (125,125). The top 3 to 4 $g.cm^{-2}$ of flat section in ^{26}Al and ^{53}Mn depth profiles may be explained by mixing due to micrometeorite impacts. The mixing rates of $\sim$ 1 $g.cm^{-2}.Myr^{-1}$ in 15010 and in 60010 cores in lunar regolith gardening due to micrometeorite impacts are consistent with the fluxes deduced by Horz et al (1975). This comparison thus indicates that the regolith gardening has been responsible for flattening of the depth profile and the effects of soil slumping and accretion are negligible/or unimportant.

The ^{26}Al depth profiles in rocks 61016, 69935 and in soil cores 15010/11 and 60010, show that the long-term (0.4-1.5 Myr to 10 Myr) averaged SCR flux is best represented by (Js, Ro) = (125,125).

(D) Ancient Solar Flare Activity :

The long-term averaged SCR proton flux and spectrum given by (Js, Ro) = (125, 125) is higher than the solar cycle 20 flux given by (90,85) based on data of Webber (1966), King (1979), Kinsley (1969), Blake et al. (1969) and SPME (Bostrom et al. 1967-73). These data have been discussed in detail by Reedy (1977). The sunspot activity of cycle 20 is similar to the average of last 20 cycles since 1950 (Waldmeir, 1961) and can be taken to be representative cycle for the present day solar activity. The solar cycle 19 was the most active period of sunspot activity with $R_{Z,max}$ = 210 compared to $R_{Z,max}$ = 110 for cycle 20 which is equal to the average sunspot number over the last 20 cycles ($\simeq$ 100). The SCR flux averaged over cycle 19 was (378, 100-130) deduced from data of Webber (1966), Weddell and Haffner (1966), Modisettee et al.(1965) and was a factor of 4-5 times higher than the flux during the cycle 20 and average flux during last 230 yrs. If this correlation between the maximum sunspot number and average SCR fluxes is real, then it can be said that occassionally the solar sunspot activity goes through a cycle such as

cycle 19 during which a few gaint solar flares of fluence $\sim 2\times10^{10}$ protons/cm^2 and, of high regidity (100-150 MV) are produced and these flare particles dominate the interplanetary medium which are responsible for observed activities of long and short half-life radionuclides in lunar samples. Contrary to this type of behaviour, there are indirect evidences that periodically our sun goes through low and high sunspot activity such as Maunder minimum, (1645-1715 A.D.), Sporer minimum (1450-1550 A.D.), Wolf minimum (1282-1342 A.D.) preceeded by with grand maximum of sunspot activity (Eddy, 1976). The SCR activity is expected to be almost zero during the minima. The Maunder, Sporer and Wolf minima represent periods of 236 years of past 700 years. During the maxima following such minima several giant solar flares of fluence $\sim 2\times10^{10}$ occur during some solar cycles. If all periodicities in the earth's climatic variation are attributed to the solar activity variations, then the well observed periodicities (Mitchell, 1976) in earth's climate at 100-400, 2500, 2&4x10^4 and 10^5 yrs do suggest enhances of solar flare activity with above periodicities. The periods of 100-400 yrs agree with recent Maunder, Sporer and Wolf minimas. If a few largest flares of 2×10^{10} protons/cm^2 fluence occur with 2×10^4, 4×10^4 and 10^5 yr time spans, one can account for the higher average SCR flux given by (125, 125) over 0.4 to 1.5 Myr than (90,85) observed during average sunspot activity period. The periodicity of 3×10^8 yr seen in the earth's climatic variation

(Mitchel, 1976) can be attributed to sudden mixing of ^{3}He in solar core leading to sudden change in solar luminosity and neutrino flux (Ezer and Cameron 1972). Zook (1980) has evaluated critically the craters and track production rates used so far and from ^{14}C, ^{59}Ni (Lanzrotti et al. 1973) and T.L. data (Hoyt et al.1973) in lunar samples has tried to show that if the results obtained so far are correctly interpreted then the data show that solar activity was $\sim$ 35 times higher than the present day activity about 2×10^{4} yrs ago.

In summary, it can be said that the solar activity has periodicities of several time-scales and the SCR particles from a few giant flares occurring at 100-400, 2500, 2×10^{4}, 4×10^{4} and 10^{5} yrs dominate the interplanetary medium.

(E) GCR produced ^{26}Al in boulder chip 69955 and Luna-24 core soil 24087,1 :

i) Irradiation history of parent boulder of 69935 & 69955:

In deriving the SCR parameters, based on ^{26}Al profiles in rocks and soil columns, the contribution due to GCR particles is calculated based on long-term average GCR flux of 1.7 protons/(cm^2.sec. 4 Π sr.> 1 GeV) and Reedy-Arnold (1972) spectral shape parameters. It was shown by Reedy and Arnold (1972) and Kohl (1975) that the model GCR calculations agree with the measured depth variation in lunar rocks and soils. The SCR flux deduced from ^{26}Al depth profiles will be affected by the preirradiation, if any, the sample had within about last three million years. Such samples are not suitable for SCR studies. Here, we have measured ^{26}Al activity in a deep shielded rock sample from the same parent boulder of sample 69935, in which we have measured ^{26}Al depth profile.

The exposure age of the parent boulder based on ^{81}Kr-^{83}Kr, ^{21}Ne are given in Table-IV.6 (Drozd et al. 1974). From the non-concordant Kr and Ne exposure ages, it is seen that the parent boulder had preirradition effects in Kr and Ne isotopes.

Based on the rare gas isotope concentrations, the size of the boulder ($\sim$ 60 cm) and the track density measurements Drozd et al. (1974) have described the irradiation history of this boulder. According to their model,about 2 Myr ago,

when the south ray crater was formed, this boulder was excavated from deep shielded condition to the lunar top surface and during this process the boulder was turned through 180°. The shielding depth during previous irradiation of rock chip 69955 was about 180 $g.cm^{-2}$ below the lunar top surface. Thus effectively, the rock sample 69955 has been exposed to cosmic rays at shielding depth of 180 $g.cm^{-2}$ during the preirradiation and during last $\sim$ 2 million years and the sample 69935 was shielded at a depth of 360 $g.cm^{-2}$ before 2 Myr.

The production rate of ^{26}Al in this sample with shielding depth of 180 $g.cm^{-2}$ calculated based on Reedy-Arnold model is 60 dpm/kg which agrees with the measured activity of 68 ± 21 dpm/kg. The above discussions indicates that the pre-irradiation effects on ^{26}Al in the sample 69935,14 are insignificant and the fact that the SCR flux derived from the ^{26}Al depth profile in 69935,14 agrees with those deduced from ^{26}Al and other radionuclide depth profiles in lunar rocks and soil columns, establishes that the SCR activity is best represented by $(J_s, R_o) = (125,125)$.

(ii) Shielding depth of 24087,1 Soil :

The nature of soil column and the uncertainty involved in the assignment of the depths to the luna-24 core samples are discussed in Chapter II. The non-destructive $\beta \pm \gamma$ measurement of total β^+ activity due to ^{26}Al and ^{22}Na in one soil layer 24087,1 are given in Table II.12.

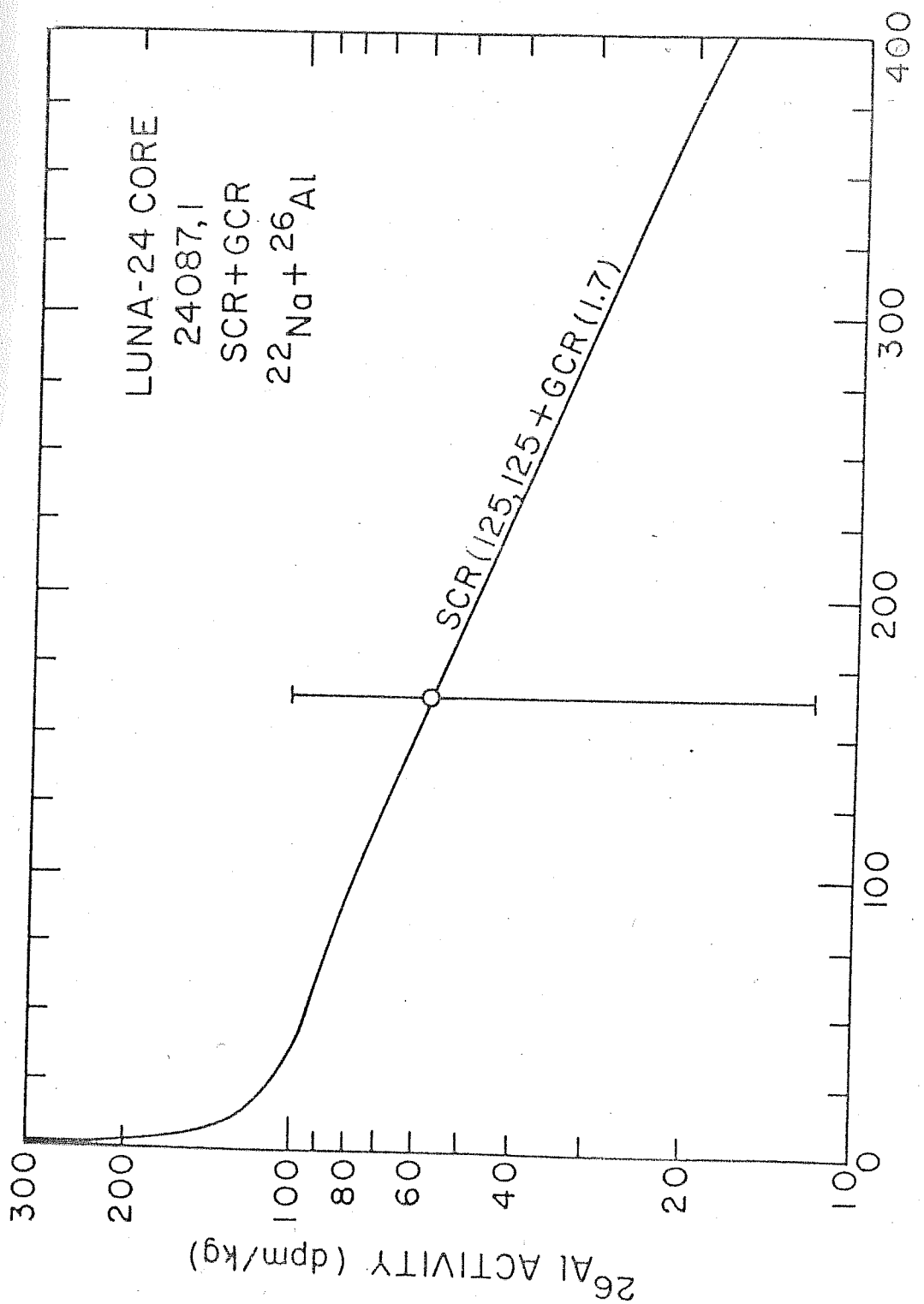

Fig.IV.11 Calculated depth profile of ^{26}Al in Luna-24 soil core and ^{26}Al in 24087,1 soil layer.

Although, the counting error is large because of small amount (162 mg) of soil sample available, still it allows us to estimate roughly the irradiation depth of the sample on the Moon. In Fig.IV.11, the expected (^{26}Al+^{22}Na) activity depth profile based on the adopted chemical composition of the mare soil and the Reedy and Arnold model calculations is shown. The effect of GCR modulation during solar cycle 20 on ^{22}Na production is estimated using the deduced GCR fluxes during all the years of solar cycle 20 (Potdar and Bhandari, 1979) and the activity is equivalent to the production due to a GCR flux of 2 protons/(cm^2.sec.4 π sr.> 1 GeV). The measured total activity is shown in the figure IV.11.

From the figure it is seen that the activity of 57$\pm$45 dpm/kg in 24087,1 corresponds to a shielding depth of $\geq$53 g.cm^{-2}. The density of core soils vary between 1.4 to 1.7 g.cm^{-3} (Apollo-16 preliminary science report). Taking an average density of 1.55 g.cm^{-3}, we obtain the shielding depth of the sample of $\geq$35 cm.

The actual depth of the sample 24087,1 from the top of the core tube is 86 to 87 cm. The tube was empty upto a depth of 47 cm and it was scantily filled upto 58 cm. From 58 cm to 73 cm of the core tube, according to Barsukov et al. (1977), contained only coarse grains. Bogard and Hirsch(1977) have discussed the problem of real sample depths of the Moon.

The following three possibilities have been suggested to explain the smaller recovered core length (140 cm) compared to the 223 cm of depth of penetration; viz.

(i) shortening due to compaction, (ii) Expansion due to large core diameter compared to that of drill bit, or (iii) incomplete sampling.

Unlike the case of rare gases, the pre-irradiation effects are absent in case of ^{26}Al. The ^{26}Al measurement can be used to determine the actual sample depth on the moon, with the help of a suitable model for calculation of depth profile, such as Reedy and Arnold (1972) model. If the level of 58 cm is assigned to the lunar surface, then our results indicate that some part of the soil was not contained in the core tube. Furthermore, as discussed by Bogard and Hirsch (1977), if the core was not taken vertically, but at an angle of 30° our results indicate a loss of upper 10 cm of core material.

CHAPTER-V

COSMOGENIC ^{21}Ne AND ^{22}Ne PRODUCTION DEPTH PROFILES IN CHONDRITES

A. INTRODUCTION:

Interaction of cosmic rays with meteorites in space produces several stable and radioactive isotopes. Of these, ^{21}Ne is produced so dominantly that ^{21}Ne content can directly be used to estimate its cosmic ray exposure in interplanetary space. To obtain the exposure age, one needs the production rate which depends on cosmic ray flux, shielding depth, size and shape of the meteoroid and finally, on its chemical composition. The cosmogenic ^{3}He was first measured in meteorites by Paneth et al. (1953). Since then a number of different methods have been used to calculate production rates of ^{3}He, ^{21}Ne and other rare gas isotopes. The results of various calculation are summarised in Table V.1. From the studies of the several rare gas isotopes in 30 meteorites, Eberhardt et al. (1966) showed that, if ^{3}He production rate is assumed to be constant with depth, the ^{21}Ne production rate, $P(^{21}Ne)$, generally increases and $(^{22}Ne/^{21}Ne)_{sp}$ decreases with depth. Later, Herzog and Anders (1971) used ^{26}Al and ^{21}Ne pair in 14 short exposure age meteorites (i.e. the meteorites with unsaturated ^{26}Al activity) to obtain $(p^{21}Ne)$. The production rates thus obtained were 25% higher than the production rates based on $(^{3}He/^{21}Ne)$ measurements Kirsten et al. (1963). The measurements in St.Severin (Schultz and Signer 1976) and Keyes (Wright et al.1973)

TABLE-V.1

Estimated ^{21}Ne Production Rates

S.No.	Authors	Method	$P(^{21}Ne)$ corresponding to $\left[\frac{^{22}Ne}{^{21}Ne}\right]_{sp} = 1.114$ 10^{-8} cc STP/g/Myr.	Shielding correction
1.	Kirsten et al.(1963)	$\left(\frac{^{3}He}{^{21}Ne}\right)$	0.377	Not discussed
2.	Eberhardt et al.(1966)	$\left(\frac{^{3}He}{^{21}Ne}\right)$	0.400	$5\left[23.4\left\{\left(\frac{^{22}Ne}{^{21}Ne}\right)_{sp}-1\right\}+2.40\right]^{-1}$*
3.	Herzog & Anders(1971)	^{26}Al Age	0.466	Not discussed
4.	Cressy & Bogard(1976)	-	0.440	(i) $38.27-62.53\left(\frac{^{22}Ne}{^{21}Ne}\right)_{sp}+26.1\left(\frac{^{21}Ne}{^{21}Ne}\right)^{2}_{sp}$ (ii) 1.181 for $\left(\frac{^{22}Ne}{^{21}Ne}\right)_{sp} \leq 1.08$ (iii) 0.818 for $\left(\frac{^{22}Ne}{^{21}Ne}\right)_{sp} \geq 1.20$
5.	Nishiizumi et al.(1980)	^{26}Al Age	0.507	$4.845 \times f \times \left[21.77\left(\frac{^{22}Ne}{^{21}Ne}\right)_{sp}-19.32\right]^{-1}$
		^{53}Mn) ^{81}Kr-^{83}Kr) Ages ^{22}Na-^{22}Ne)	0.31	where f = 1.0 for L & LL chondrites = 0.93 for H chondrites
6.	Muller et al.(1981)	^{26}Al Age	0.46	Similar to that of Eberhardt et al. (1966)
		^{53}Mn Age	0.30	
7.	Present work	Depth Profile calculations	0.40 for $R_E \leq 25$ cm 0.32 for $R_E \sim 50$ cm 0.20 for $R_E > 500$ cm	Discussed in the text

* Discussed in Bhandari et al. (1980)

chondrites agreed with the results of Eberhardt et al. (1966). Subsequently Cressy and Bogard (1976) suggested the use of $(^{22}Ne/^{21}Ne)_{sp}$ ratio to calculate shielding correction to $P(^{21}Ne)$ at any depth. The shielding correction included the effects of variation in chemical composition. From the measured $(^{21}Ne)_m$ and $P(^{21}Ne)$ calculated for the corresponding $(^{22}Ne/^{21}Ne)_{sp}$, one could obtain the cosmic ray exposure age of chondrites.

The recent work on ^{21}Ne production rate of Nishiizumi et al. (1980) based on the various exposure ages viz. ^{26}Al, ^{81}Kr-^{83}Kr, ^{53}Mn, ^{22}Na-^{22}Ne, of several chondrites have given discondant production rates, and their production rate based on ^{26}Al is higher than those based on ^{53}Mn and ^{81}Kr-^{83}Kr ages. The work of Müller et al. (1981) has given production rate in agreement with those of Nishiizumi et al. (1980).

Depth profiles of $P(^{21}Ne)$ and $(^{22}Ne/^{21}Ne)_{sp}$ depend sensitively on R_E (the effective preatmospheric radius) of the meteorids. In the all works cited above, this effect is not investigated. The empirical curves of $P(^{21}Ne)$ vs. $(^{22}Ne/^{21}Ne)_{sp}$ of Eberhardt et al. (1966) and those of Cressy and Bogard (1976) are being used to obtain exposure ages of meteorites irrespective of their sizes.

As already discussed in Chapter-IV, Reedy and Arnold (1972) developed a semi-empirical model for calculating the production depth profile of some radionuclides in the moon in GCR and SCR interactions. These calculations have shown reasonable

agreement with the measured depth profiles of some radionuclides in lunar rocks and soil cores. These calculations, when applied to meteorites require a priori knowledge of energy spectrum of nucleons as a function of depth within a meteoroid which is difficult to calculate from the intranuclear evaporation - cascade theory of development of secondary nucleons. Applying this method to meteorites, Bhandari et al. (1979) calculated the spectral shape parameters for various size chondrites based on ^{22}Na depth profiles of Trivedi and Goel (1969). Reedy et al (1979) calculated the depth profiles of ^{21}Ne and ^{22}Ne production rates in St.Severin and Keyes chondrits, which agreed with the measured profiles within $\sim 30\%$. Recently, Bhattacharya et al. (1980) have experimentally deduced α depth profiles for small chondrites ($R_E \leq 25$ cm) based on measured ^{53}Mn depth profiles. These values of α are significantly different from those of Reedy et al. (1979) which were based on semi-empirical considerations. These experimentally deduced α-depth profiles are used here for calculating the depth and size dependence of production rates of ^{21}Ne and ^{22}Ne.

B. CALCULATION OF DEPTH PROFILES OF $P(^{21}Ne)$ AND $(^{22}Ne/^{21}Ne)_{sp}$ IN CHONDRITES :

The production of cosmogenic nuclides in meteorites and lunar samples is due to two distinct sources. The SCR protons are mainly responsible for significant production at depths less than 10 g. cm^{-2} whereas the GCR protons and their secondaries dominate the productions in deeper regions.

I. GCR Production :

The GCR contribution is calculated following the procedure of Reedy and Arnold (1972).

The Reedy-Arnold model requires a priori knowledge of the following parameters :

(i) The primary cosmic ray flux during the exposure of meteoroid in the interplanetary space.

As discussed in Chapter-IV, the annual flux of GCR proton ($E > 1$ GeV) at 1 A.U. during solar cycle 20 varied between 1.32 and 2.36 protons/(cm^2.sec.4 π sr) leading to an average GCR proton flux over solar cycle 20 of 1.9 ± 0.1 protons/(cm^2.sec.4 π sr.) (Potdar and Bhandari 1979). However, here we adopt a value of 1.7 protons/(cm^2.sec.4 π sr) as the average over a few million years period (Reedy and Arnold 1972).

(ii) The spectral Shape Parameter (α) :

The spectral shape parameter as a function of depth 65 cm (Madhipura chondrite), 9 cm (Udaipur chondrite), 15 cm (Bansur chondrite) and 25 cm (St. Severin chondrite) were taken from Bhattacharya et al. (1980) which were obtained from measured ^{53}Mn depth profiles in these chondrites. In obtaining these α values, the excitation function for the following nuclear reactions:

$$^{56}Fe(n,x)^{53}Mn$$

and $$^{56}Fe(p,x)^{53}Mn$$

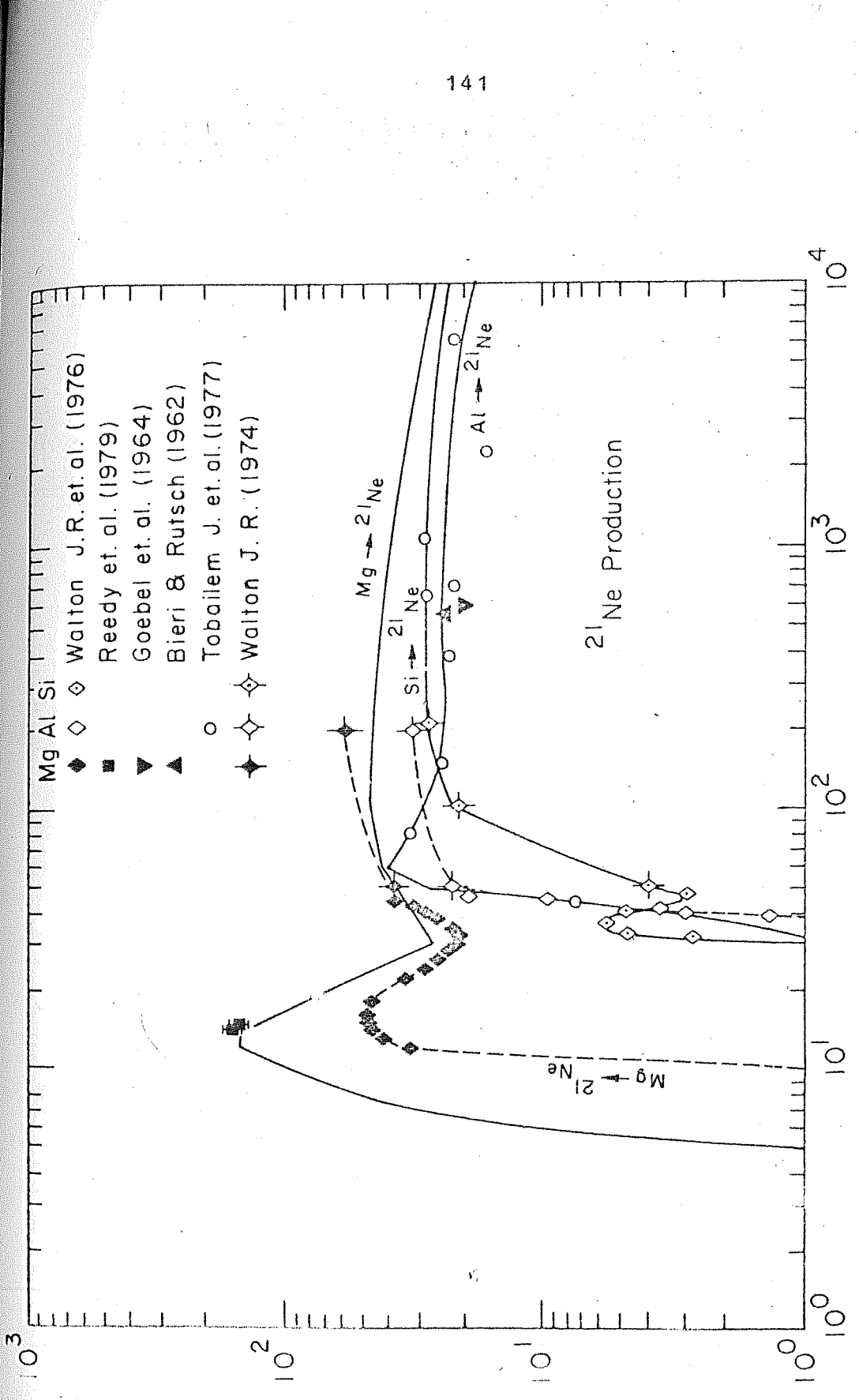

Fig.V.1(a) Excitation functions for ^{21}Ne production from Mg, Al and Si targets.

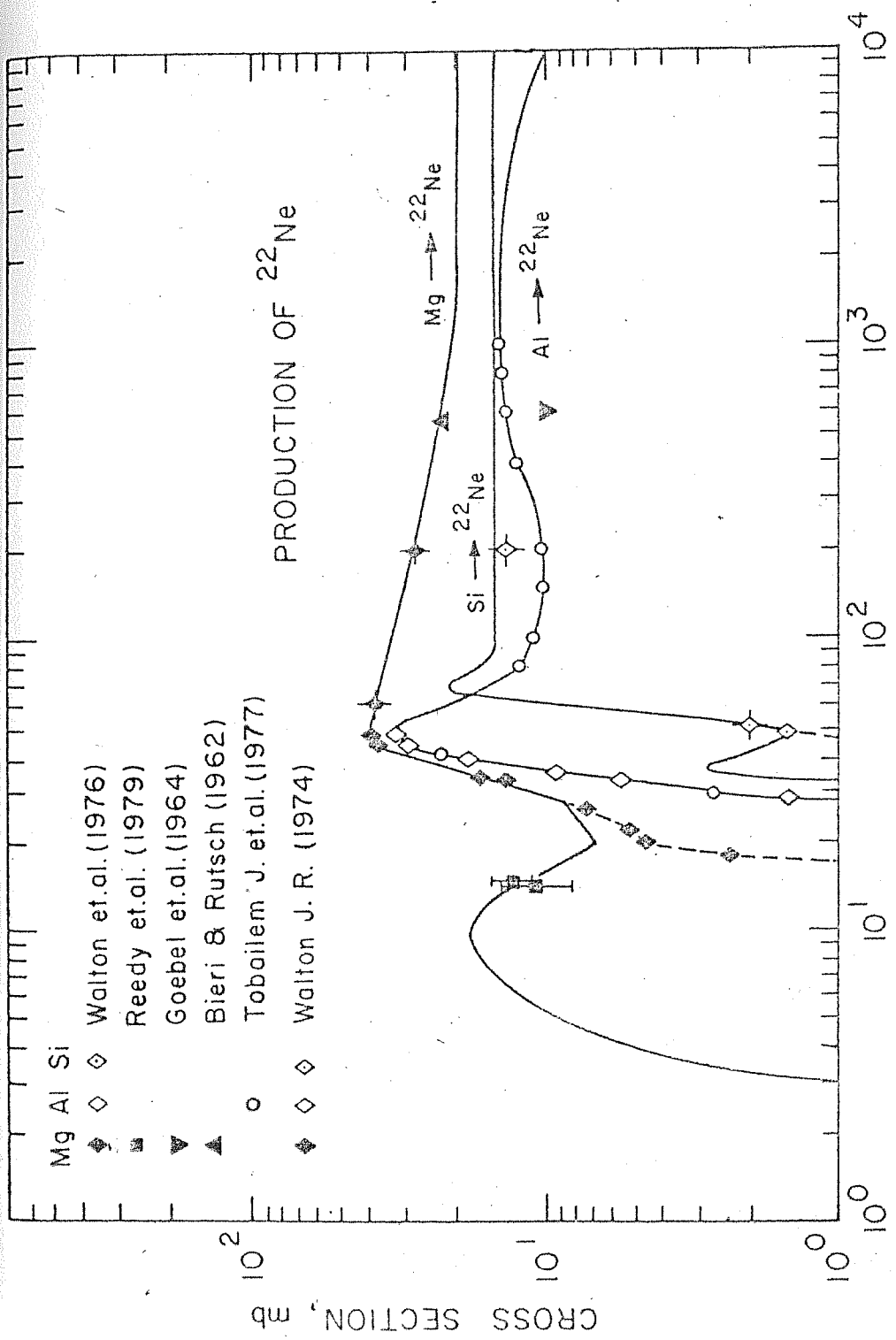

Fig.V.1(b) Excitation functions for ^{22}Ne production from Mg, Al, and Si targets.

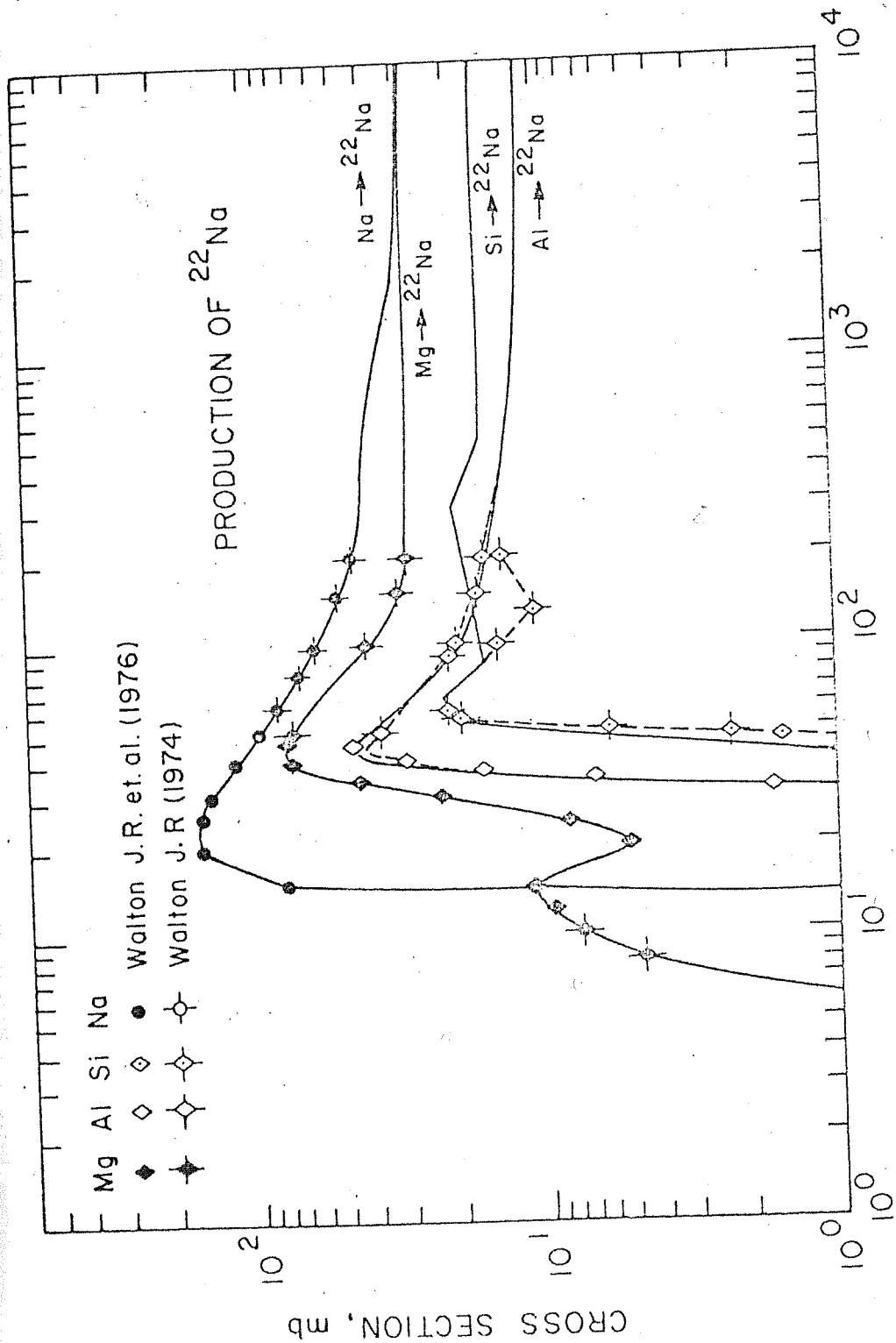

Fig.1(c) Excitation function for ^{22}Na production from Na, Mg, Al and Si targets.

were taken from Gensho et al. (1977). The ^{55}Mn to ^{53}Mn contribution was estimated to be $\sim 1\%$. The α depth profile for a meteoroid of size R_E ~ 50 cm (Dhajala chondrite) was obtained from the ^{26}Al depth profile determined in the present work (Chapter-IV). For a large size (> 5m) (moon size) meteoroid the Reedy-Arnold α depth profile was used. Reedy-Arnold α values and their adopted $^{56}Fe(n,x)^{53}Mn$ excitation function underestimate ^{53}Mn in Apollo-15 core by about 33%. It was found that Gensho et al. excitation function and Reedy-Arnold α values correctly reproduce ^{53}Mn depth profile in Apollo-15 core sample obtained by Kohl (1975), and hence we have used excitation function of Gensho et al. throughout the energy region of interest.

The production cross-sections of ^{21}Ne, ^{22}Ne and ^{22}Na from targets Mg, Al, Si and Na were taken from Walton (1974), Walton et al. (1976), Tobailem (1977), Bieri and Rutsch (1962) and Goebel et al. (1964).

The production cross-section due to neutrons and protons are different at low energies, so that strictly one should consider relative fluxes and spectra of neutrons and protons and corresponding cross-sections. However, in view of uncertainties involved in the estimation of their relative fluxes and the scarcity of neutron cross-section data, the flux of all nucleons are considered together and we use neutron induced reaction cross-sections at low energies and proton induced reaction cross-sections at high

TABLE-V.2

Production of ^{21}Ne and ^{22}Ne from various target elements

(in 10^{-8} cc STP/g/Myr.)

Nuclide	Depth	R_E = 6.5 cm				R_E = 25 cm				R_E = 50 cm			
		Mg	Al	Si	Na	Mg	Al	Si	Na	Mg	Al	Si	Na
^{21}Ne	10 g.cm^{-2}	1.34	0.53	0.47	-	1.77	0.60	0.50	-	1.58	0.52	0.44	-
	Center	1.39	0.54	0.47	-	2.45	0.71	0.57	-	1.63	0.45	0.36	-
^{22}Ne (total)	10 g.cm^{-2}	1.50	0.63	0.60	1.52	1.85	0.75	0.66	2.02	1.63	0.65	0.58	1.80
	Center	1.54	0.65	0.60	1.57	2.40	0.92	0.78	2.79	1.56	0.60	0.49	1.86

energies. The excitation functions for various reactions are shown in Fig.V.1(a,b,c). Since the cross-sections have not been measured throughout the energy regions of interest, some interpolations and extrapolations have been made, within the errors of cross section measurements, to reproduce the $(^{22}Ne/^{21}Ne)_{sp}$ and $P(^{21}Ne)$ profiles in St.Severin amphoterite (LL chondrite) as precisely as possible. The St.Severin was taken as standard because:

(i) precise measurement of rare gas depth profiles have been made in a core taken radially through it (Schultz and Signer, 1976).

(ii) the exposure age as obtained by various methods including ^{81}Kr-^{83}Kr method, cluster around 11 Myr (Range 10.8 Myr to 13.0 Myr), (Marti et al. 1969), and

(iii) its preatmospheric size (R_E=25 cm) and shape are known well from extensive particle track studies (Bhandari et al. 1980).

It should be noted that ^{21}Ne is predominatly produced in $^{24}Mg(n,^{4}He)$, and ^{22}Ne in $^{25}Mg(n,^{4}He)$ reactions as well as from insitu decay of ^{22}Na. The contributions due to Ca, Fe etc are estimated to be only 3% (Reedy et al.1979). Table-V.2 gives the typical production rates in different target elements for R_E = 6.5, 25 and 50 cm.

II. SCR Production:

Long-term average SCR flux at 1 A.U. is given by J_s = 125 protons/(cm^2.sec.4 Π sr) and R_o=125 MV (Chapter-IV). At meteorite aphetion distances ($\sim$3-4 A.U.), the solar fluxes are expected to be lower than those at 1 A.U. Lal and Marti (1977) have mentioned that the Ne production in near surface regions of St.Severin (X $\sim$4-8 g.cm^{-2}) require higher fluxes of low energy protons, but whether this excess flux is entirely of solar or galactic origin(due to less solar modulation) is not very clear. Considering the entire production to be due to SCR particles, they find that a flux of J_s = 70 protons/(cm^2.sec.4 Πsr) and R_o = 100 MV will be required under the assumption of no gas loss to match the observations. For the sake of discussions we present here calculations for J_s = 110 protons/(cm^2.sec.4 Πsr) and R_o = 100 MV.

(C) RESULTS:

The calculated production depth profiles of ^{21}Ne and $(^{22}Ne/^{21}Ne)_{sp}$ are shown in Fig.V.2, 3 and 4 for H, L, LL group chondrites of various sizes. It is seen that $P(^{21}Ne)$ depth profile is more sensitive to J_G and α values as compared to $(^{22}Ne/^{21}Ne)_{sp}$ depth profiles. The experimental data in San Juan Capistrano (Finkel et al. 1976) and Keyes (Wright et al.1973) chondrites are shown and compared with the calculated profiles.

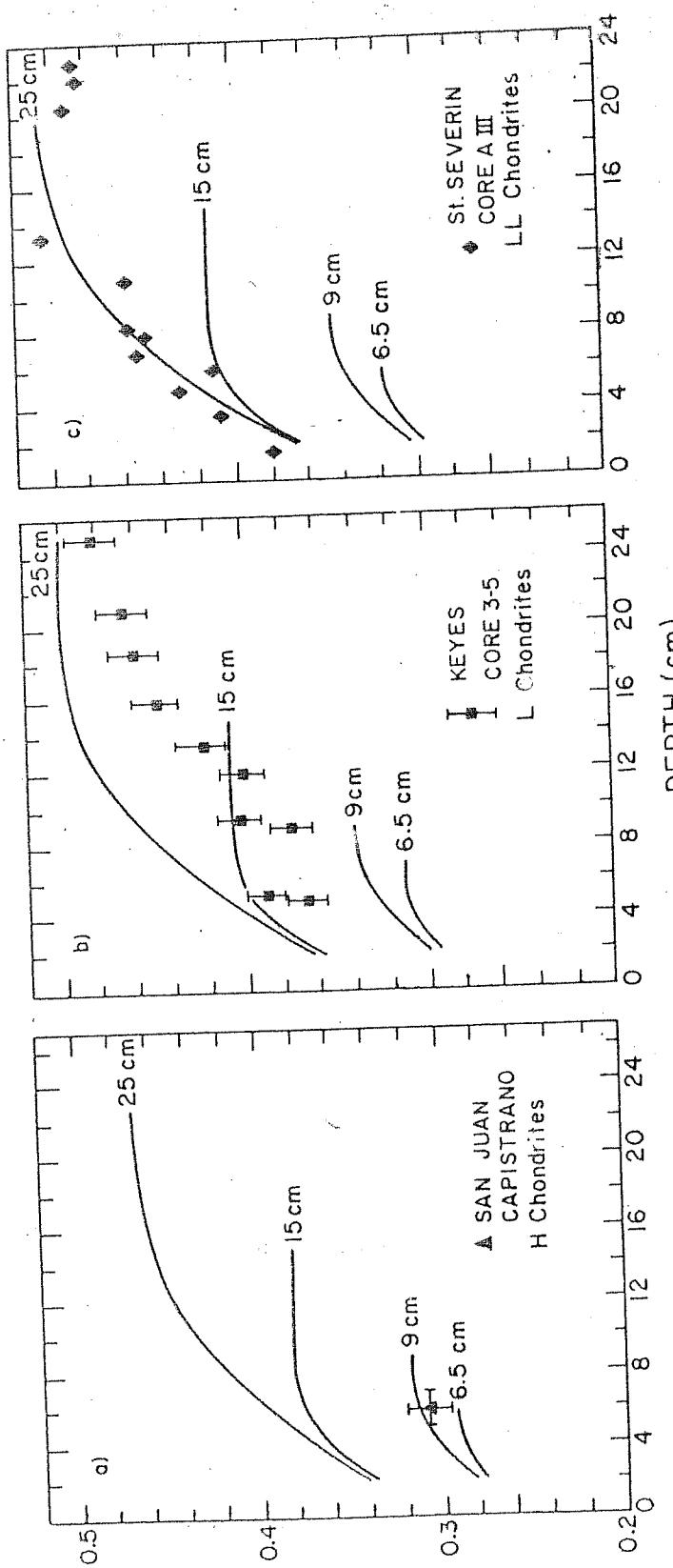

Fig. V.2 Calculated GCR ^{21}Ne production depth profiles in 6.5, 9.0, 15.0 and 25 cm radius H(a), L(b) and LL(c) chondrites and comparision with the measurements in Keyes (30 cm), St.Severin (25 cm) and San Juan Capistrano (8 cm) meteorites. Appropriate shielding corrections have been made based on track data of Bhandari et al. (1980) and Bhattacharya et al. (1980).

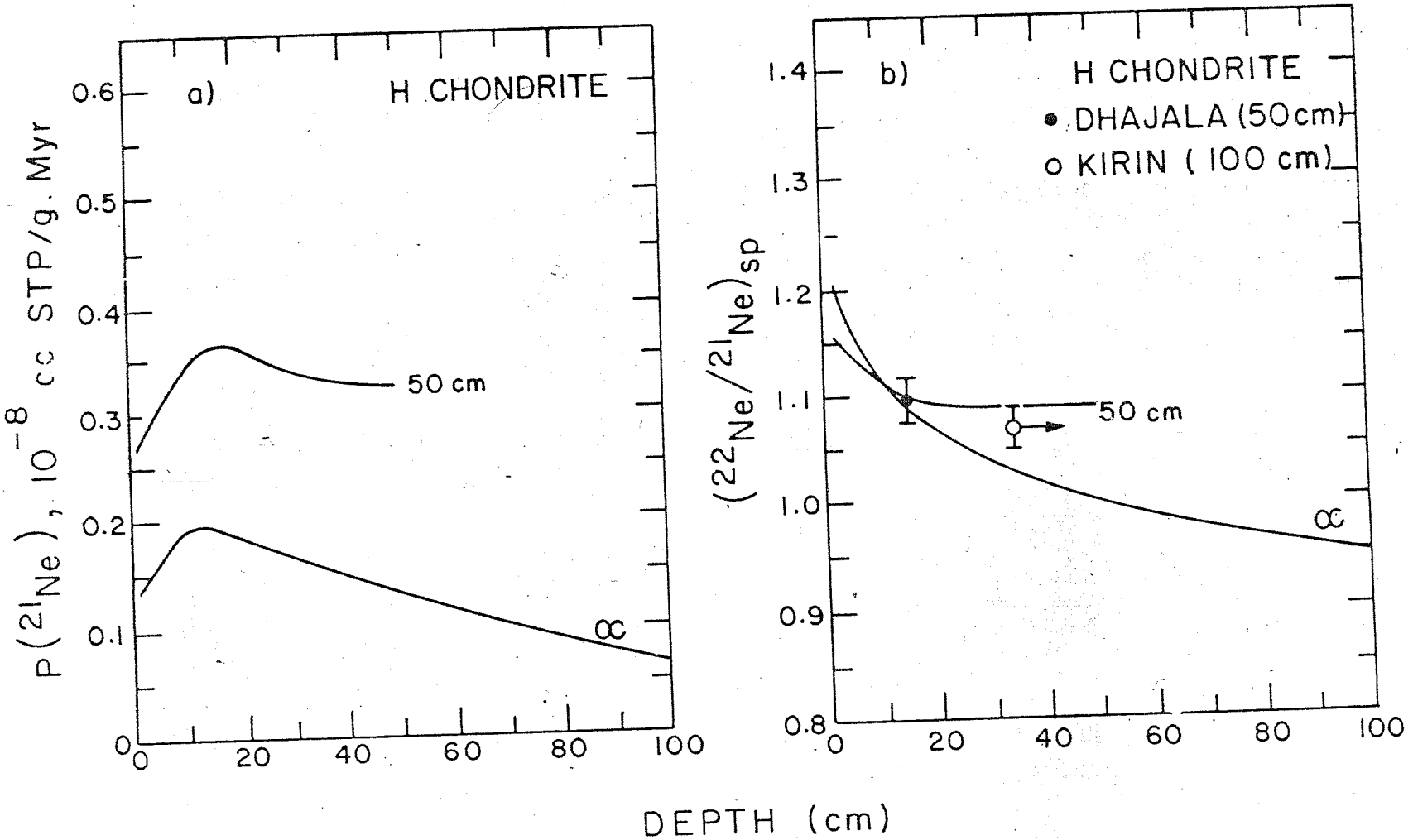

Fig.V.3 (a) Calculated ^{21}Ne production profiles, and (b) the $(^{22}Ne/^{21}Ne)_{sp}$ profiles in R_E=50 cm and ∞ (i.e. $R_E > 500$ cm) H chondrites and comparison with data in Dhajala and Kirin chondrites.

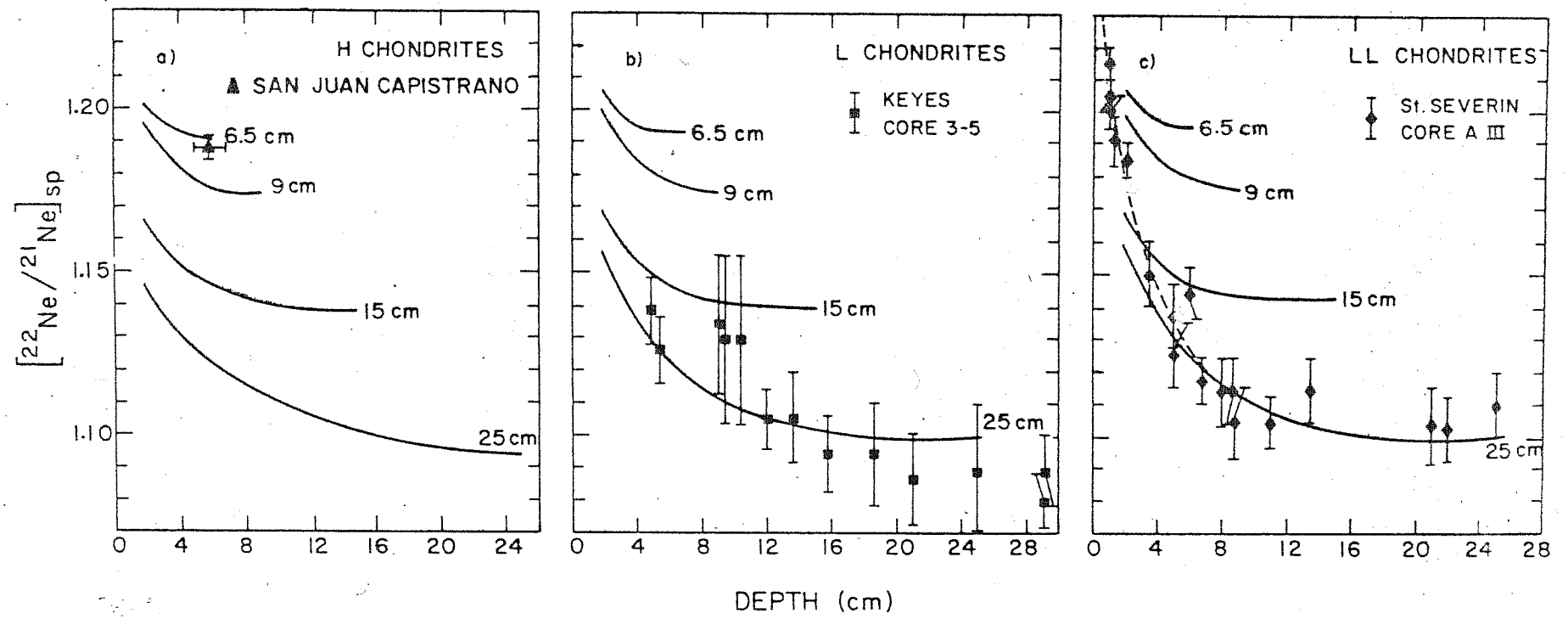

Fig.V.4 Calculated $(^{22}Ne/^{21}Ne)_{sp}$ depth profiles for H(a), L(b) and LL(c) chondrites and comparison with data on San Juan Capistrano, Keyes and St.Severin chondrites.

The exposure ages of these chondrites based on different methods like ^{3}He, ^{38}Ar and ^{81}Kr-^{83}Kr, differ substantially. The differences are not clearly understood and may be due to uncertainties in their production rates, degassing and multiple stage exposures to cosmic rays. Since there is no evidence of ^{3}He loss in these chondrites and it may represent production during final stage of exposure history, we use here ^{3}He exposure ages for comparing the experimental data with the calculations. The ^{3}He exposure ages of San Juan Capistrano and Keyes are 19 and 21 Myr and the preatmospheric radii are approximately 8 and 30 cm, respectively.

I. Production due to GCR:

As the α values obtained for meteorites are from the measured radionuclide depth profiles, the SCR and GCR contributions cannot be resolved. Thus, the production rates in depth < 20 $g.cm^{-2}$ given in Fig.V.2, 3 and 4 are composite of both the SCR and GCR contributions. These calculations have uncertainties inherent in (1) long-term cosmic ray intensity, (2) excitation functions and (3) the departure from sphericity of meteorites. In the present calculations we have tried to minimise the above uncertainties in the following way. We use α profiles dervied from the measured ^{53}Mn profiles in various meteorites and the same GCR flux (J_G = 1.7 protons/(cm^2.sec.4 π sr.). Since the production rates depend on the combination of J_G and α the uncertanty mentioned in (1) above is thus, minimised. Only if, the

primary GCR flux were different about 5 Myr ago, such variation will introduce the error in the production rates in meteorids with long exposure ages. The uncertainty due to departure from sphericity decreases with increasing shielding depth and it is important only when shallow depths are considered. In the present calculations, since the emphasis is laid on measurements in the near central or deep shielded (> 15 g.cm^{-2}) samples, the error due to non-spherical geometry is minimised.

The dependence of production rate of an individual nuclide due to uncertainties in the excitation function could be significant. This uncertainty is reduced by adjusting excitation functions within the permissible limits of errors of cross-section measurements, so that the $(^{22}Ne/^{21}Ne)_{sp}$ and $P(^{21}Ne)$ in St.Severin chondrite are reproduced very well. Since the calculations agree with the measurements in several chondrites, it is clear that the relative production rates for sizes and depths given here are reasonably accurate (Bhandari et al. 1980a).

The following observations can be made regarding the GCR profiles:

1. The calculated depth profiles are quite sensitive to the size of the meteoroids. The production rate increases with depth for size of upto 25 cm, and in large size meteoroids, the production rate initially increases upto depth of 15-20 cm and then decreases (Fig.V.2 and 3). The

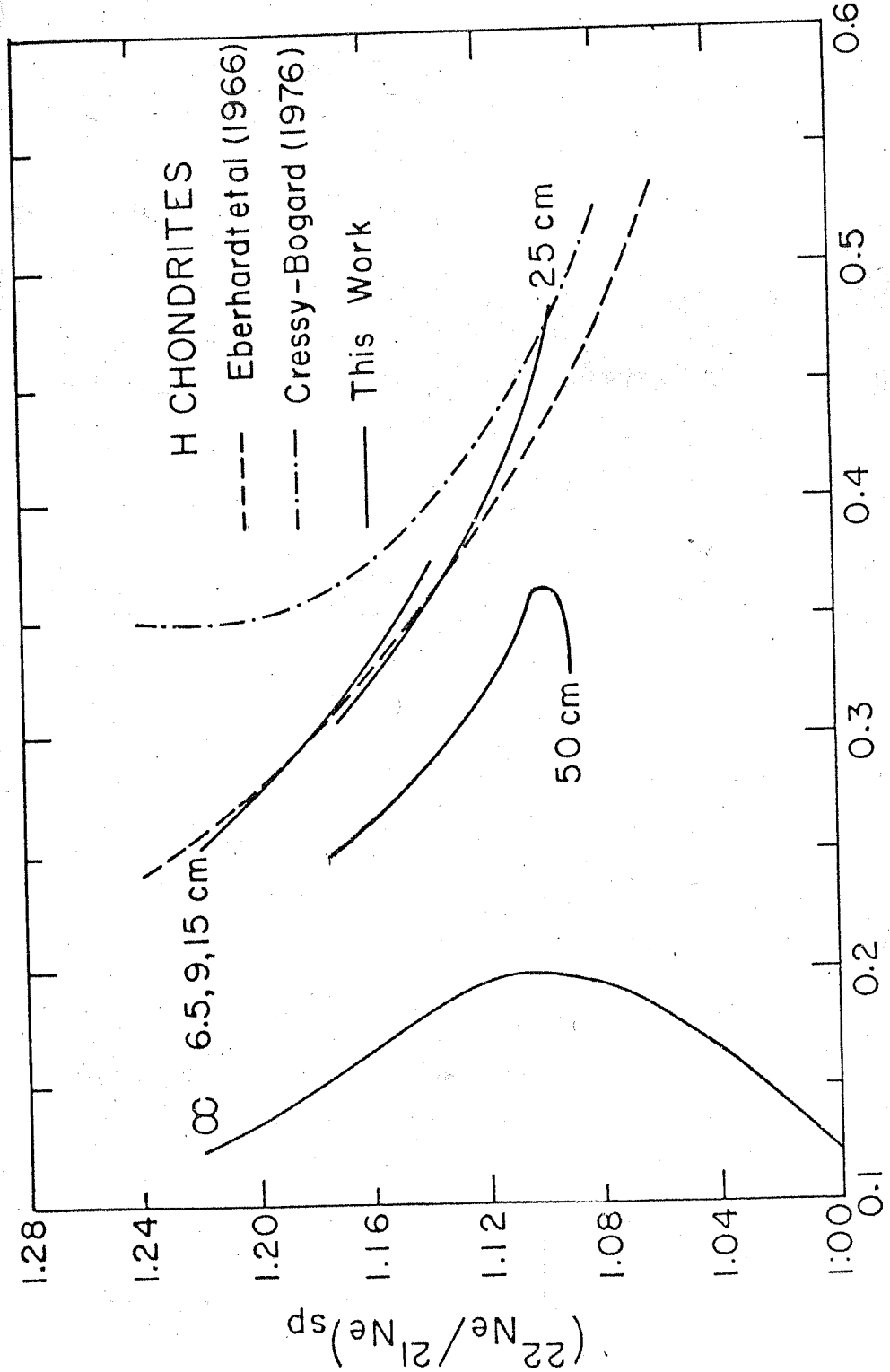

Fig.V.5 $(^{22}Ne/^{21}Ne)_{sp}$ vs. $P(^{21}Ne)$ correlation diagram for H chondrites. The empirical curves of Eberhardt et al.(1966) and, Cressy and Bogard (1976) are also shown.

calculated $P(^{21}Ne)$ depth profiles are consistent with the measured profiles (within ∿10%) for various size meteorites ranging from R_E = 8 cm (San Juan Capistrano) to R_E ∿ 100 cm (Kirin). The $(^{22}Ne/^{21}Ne)_{sp}$ profiles show agreement with measured profiles within about 2%, which is quite satisfactory in view of uncertainties in the shapes of the meteoroids.

2. It is clear that the $P(^{21}Ne)$ is not a simple function of $(^{22}Ne/^{21}Ne)_{sp}$ as has been assumed by Eberhardt et al. (1966) and Cressy and Bogard (1976), in their procedure for calculating the meteoroid exposure ages wherein the shielding factors are calculated from the measured spallation neon ratios. In Fig.V.5 these correlation curves of $P(^{21}Ne)$ vs. Ne spallation ratio for different preatmospheric sizes are plotted along with the empirical curves of Eberhardt et al. and Cressy and Bogard. The agreement between our calculated curves and the empirical curve of Eberhardt et al. (1966) is good for size range of 6.5 cm to 25 cm, but for large meteoroids (R_E > 25 cm), there is marked disagreement. The measured value of spallation neon ratio 1.07 (Heusser et al. 1979, Begemann et al. 1980) in Kirin (R_E ∿ 100 cm) which is similar to that in Dhajala (R_E ∿ 50 cm) and Keyes (R_E ∿ 30 cm), further support our conclusion that the $(^{22}Ne/^{21}Ne)_{sp}$ does not decrease much with size (for R_E > 25 and depth > 30 cm).

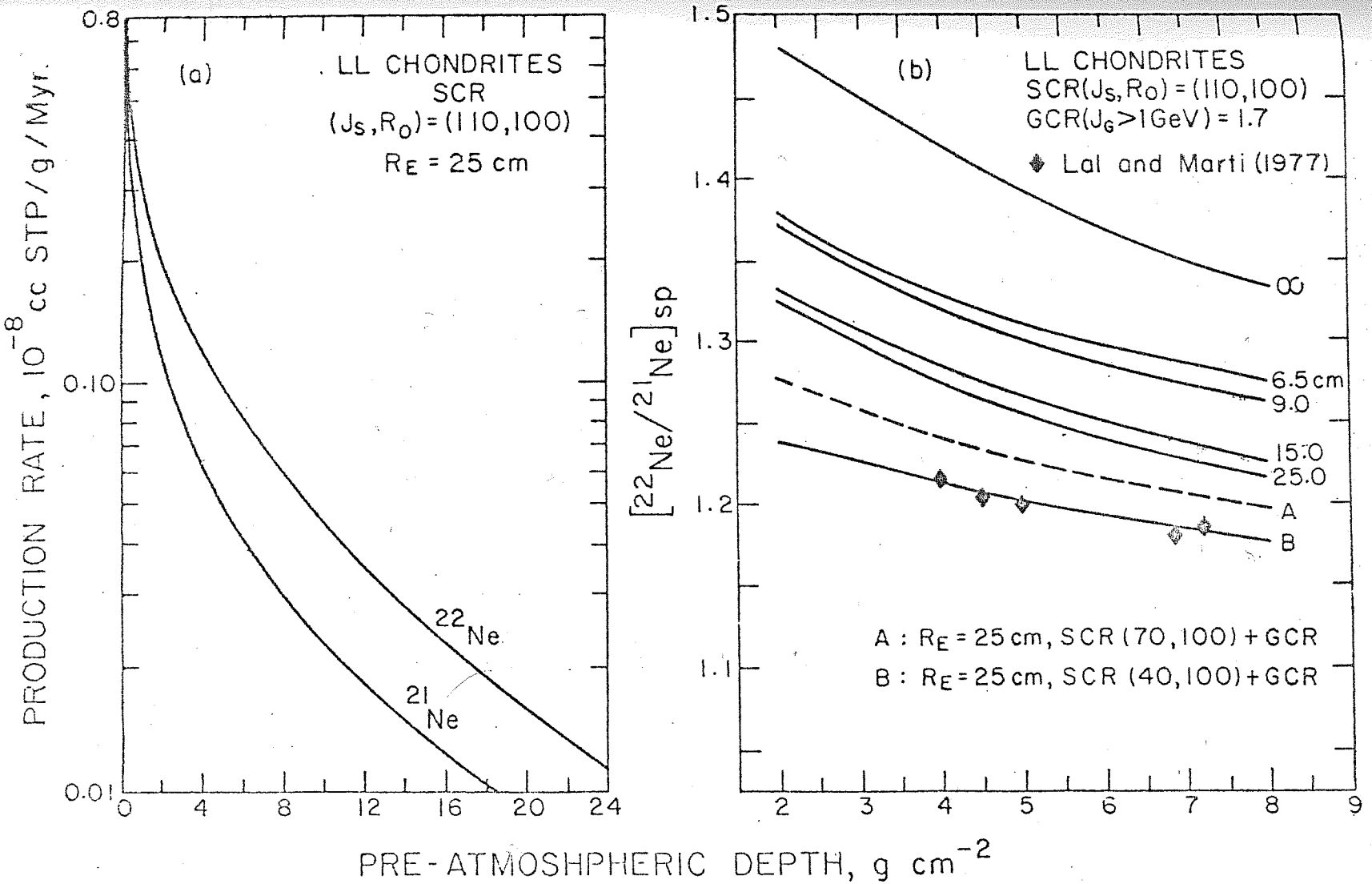

Fig.V.6 (a) Calculated SCR produced ^{21}Ne and ^{22}Ne profiles based on $(Js,Ro)=(110,100)$, (b) SCR and GCR produced $(^{22}Ne/^{21}Ne)_{sp}$ profiles in LL group chondrite of various sizes.

II. Production due to SCR :

For calculating ^{21}Ne and ^{22}Ne production depth profiles in chondrites we have chosen the SCR flux given by $(J_s, R_o) = (110,100)$, as discussed previously. The SCR production profiles of ^{21}Ne and ^{22}Ne for R_E = 25 cm are shown in Fig. V.6(a) and the total (SCR+GCR) production depth profiles of spallation neon ratio are shown in Fig.6(b) for meteorites of various preatmospheric sizes. In Fig.6(b) the measured $(^{22}Ne/^{21}Ne)_{sp}$ depth profiles in shallow regions of St. Severin meteorite due to Lal and Marti (1977) are plotted which seem to fit well with SCR parameters $(J_s, R_o) = (40,100)$, if the GCR flux of 1.7 protons/(cm^2.sec.4 π sr. > 1 GeV) is assumed to be the same even at the meteorite aphelion distances. This is the upper limit on SCR flux at meteoroid aphelion distances.

However, in shallow depth regions one cannot rule out the possibility of gas loss due to heating during ablation. From the analysis of rare gas data and cosmogenic particle track data it appears that the solar contribution is responsible for the observed high $(^{22}Ne/^{21}Ne)_{sp}$ in small meteorites like Narellan and Gopalpur having preatmospheric masses of 1.5 and 10 kg, respectively (Bhandari et al.1980).

(D) TRACK PRODUCTION RATE - $(^{22}Ne/^{21}Ne)_{sp}$ CORRELATION AND PARENT BODY EXPOSURE OF CHONDRITES:

It was pointed out by Bhandari et al. (1980) that TPM (Track Production rate expressed in tracks/cm^2.Myr) and $(^{22}Ne/^{21}Ne)_{sp}$ are correlated for different size meteoroids. The spallation neon ratio vs. TPM correlation curves based on the production profiles calculated in the present work and TPM profiles of Bhattacharya et al.(1973a)are given in Fig.V.7. The curve for R_E = 10 and 25 cm agree closely with the curves predicted by Bhandari et al. (1980) and the present calculations support the view, expressed therein, that TPM-$(^{22}Ne/^{21}Ne)_{sp}$ values in interior sample of small bodies (R_E=6-25 cm) are sufficient to determine the preatmospheric size of meteorites. However, for large bodies (R_E > 25 cm) the curves cluster together and overlap so that it is not possible to distinguish meteorites of different preatmospheric sizes. The present calculations are in agreement with measurements in Dhajala ($R_E \sim 50$ cm) chondrite (Gopalan et al.1977) and Kirin ($R_E \sim 100$ cm) chondrite (Heusser et al.1979) and in many other meteorites (Bhandari et al.1980a). The calculations also indicate that the forbidden zone of a single stage cosmic ray exposure extends beyond the regions indicated by Bhandari et al (1980). This extended forbidden zone is indicated as zone of parent body exposure in Fig.V.7.

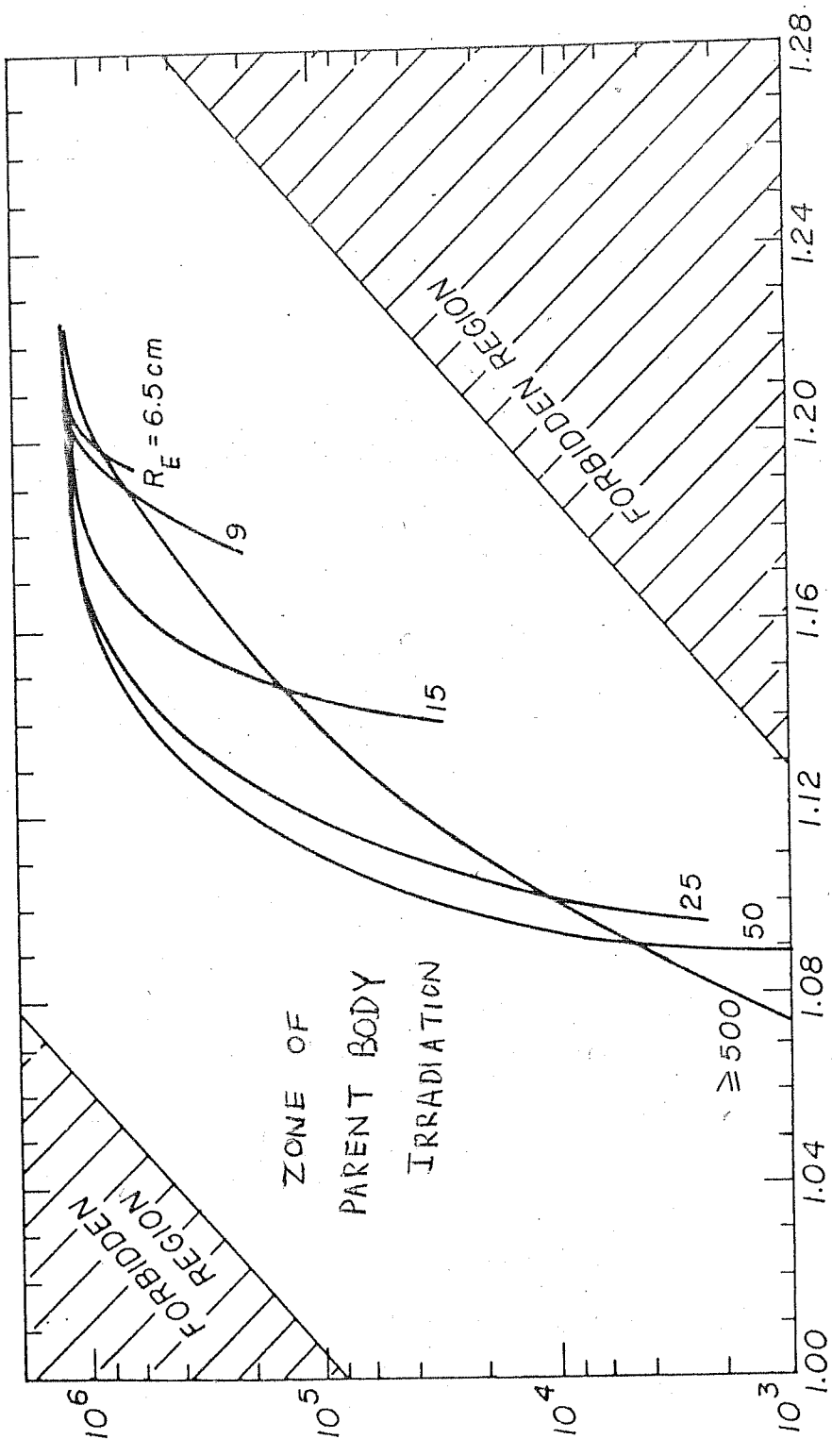

Fig.V.7 Track production rate vs. $(^{22}Ne/^{21}Ne)_{sp}$ correlation diagram. Forbidden regions are shown following Bhandari et al.(1980).

If we consier nearly 50 meteorites with aliquot samples analysed for rare gas contents and cosmogenic particle tracks (Bhandari et al.1980), we find that there are several chondrites which fall in this extended forbidden zone (or in the zone of parent body exposure, as indicated in Fig.V.7) of the TPM-$(^{22}Ne/^{21}Ne)_{sp}$ correlation diagram. The chondrites with measured neon isotopic ratio less than that expected for the shielding depth and size are also the ones with multiple cosmic ray exposure history. Nine such chondrites have lower $(^{22}Ne/^{21}Ne)_{sp}$ values than expected and are the definite cases of pre-irradiation. These are listed in Table V.3, together with the tracks and rare gas data. Since $(^{22}Ne/^{21}Ne)_{sp}$ is independent of the exposure age and its measurements are precise within $\pm 1\%$, the discrepancy between the calculated and measured values seems to be real. Based on the calculations presented in this work only a deep shielded exposure can result in lower neon ratios than the expected. Two possible geometries of deep shielded exposure can be visualised:

(i) exposure in Asteroidal regolith, and

(ii) exposure as a part of a large body (parent body), which undergoes collisional fragmentation in space.

In general, both these processes must be occurring frequently and the meteoroids are subjected to multiple exposure to cosmic rays, as pointed out by Wetherill (1979). Experimentally, they can be resolved only if two exposures produce comparable amounts of spallation neon but sifnificantly

different track densities. Since the track production rate (TPM) decreases steeply with the shielding depth, the track densities aquired during parent body irradiation period will, in general, be orders of magnitude smaller than that aquired during the last exposure period. Therefore, the TPM value will correspond to the final size of the meteoroid. Rare gas production rate and spallation neon ratio, on the other hand, decrease slowly with depth and hence, in case of multiple exposures, the data points will lie to the left of the predicted curves.

(E) CALCULATION OF MODEL AGES:

Under some plausible assumptions of shielding depth during parent body exposure, it is possible to calculate the cosmic ray exposure period in the parent body prior to the fragmentation, from the measured $(^{22}Ne/^{21}Ne)_{sp}$ by using two stage irradiation model.

For a meteorite with complex exposure history (2 stages of irradiation), we can write the following two equations:

$$T = T_2 + T_1 \times P_R \qquad \ldots.(V.1)$$

where T_2 = meteoroid exposure age as a small body, Myr.

T_1 = parent body exposure age, Myr.

T = exposure age if the meteoroid had simple exposure history with $P(^{21}Ne)$ equal to $P(^{21}Ne)_{T_2}$

TABLE V.3

Meteorites with complex exposure history

Meteorite	Size* R_E (cm)	Sample depth* (cm+)	$P(^{21}Ne)$ 10^{-8}ccSTP/g Myr.	$P(^{21}Ne)_m$ 10^{-8}ccSTP/g	$\left[\frac{^{22}Ne}{^{21}Ne}\right]_{sp}$ measured	Apparent exposure age, T (Myr)	$\left(\frac{^{22}Ne}{^{21}Ne}\right)_{sp}$ expected	Model exposure age (Myr) T_1	T_2
De Nova (L)	18	7	0.415	7.37	1.08	17.8	1.135	46	12.5
Gilgoin (H5)	27	8	0.403	1.86	1.04	4.65	1.110	17	2.6
Hayes Center(L)	22	17	0.470	10.70	1.04	22.8	1.110	98	12.8
Kesen (H4)	29	8	0.400	2.37	1.02	5.9	1.105	27	2.7
Roy (L5)	27	12	0.462	7.50	1.00	16.0	1.110	106	5
Temple (L)	13	12	0.440	9.90	1.07	22.5	1.125	65	15.4
Ulysses (H)	14	7	0.365	1.44	1.10	4.0	1.148	7.4	3
Walters (L6)	14	10	0.405	1.39	0.98	3.45	1.142	24.4	0.5
Wellman (H)	24	11	0.430	2.06	1.05	4.80	1.110	16	3

* These data are taken from the compilation of Bhandari et al. (1980)

\+ The errors on these estimates are about 15%

and $P_R = P(^{21}Ne)_{T_1} / P(^{21}Ne)_{T_2}$, i.e. the ratio of ^{21}Ne production during time T_1 to that during time T_2,

$$R_m = \frac{T_2}{T} R_2 + \frac{P_R \; T_1}{T} R_1 \qquad \ldots\ldots (V.2)$$

where R_m = measured $(^{22}Ne/^{21}Ne)_{sp}$

R_1 = Spallation neon ratio during T_1,

and R_2 = Spallation neon ratio during T_2

If depth of irradiation on the parent body is known or assumed to be about 100 cm ($P_R = 0.15$), then R_1 and R_2 from Fig.V.2, 3, 4 can yield the values of T_1 and T_2. These estimates are given in Table V.3.

As mentioned earlier, R_1 and R_2 are quite insensitive to α value and hence, the departure of the measured $(^{22}Ne/^{21}Ne)_{sp}$ from expected $(^{22}Ne/^{21}Ne)_{sp}$ cannot be just explained by the choice of parameters used in the calculations. Thus, a complex irradiation seems to be the only plausible way in which such low ratios can arise. Although, in the above calculations we have assumed the irradiation depth in the parent body to be 100 cm, it is possible to deduce the actual shielding depth if additional measurements of a long-lived radionuclides like ^{53}Mn or ^{26}Al in the same aliquot samples are made. Unfortunately, such data are not available at present.

(F) SUMMARY:

In this chapter we have calculated the depth and size dependent production of cosmogenic ^{21}Ne and $(^{22}Ne/^{21}Ne)_{sp}$ which were not available heretofore. From the track production rate (TPM) vs. $(^{22}Ne/^{21}Ne)_{sp}$ correlation diagram and the data on aliquot samples of several meteorites it is seen that there are several meteorites with Ne ratio less than 1.06 and those expected for their shielding depth and size and these meteorite data are interpreted to be due to multiple exposure to cosmic rays. A model for two stage exposure history is developed and model exposure ages are obtained for such cases.

CHAPTER-VI

ABLATION OF METEORITES IN THE EARTH'S ATMOSPHERE

A. INTRODUCTION:

There are several processes which occur in the interplanetary space and earth's atmosphere resulting in change of the production rates of nuclides in meteorites. The most important of these are (i) fragmentation of meteoroids and their parent bodies in the collisional events in the interplanetary space, leading to multiple exposure of the meteoroids to the cosmic rays,(ii) erosion due to micro-meteoroid impacts leading to secular changes in the shielding conditions of meteoroids and, (iii) the ablation of meteoroids during their entry into the earth's atmosphere. The effects of these processes on cosmic ray exposure history and shielding conditions have to be considered adequately before the depth and size dependence of nuclide production rates are to be evaluated.

The time scales involved in collisions of meteorite parent bodies are large and these are of the order of meteorite exposure ages, because during the deep shielded exposure of meteoroids on their parent bodies the cosmic ray effects are negligible and the cosmogenic products seen in the meteorites are largely due to their recent exposure to cosmic rays. Since the cosmic ray effects are confined to first a few meters ($\sim$5 meters) of depth in large parent bodies, the multiple exposure effects can be observed in

meteorites if the production of some stable and radioactive nuclides during their parent body exposure are comparable to those produced in their recent exposure period. From the study of estatistical fragmentation process in the catastrophic cratering events (Wetherill, 1980) large number of meteorites are expected to have undergone multiple exposures and the method of identification of such meteorites (from neon isotopic compositions) has been discussed in Chapter V.

The erosion rate due to micrometeorite impacts is quite small and it is independent of the hardness of the rocks (Geiss and Oeshger 1960). The erosion rate of chondrites is less than 1 mm/Myr (or $\lesssim$ 0.35 g.cm.$^{-2}$Myr^{-1}) (price et al.1967, Lal et al.1969). During exposure duration of meteoroids, which is of the order of a few Myr hardly upper 1 to 2 cm layer of matter is eroded and the affected regions are, usually, lost during the atmospheric ablation of these meteoroids. Unlike meteorites, the moon samples have well preserved top layers (since they are brought safely to the earth by astronauts) and the effect of erosion in true production rates of cosmognic nuclides in these top layers is significant and is discussed in Chapter-IV.

Atmospheric ablation is the major physical process leading to a significant mass loss (varying from $\sim$15% to $\sim$ 99.9%) resulting in large uncertainties in the information the preatmospheric shape, size and the shielding depths of meteorite samples. Due to the large aerodynamic stresses,

the meteoroids usually undergo fragmentation resulting in uncertainty in the relative shielding depths of the fragments. We discuss here the ablation phenomena in detail.

Meteoroid interaction with the earth's atmosphere is random and unpredictable. When they enter in the atmosphere with high velocity and glow due to ablation, their arrival is noted. Due to aerodynamic drag they are slowed down quickly and due to the atmospheric friction the meteoroid surface melts and evaporates resulting in the loss of mass, and information on their arrival direction and velocity. There are only three meteorite with their bright fireball trails photographed by camera networks and hence their preatmospheric velocities and heliocentric orbits are known. From the analysis of strewnfield data of several meteorite falls, Simonenko (1978) has tried to derive their orbital elements for a set of possible preatmospheric velocities. If the preatmpspheric velocities can be deduced for these meteorites their heliocentric orbits can be deduced, which are important in understanding about their origin and evolution of their population. In the present chapter an attempt has been made to deduce the preatmospheric velocities of some meteorites from their ablation characteristics.

Frictional heating, subsequent melting and rapid evaporation is the main cause of mass ablation. The classic work of Whipple and Hawkins (1959) marked the beginning of the theoretical treatment of the ablation proces. They

formulated the basic equations of the meteoric process and showed that the ablation depends sensitively on the heat transfer coefficient. Opik (1958) had discussed extensively the physical processes occurring during ablation. He showed that the ablation depends on entry velocity of meteoroids. Bronshtein(1964) also discussed the theoretical and aero-dynamical problems involved.

The recent work of Baldwin and Sheaffer (1971) is based on cumulative data obtained by simulation experiments carried out at NASA's AMES Research Center. The calculations consider the ablation by vapourisation, liquid runoff and surface spalling due to thermal stresses. The relative importance of these modes of mass loss depends on meteoroid surface conditions, the size and velocity.

An approximate and empirical ablation model of ReVelle (1979) in which the local Knudsen number, Kn (defining the relative rarification of air) is taken as a criterion in choosing the dominating mode of heat transfer gives better agreement with the experimental data on Lost City and Pribram and Innisfree, provided the assumptions made by ReVelle regarding the initial and final masses of the meteorites are acceptable. However, there still remain several short-comings and no satisfactory model exists as will be discussed later.

Since Baldwin-Sheaffar model is more analytical and is based on physical and aerodynamical parameters measured in simulation experiments, we basically follow this model here. In the present chapter we examine the Baldwin-Sheaffer model in the light of experimental data on meteorite ablation and suggest some possibilities of modifications. Using the model we obtain the preatmospheric velocities of meteorites for which ablation data are available from the cosmogenic particle tracks and rare gas studies (Bhandari et al. 1980).

(B) CALCULATION OF TRAJECTORY AND MASS ABLATION:

We consider here the high velocity entry of a large meteoroid body in the earth's atmosphere. The meteoroid shapes are irregular but for simplicity, in the present calculations, they are assumed to be spherical in shape. The fragmentation has been considered by Baldwin and Sheaffer (1971) in detail and here we confine to a single body motion without fragmentation. The trajectory, the motion and mass loss of a non-fragmenting meteoroid during atmospheric flight at any time t, are described by following equations (Whipple and Hawkins 1959, Baldwin and Sheaffer. 1971).

(i) The equation of motion :

$$m \frac{dv}{dt} = -\frac{1}{2} C_D v^2 \rho_a \frac{A}{m} + g \sin\theta' \qquad \ldots.(VI.1)$$

(ii) The equation of mass loss:

$$\frac{dm}{dt} = \frac{1}{2} C_H \rho_a v^3 \frac{A}{Q} \quad \ldots\ldots (VI.2)$$

(iii) The equation of angle of elevation:

$$\frac{d\theta'}{dt} = - \frac{g}{v} \sin\theta' \quad \ldots\ldots (VI.3)$$

(iv) The equation for altitude (h) :

$$\frac{dh}{dt} = v \sin\theta' \quad \ldots\ldots (VI.4)$$

where v = instantaneous velocity at time t,

C_D = aerodynamic drag coefficient,

C_H = total heat transfer coefficient,

θ' = angle of elevation of velocity vector,

g = acceleration due to gravity,

m = instantaneous mass of the meteoroid,

ρ_a = atmospheric density,

A = cross-sectional area,

and Q = heat of ablation

All the above four differential equations are inter-dependent and they are solved simultaneously for mass, velocity and angle of elevation at any time, t, given the initial entry velocity, mass and angle. The aerodynamic constants C_D, C_H are evaluated at all the points on the trajectory.

Unlike Baldwin and Sheaffer (1971), in the present treatment we consider time as the independent parameter. The equations are integrated assuming that the meteoroid properties, the aerodynamic constants and the atmospheric density remain constant over the time interval of 0.01 sec used for calculation i.e. first order approximation is used. It is found that smaller time steps do not introduce any significant changes in the trajectory and mass ablation. The starting height is taken to be 100 km.

The aerodynamic coefficients C_D, C_H and the heat of ablation are intricate functions of meteoroid properties, atmospheric density, meteoroid mass and velocity, as discussed below.

The drag coefficient C_D and the heat transfer coefficient C_H are calculated following the procedure described in Appendix of Baldwin and Sheaffer (1971). The total heat transfer coefficient (C_H) depends on continuum flow heat transfer coefficient (C_{Hu}) by

$$C_H = C_{Hu}\, e^{-C_{Hu}} + (1-e^{-C_{Hu}})^2 \qquad \ldots\ldots (VI.6)$$

where

$$C_H = C_{Hcvu} + C_{HR}$$

The convective heat transfer coefficient (C_{Hcvu}) is given by

$$C_{Hcvu} = C_r\, v^p \{\sigma_1 + (1-\sigma_1) f(v, r, T, W)\} \qquad \ldots\ldots (VI.6)$$

where C_r = Constant dependent on size, r, of the meteor body

P = aerodynamical constant (Baldwin and Sheaffer, 1971)

f = $f(v,r,T,W)$ is a known function of velocity v, radius, r, vapour temperature, T, and total mass loss rate $W(T)$.

From equation (VI.6) it can be shown that the convective heat transfer coefficient depends sensitively on P, an aerodynamical constant.

The radiative heat transfer coefficient (C_{HRT}) for an optically thin gas cap layer is given by

$$C_{HRT} = C_{Heu} + C_{Hnu} \qquad \ldots\ (VI.7)$$

where C_{Heu} = The equilibrium radiative heat transfer coefficient for an optically thin gas-cap and is given by

$$C_{Heu} = 41.6\, \rho'^{0.8} \left[\frac{v}{10^4}\right]^{P_1} \exp\left[-\frac{7.2\times10^{-8}}{\rho' r}\right], \text{ for } v \geqslant 13.7 \text{ km/sec}$$

$$\text{or} \quad = 1.58 \left[\frac{v}{10^4}\right]^{P_2} r \exp\left[-\frac{7.2\times10^{-8}}{\rho' r}\right], \text{ for } v \leqslant 13.7 \text{ km/sec}$$

$$\ldots\ (VI.8)$$

where $P_1 = 2.05$ and $P_2 = 12.45$.

And, the non-equilibrium radiative transfer coefficient, C_{Hnu}, is given by

$$C_{Hnu} = 0.6\times10^{-6}\ \frac{1}{\rho'^{1.5}}\left[\frac{v}{10^4}\right]^{p_3}\ \exp\left[\frac{-7.2\times10^{-8}}{\rho' r}\right],\ \rho' \geq 10^{-3}$$

$$\text{or} = 0.6\times10^{-3}\left[\frac{v}{10^4}\right]^{p_3}\ \exp\left[\frac{-7.2\times10^{-8}}{\rho' r}\right],\ \rho' \leq 10^{-3}$$

.... (VI.9)

where $\rho' = \frac{\rho(h)}{\rho(o)}$ & $p_3 = 4.0$, Baldwin and Sheaffer (1971)

Then, the total radiative heat transfer coefficient (C_{HR}) is given by

$$C_{HR} = C_{HRMAX}\cdot \exp\left\{\frac{-2C_{HRT}}{C_{HRMAX}}\right\} + C_{HRMAX}\left\{1 - \exp\left[\frac{-C_{HRT}}{C_{HRMAX}}\right]\right\}^2$$

....(VI.10)

where C_{HRMAX} is an aerodynamic constant (Baldwin and Sheaffer, 1971) and is equal to 0.1363.

The heat of ablation Q is obtained by

$$Q = \frac{C_H \rho_a v^3}{2W_s} \qquad \text{....(VI.11)}$$

where W_s = total mass loss rate per unit meteoroid surface area due to vapourization, liquid flow and spalling.

In the present calculations only ordinary chondrites (chondrites and achondrites) are considered. For ordinary chondrites the main process of mass ablation is due to vapourization and liquid run off. The mass loss due to spallation is usually negligible. For lower entry mass meteoroids convective heating and for higher mass meteorites the radiative heating dominate.

(C) RESULTS OF THE CALCULATIONS AND COMPARISON WITH METEORITES DATA :

There are only three meteorites viz. Pribram, Lost City and Innisfree for which the velocity and angle of entry and hence heliocentric orbits are known (Ceplacha 1961, McGrosky 1971 and Halliday et al.1978). Also, from cosmogenic particle track density and rare gas measurements their preatmospheric masses are known (Bhandari et al.1980, and Goswami et al. 1979). Table VI.1 summarises data on these meteorites. In estmating the ablation suffered by these meteorites, it is assumed that the recovery of meteorites fragments is nearly complete, although recently Bagolia et al. (1977) have shown that the most probable recovery efficiency in a meteorite shower is about 60%. Since the preatmospheric mass is deduced from the measured particle track production rates and in some cases from track density gradients, the estimated are reliable within $\sim$ 20%. If ΔA is the uncertainty in deduced ablation A and ΔMo is the uncertainty in the estimated preatmospheric mass

of a meteoroid, we can write

$$\frac{\Delta A}{A} = \frac{\Delta Mo}{Mo} \times \frac{(1-A)}{A} \qquad \ldots\ldots(VI.12)$$

From above equation it is seen that for $\sim$ 20% uncertainty in A, the $\Delta Mo/Mo$ value varies from $\sim$3% for A = 15% to $\sim$ 20% for A = 99%.

Fig.VI.1 shows the comparison of meteorite ablation data and the calculations based on Baldwin and Sheaffer(1971) model. While the Baldwin-Sheaffer model calculations agree in case of Pribram, the model grossly disagrees with the data on Lost City and Innisfree meteorites. The predicted ablation of Lost City meteorite of 30% is small compared to experimentally determined ablation of (75$\pm$24)%. Although the error in ablation estimate is large, certainly the ablation is greater than 50% (Bhandari et al.1980). Baldwin-Sheaffer model underestimates the ablation of low entry velocity meteorites. Unfortunately, there is no other meteorite with known preatmospheric velocity towards lower end of velocity scale to compare, but for Innisfree meteorite.

In case of Innisfree meteorite, whose preatmospheric entry velocity and angle were similar to those of Lost City meteorite, the model predicts initial mass of $\sim$25 kg. This is much lower than the estimated mass of 350$\pm$100 kg based on particle tracks and rare gas data (Goswami et al.1979). The case of Innisfree looks to be grossly anomalous. One

TABLE-VI.1

Basic data on Meteorite Orbits

Meteorite	Date of fall	Recovered mass (kg)	M_o (kg)	V_o (km/sec)	θ (deg)	a (a.u.)	e	i (deg)	References
Pribram (LL)	7 April '59	9.5	200 ± 80	20.9	43	2.42	0.67	10	a,b
Lost City (H)	3 Jan. '70	16.5	65 ± 32	14.2	38	1.88	0.41	12	a,c
Innisfree (L)	6 Feb. '77	5	350 ± 180	14.5	67	1.80	0.44	12	a,e
St.Severin (LL)	27 June '66	271	372 ± 14	14.0	17	1.94	0.49	1.1	a,f

a) Bhandari et al. (1980)
b) Ceplacha (1961)
c) McCrosky et al. (1971)
d) Goswami et al. (1979)
e) Halliday et al. (1978)
f) Nordemann et al. (1970)

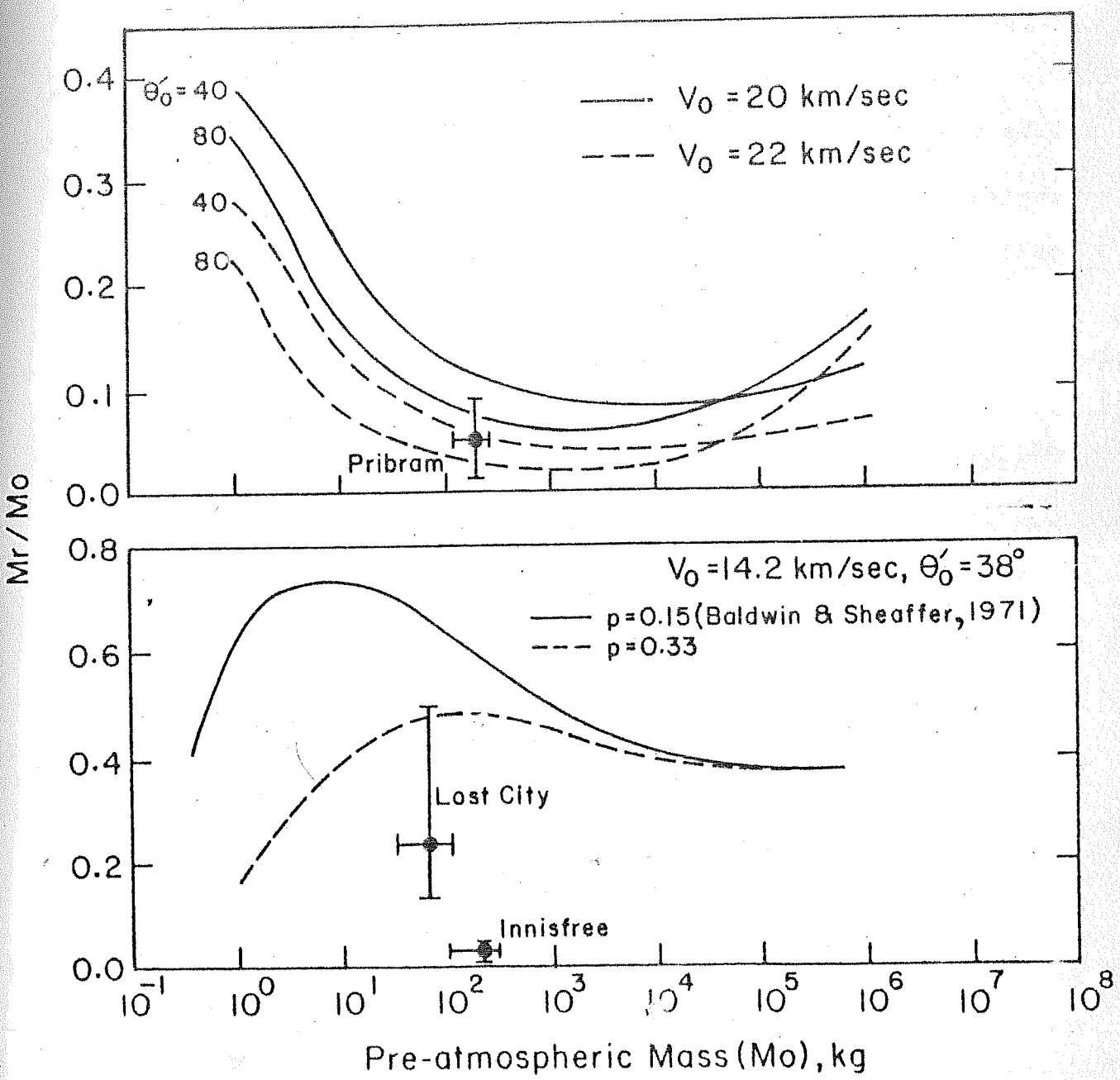

Fig. VI.1 Comparison of ablation data on Pribram, Lost City and Innisfree with the calculations based on Baldwin and Sheaffer (1971) model and the modified calculations discussed in the text.

possibility is that the meteorite recovery is far from complete, although Halliday et al. (1978) cliam the complete recovery. Another possibility is that the meteorite had complex exposure history resulting in over-estimation of the preatmospheric mass. In the present discussion, this anomalous case of Innisfree is excluded.

Many parameters which go into the model calculations are uncertain. The parameters used in the Baldwin-Sheaffer model are determined by laboratory simulation experiments at NASA/Ames Research Center. The ablation depends sensitively on the total heat transfer coefficient (C_H); which constitutes of two modes viz. convective and radiative which in turn depend on velocity through aerodynamical parameters p, p_1, p_2 and p_3. Although these parameters are determined from numerous laboratory simulation experiments, the validity of their values when applied to large meteoroid bodies entering into the atmosphere are to a certain extent doubtful.

(D) MODIFICATION OF BALDWIN-SHEAFFER MODEL :

To match the ablations of Lost City and Pribram meteorites simultaneously we have tried to investigate the dependence of ablation on certain crucial parameters p, p_1, p_2 and p_3 in expressions for convective and for radiative heat transfer coefficients. The ablation of Lost City meteorite is assumed to be 53% . The ablation of Lost City meteorite given by ReVelle (1979) is 67% which is higher than 53% ablation adopted in our calculations.

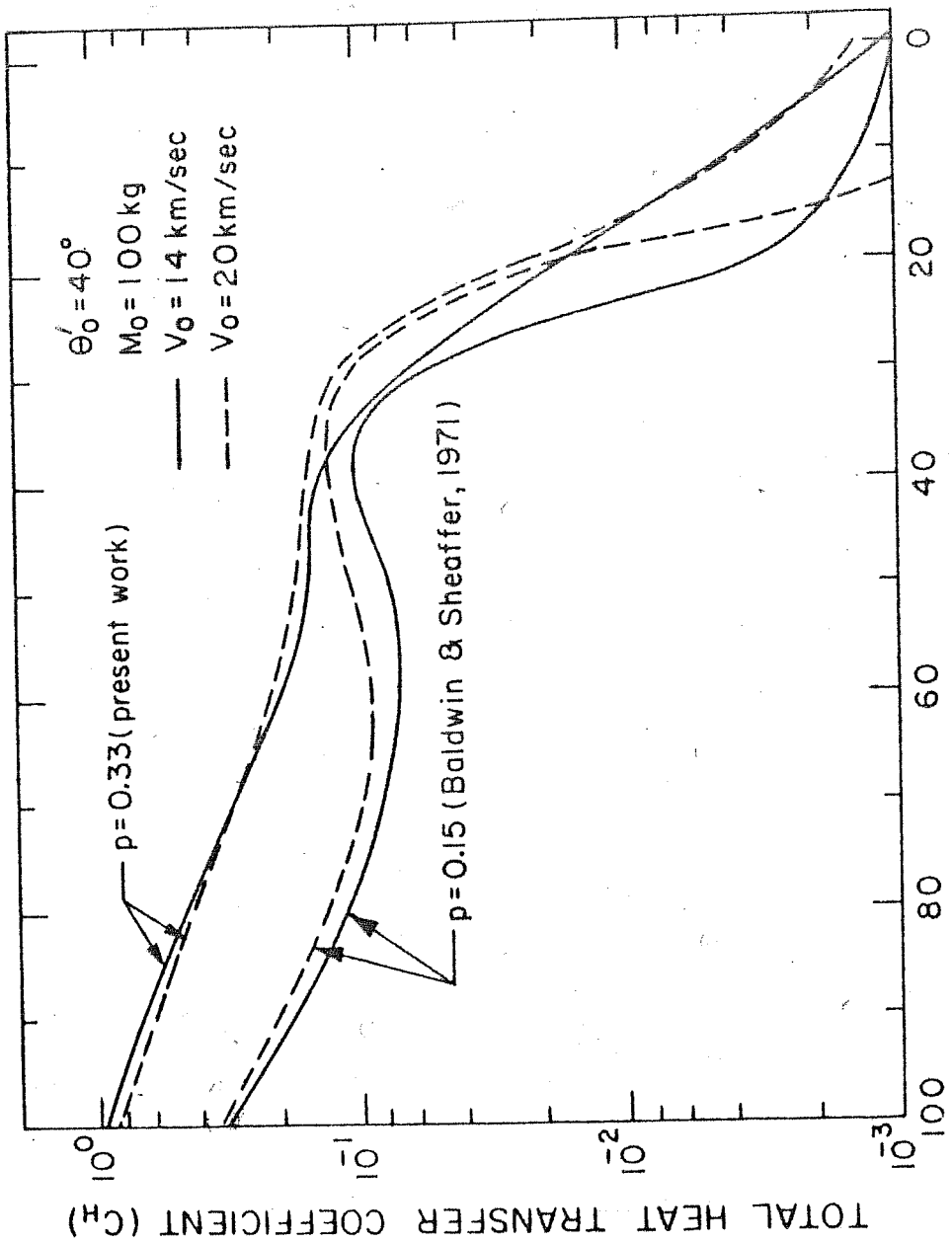

Fig. VI.2 Altitude dependence of total heat transfer coefficient (C_H) for M_0=100 kg, $\theta_0' = 40°$ and V_0=15 and 20 km/sec based on Baldwin-Sheaffer (1971) model and modified calculations discussed in the text.

Since for smaller velocities, the convective heat transfer mode dominates, it is obvious that increase in convective heating for smaller bodies can result in higher mass ablation. This can be achieved if the value of the parameter P appearing in the equation for convective heat transfer coefficient (Equation VI.6) is 0.33 instead of 0.15, given by Baldwin and Sheaffer. This value, according to Baldwin (personal communication, 1981) is reliable within a factor of two. The radiative heat transfer coefficient is not very sensitive to parameters p_1, p_2 and p_3. Even a factor of 4 increase in p_1 and a factor of 2 increases in p_3 (p_2 is calculated by equating the C_{Heu} obtained by two equations (VI.8) for velocity V = 13.7 km/sec), the calculated ablation of Lost City meteorite can be increased to only 33%. Thus, it is necessary to change only p . This is adjusted to 0.33 in the following calculations & other parameters are kept unchanged.

In Fig.VI.2, the total heat transfer coefficient as a function of altitude for initial velocities of 14 and 20 km/sec and for 100 kg initial mass calculated by Baldwin-Sheaffer model for the two values of p are shown for comparison. At high altitudes, the total heat transfer coefficient with P = 0.33 is higher than Baldwin-Sheaffer value. In the altitude range of 40-10 km, in which most of the ablation occurs, the total heat transfer coefficient is about a factor of 2 above the heat transfer coefficient with P = 0.15. This is true for both the low and high entry velocities.

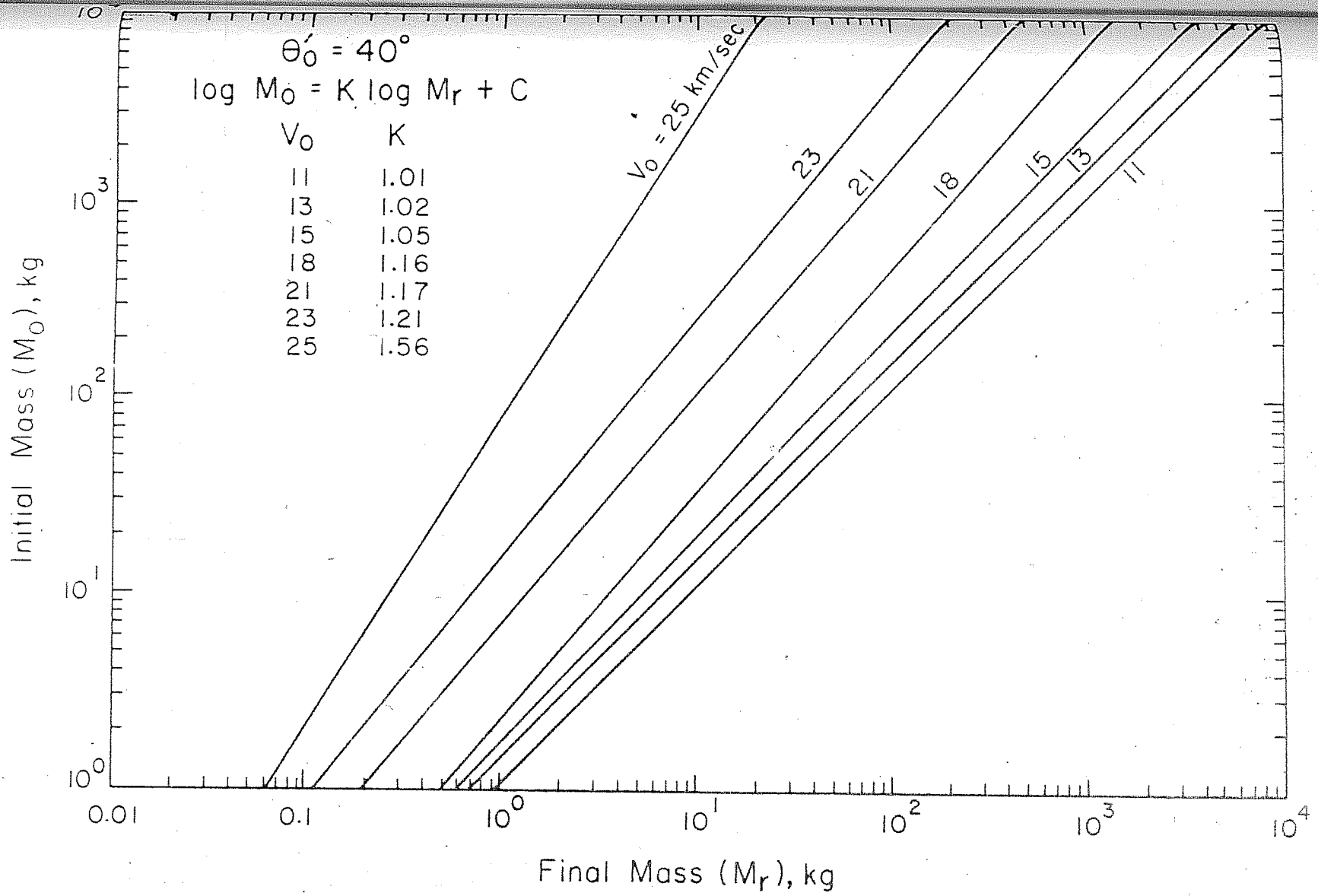

Fig. VI.3 Ablation dependence on preatmospheric velocity of ordinary chondrites for typical angle of entry 40°.

The results of calculations are shown in Fig.VI.3. For entry velocities ranging from 11 km/sec to 25 km/sec the surviving mass for various preatmospheric masses are shown. It is interesting that such elaborate and intricate calculations ultimately lead to a simple relation between surviving mass, M_r, and the preatmospheric mass, M_o. The curves are plotted for typical entry elevation angle of 40°. It is found that the uncertainty in the initial angle of entry ($10 \leq \theta \leq 80°$), leads to an uncertainty of $\sim \pm 0.5$ km/sec in entry velocity. From Fig.VI.3 the relation between M_r and M_o for various entry velocities is described by equation

$$\log M_o = K \log M_r + C \qquad \ldots.(VI.12)$$

where K and C are constants and function of V_o. The value of K and C are given in a table in set in Fig.VI.3.

According to the calculations, the ablation for a given mass increases rapidly with velocity. For $M_o \sim 1$ kg, the ablation suffered for V_o = 25 km/sec is $\sim$ 16 times more than that for V_o = 11 km/sec. The corresponding ablation value for $M_o = 10^4$ kg are 99.9 and 90%. At higher entry velocities the ablation does not depend very much on the mass (M_o) whereas at lower entry velicities the dependence is quite significant.

(E) PREATMOSPHERIC VELOCITIES OF METEORITES:

One of the important applications of an ablation model is to obtain the preatmospheric velocity distribution of

TABLE-VI.2

Preatmospheric Velocities of meteorites

Meteorite	Abbrev. used	Class	M_r (kg)	Ablation (%) (Bhandari et al.1980)	Preatmospheric Veolcity(V_o),km/sec Present work	Rajan et al. (1978)	Millman (1969)
Adrian	ADR	H	22.8	74 ± 7	$16^{+1.5}_{-0.5}$	14.8 ± 1	-
Ambapur Nagla	AMB	H	6	91^{+8}_{-15}	19 ± 2	-	-
Akaba	AKB	L	11	96^{+3}_{-12}	20 ± 2	-	-
Andura	AND	H	17	$82+5$	17.5 ± 1	16.5 ± 1	-
Archie	ARC	H	5	94 ± 5	20 ± 2	-	17.7 ± 2.0
Aztec	AZT	L	2.8	84 ± 8	18 ± 1.5	-	-
Barwell	BAR	L	46	35 ± 12	13 ± 1	-	-
Binda	BIN	HOW	6	84 ± 8	18 ± 2	-	-
Chasslgny	CHA	ACH	4	89 ± 6	19 ± 1	-	-
Cynthiana	CYN	L	6	78 ± 11	17 ± 2	-	-
Dhajala	DHA	H	65	95^{+4}_{-8}	20.5 ± 1.5		-
Finney	FIN	L	10	63 ± 11	15 ± 1	13.8 ± 1.3	-
Harleton	HAR	L	8.4	90 ± 5	19 ± 2	-	-
Hugoton	HUG	H	322	58 ± 13	14.5 ± 1	-	-
Kapoeta	KAP	HOW	12.6	56 ± 14	14 ± 2	12.3 ± 1.1	-
Keyes	KEY	L	136	58 ± 13	14.5 ± 1	13 ± 1	-
Kiel	KIE	L	0.74	87 ± 6	17 ± 2	-	-
							-
Lost City	LOS	H	16.5	73 ± 24	16^{+1}_{-2}	14.7 ± 1.2	-
Madhipura	MAD	L	0.94	75 ± 10	15 ± 2	12.3 ± 1.1	-
					$+2.5$		
Norton County	NOR	AUB	1250	69 ± 15	$15.5_{-1.0}$	-	16 ± 2.0
Pribram	PRI	H	9	95 ± 3	21 ± 2	-	20.9 ± 0.1
St.Severin	STS	LL	372	27 ± 3	12.2 ± 0.5	-	-
San Juan Capstrano	SAN	H	0.05	99.5	25 ± 0.5	-	-
Shalka	SHA	DIO	4	97 ± 1	23 ± 0.5	-	-
Utzenstorf	UTZ	H	3.2	66 ± 10	14.5 ± 1.5	14.2 ± 3	-

meteorites to see if the meteoroids have any preferential velocity. An attempt was made by Bhandari (1969a) to deduce preatmospheric velocities from mass ablation based on Opik's meteor theory. The Baldwin and Sheaffer model is more sophisticated and we use this model to deduce the preatmospheric velocities. To deduce the preatmospheric velocities of the meteorites, which are listed in Table VI.2, we have plotted ablation as a function of recovered mass for various entry velocities (Fig.VI.4). The angle of entry has been assumed to be 40°. The ablation data of the meteorites are plotted. From the theoretical curves it is seen that the minimum amount of ablation a meteorite can suffer is 15% (V_o=11 km/sec and $M_r = 10^3$ kg) and for larger recovered masses, the ablation is by and large constant and depends solely on preatmospheric velocity. Towards lower end of the recovered mass scale the ablation range narrows down (from 50% to 99%). Although similar velocity dependent ablation curves were obtained by ReVelle (1979) based on his empirical model, the minimum ablation predicted by his model is 35%, which is much above the observed ablation of 27 ± 3 % for St.Severin chondrite. Our model calculations do incorporate the data on St.Severin chondrite and the deduced preatmospheric velocity of 12.2 ± 0.5 km/sec fairly agrees with that deduced by Nordemann et al. (1970) of 14 ± 1 km/sec. Velocities of most of meteorites can be estimated within the uncertainty of ± 2 km/sec. The deduced velocities are given in Table VI.2.

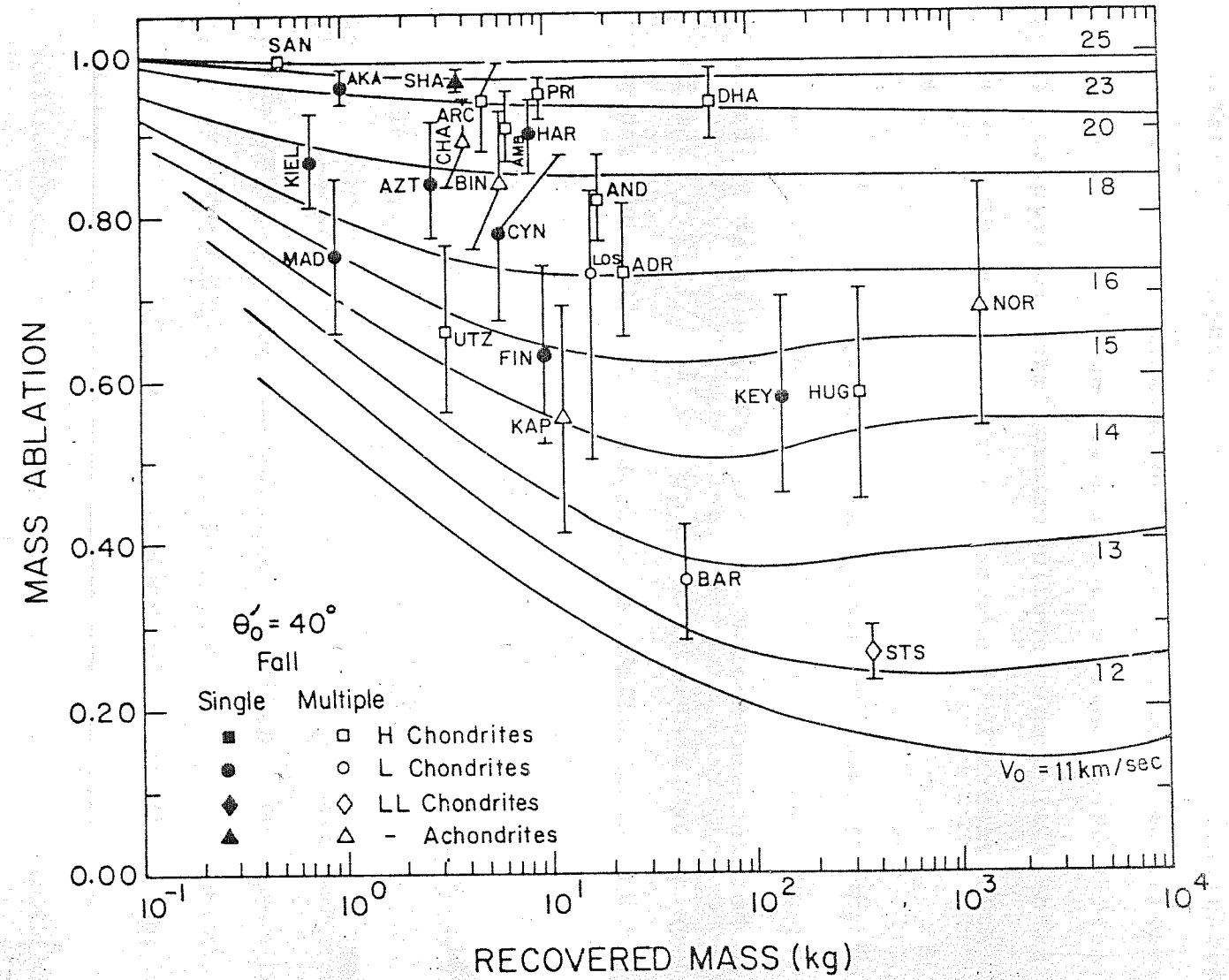

Fig.VI.4 Ablation as a function of recovered mass for typical angle of entry 40° and comparison with data on meteorites with known ablation (Bhandari et al.1980).

The velocity histogram of these meteorites is shown in Fig.VI.5. The velocity interval of 2 km/sec is chosen since, as discussed above, the velocities of most of the meteorites are known within ±2 km/sec. The distribution can be best represnted by a curve shown in the figure which resembles to the one obtained by Millman (1969) from about 250 meteorites orbit distributions. There is a sharp cut off at V_o = 11 km/sec and the frequency falls down with increasing V_o.

The preatmospheric velocities of some of the meteorites deduced by Rajan et al. (1978) based on empirical model of ReVelle (1979) and the velocities deduced by Millman (1969) from the observed radiants are given for comparison in Table VI.2. The velocities given by Rajan et al. are systematically lower than those deduce here, though they agree within the uncertainties given. The velocities of Archie and Norton County given by Millman (1969) agree with those given by us within the errors.

Several of the meteorites listed in Table VI.2 are falls and the approximate time of fall and the co-ordinates of the place of fall are known. Additional information of the radiant of showers or strewnfield along with the deduced preatmospheric velocities can be used to deduce the heliocentric orbits of these meteorites. Based on similar approaches Ballabh et al.(1978) have calculated the orbit

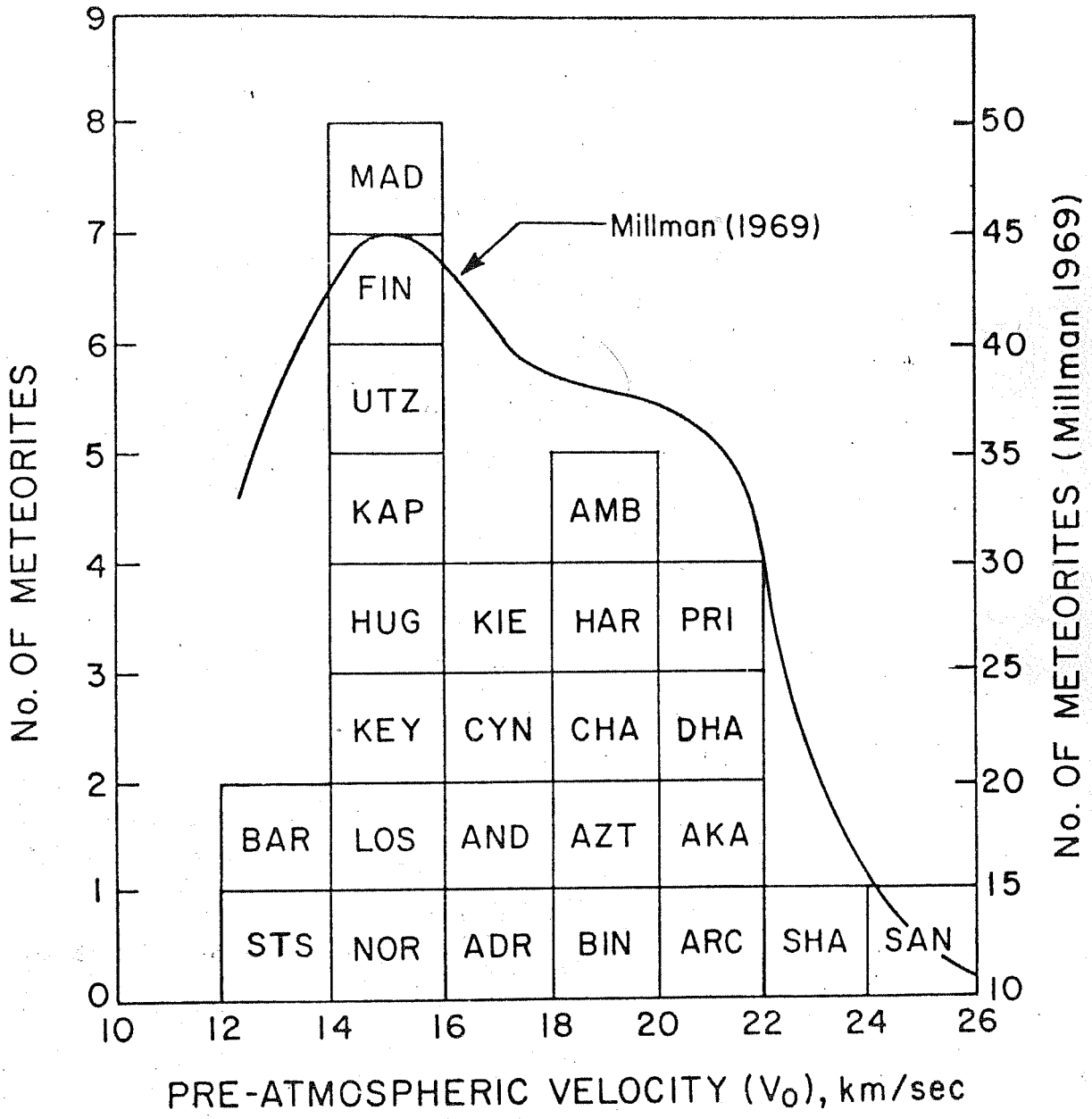

Fig.VI.5 Velocity Histogram of Meteorites.

of the Dhajala chondrite, Millman (1969) calculated the orbits of several meteorites.

(F) SUMMARY:

Baldwin and Sheaffer (1971) does not predict the observed ablation of Lost City meteorite and in general it predicts lower ablation for low velocity meteorites. The observed ablation of Pribram meteorits is correctly predicted by the model. Some of the parameters used in this model have large uncertainties. It has been found that the parameter p appearing in the equation of convective heat transfer coefficient is the most sensitive of all these parameters and according to Baldwin (personal communication, 1981) is better known within a factor of 2. To obtain a better match with Lost City and other meteorites, we have recalculated ablation with p = 0.33 and based on these curves, we have determined the preatmospheric velocities of meteorites. The preatmospheric velocity distribution deduced from the revised model shows a similar behaviour to that obtained by Millman (1969). The velocities deduced in the present calculations are accurate within ± 2 km/sec and incorporate the observed ablation of St. Severin meteorite.

CHAPTER VII

CONCLUSIONS

An attempt has been made in this thesis to determine the production rates of several cosmogenic nuclides and to assess the long-term characteristics of the SCR and GCR particles in the interplanetary space. The following conclusions are drawn on the basis of this work.

(A) Production rate of cosmogenic nuclides in chondrites :

As a result of this work and some earlier attempts, we now have a fair idea of the production profiles of several radionuclides in chondrites. Based on ^{26}Al depth profile in Dhajala chondrite, we have now deduced the energy spectrum of nuclear active particles as a function of shielding depth in a 50 cm radius body which can be used to calculate the depth profile of production rates of many other cosmogenic nuclides, provided the proper excitation functions are available, using a suitable model. Using Reedy and Arnold (1972) model, the depth profiles of ^{22}Na, ^{10}Be, ^{21}Ne, ^{22}Ne, etc. have been calculated. Such calculations when compared with measured profiles can give information on the GCR intensity over about 3 to 4 mean-lives of a radionuclide, or on the exposure history of meteorites using stable rare gas isotopes, like ^{21}Ne and ^{22}Ne etc. A comparison of measured ^{22}Na depth profile in Dhajala chondrite with the calculated profile indicates that the solar cycle modulation effect on

^{22}Na is quite significant. To assess the effect of higher GCR fluxes in the interplanetary space during solar cycle 20 on ^{22}Na activity in meteoroids, the annual average GCR fluxes during solar cycle 20, deduced from the available satellite measurements of GCR spectra, show that only about half of the measured excess ^{22}Na activity can be accounted for solar cycle modulation in the ecliptic plane. In view of the orbital parameters of Dhajala meteoroid, the residual excess indicates higher GCR fluxes at helio-latitude of $> 15°$ during the cycle 20, as earlier shown by Bhandari et al. (1979) and is supported by the present data.

Secondary neutrons constitute very important part of the nuclear active particles and the information on their flux and energy spectrum are important in calculation of nuclides produced by these neutrons, such as ^{21}Ne, ^{22}Ne (E_T = 2.7 and 0.5 MeV, respectively. See table I.1), and ^{60}Co, ^{59}Ni and ^{36}Cl produced by the thermal/epithermal neutron capture reactions. Determination of ^{60}Co depth profile in Dhajala has enabled us to deduce the epithermal (0.5-300 eV) neutrons slowing down density as a function of depth. This density varies by a factor of $\sim$ 13 from 6 cm to 50 cm depth(0.005 neutrons/ cm^3.sec. at depth of about 6 cm to 0.084 neutrons/ cm^3.sec. at the center of 50 cm radius chondritic body). The comparison of the ^{60}Co depth profiles in 50 cm and 100 cm (Kirin) chondrites and in a 100 cm carbonaceous chondrite (Allende) shows that the

calculated ^{60}Co depth profiles of Eberherdt et al. (1963) overestimate the production. The maximum slowing down density in a 100 cm H chondrite and in a 100 cm carbonaceous chondrite (cv3) occurs at 30 cm and 16 cm depths, respectively, with peak slowing down density of neutrons of 0.25 neutrons/cm^3.sec. and 0.50 neutrons/cm^3.sec., respectively. The peak neutron flux in 100 cm radius Kirin chondrite agrees with the peak flux of Eberherdt et al.

The exact shape of the energy spectrum of the nuclear active particles at any depth in a meteoroid body is not known, although it can be described by the spectral shape parameter (α) appearing in the empirical equation given by IV.1, and assumed by Reedy and Arnold (1972), which is a decreasing function of $E > 100$ MeV. The experimental ^{10}Be depth profile in a 50 cm radius body (present work), and in the Moon (Finkel 1972, Kohil 1975), show that the Reedy-Arnold model calculations of this high energy (100-1000 MeV) product is underestimated by a factor of about 2.2. Hence 100-1000 MeV flux required is about 2.2 times higher than the flux given by the equation IV.1.

The cosmogenic ^{21}Ne is, especially, useful in deducing the exposure age of meteorites, but due to the unknown depth and size dependent production rates, and the pre-irradiation effects, its use has been limited. The depth and size dependent ^{21}Ne production rate calculations made

in this thesis show that the $(^{22}Ne/^{21}Ne)_{sp}$ ratio less than 1.06 is not possible for chondrites with a simple one stage exposure history. It is found that there are several chondrites with neon isotopic ratio less than 1.06, and also the ratio less than that expected for their shielding depth and preatmospheric size. Several such chondrites with multiple exposure history are identified, and based on some plausible irradiation depth on parent bodies, model exposure ages are calculated. The statistics is not adequate at present, but togther with particle tracks, neon isotopes and ^{53}Mn or ^{26}Al measurements in some aliquot samples, the exposure history and shielding depths etc. can be determined.

To study the cosmic ray intensity in the interplanetary space, and the variation in time, it is essential to know the heliocentric orbits of the meteoroids. One of the important parameters which can be used to determine the orbits is the preatmospheric velocity of meteoroids. There are only three meteorites for which the preatmospheric velocity and the heliocentric orbits are known. The aphelia of these meteorites lie in the asteroidal belt. In this thesis, the Baldwin-Sheaffer (1971) ablation model is discussed in terms of known ablation for these meteorites and is found to underestimate the ablation of low entryvelocity meteoroids. Using some variation of this model, to match the observed ablation of Lost City meteorite,

we have calculated the preatmospheric velocities of several meteorites with known ablation from cosmogenic particle track and rare gas studies of Bhandari et al. (1980). The preatmospheric velocities can be estimated within ±2 km/sec and the error due to uncertainty in the angle of entry is about 0.5 km/sec. Even though the statistics is poor, the velocity distribution obtained is similar to that of Millman (1969) based on about 250 computed meteorite orbits. The preatmospheric velocities and the information on the meteorite radiant, strewnfield data, the meteorite orbits can be calculated.

(B) Ancient Solar Flare Activity:

The concept of the constant sun has been challenged by the recent developments in the solar neutrino astronomy, and the observations of the varying sunspot activity. Several hypothesis have been put forward to explain the non-steady nature of solar magnetic field and the energy generation processes.

Here we have an opportunity to study the ancient solar flare activity with the availability of well documented lunar samples, the solar system materials from the known heliocentric distance. Moreover, because of dynamic lunar surface processes, we have samples with exposure ages varying from a fraction of Myr onwards, which can give information on various time averaged solar flare activity.

The direct measurements of the solar proton fluxes at 1 A.U. by SPME has yielded lower proton fluxes than the long-term average from radionuclide depth profile studies. The high depth resolution and high precision measurement of ^{26}Al depth profile in several lunar rocks and soil has yielded 0.4 to 1.5 Myr averaged flux given by (Js,Ro) = (125,125), which exactly reproduces ^{53}Mn depth profile in soil column 60010 measured by Nishiizumi and Arnold (1981). This 0.4 to 10 Myr averaged SCR flux of (125,125) is higher than the solar cycle 20 average of (90,85) and lower than the solar cycle 19 average of (378,100-130) and generally in agreement with the fluxes deduced by several other radionuclide viz. ^{3}H, ^{14}C, ^{59}Ni, ^{81}Kr depth profiles. This observation can be understood in terms of several periodicities in solar sunspot and flare activity.

REFERENCES

Armstrong T.W. and Alsmiller R.G., Jr. (1971), Calculation of cosmogenic radionuclide in the Moon and comparison with Apollo measurements, Proc. Lunar Sci. Conf. 2nd, 1979.

Arnold J.R., Honda M. and Lal D. (1961), Record of cosmic ray intensity in meteorites, J.Geophy. Res., 66, 3519.

Bagolia C., Doshi N., Gupta S.K., Kumar S., Lal D. and Trivedi J.R. (1977), The Dhajala meteorite shower: Atmospheric fragmentation and ablation based on cosmic ray tracks studies, Nucl. Track Detection, 1, 83.

Bagolia,C., Bhandari N., Goswami J.N., Lal D., Lorin J.C. and Pellas P. (1980), Multiple fall of Pribram meteorite photographed : 12. Preatmospheric size of the Pribram meteorite based on studies of fossil cosmic ray tracks and spallation products, Bull.Astron.Inst.Czechosl.,31,51.

Bahcall J.N. (1979), Solar neutrinos : Theory versus observations, Sp. Sci. Rev., 24, 227.

Baldwin B. and Sheaffer, Y. (1971), Ablation and breakup of large meteoroids during atmospheric entry, J.Geophy. Res.,76, 4653.

Ballabh G.M., Bhatanagar A. and Bhandari N. (1978), The orbit of Dhajala meteorite, Icarus, 33, 361.

Barsukov V.L. and Florensky C.P. (1977), Lunar soils from Mare Crisium : Preliminary data, Lunar Science VIII, 61.

Bedijn P.J., Burger, J.I. and Swanenburg B.N. (1973), The long-term modulation of cosmic rays, 13th Int. Cosmic Ray Conf., 5, 3106.

Begemann F., Born W., Palme H., Vilcsek E. and Wanke H. (1972), Cosmic ray produced radioisotopes in Apollo-12 and Apollo-14 samples, Proc. Lunar Sci. Conf. 3rd, 1963.

Begemann F., Breun O. and Webber N.W. (1980), Uber die leichten Edelgas in dem chondriten Kirin, Z.Naturforsch., 35a, 37.

Bieri R.H. and Rutsch W. (1962), Erzengungsquerschnitte fur Edelgas aus Mg, Al, Fe, Ni, Cu and Ag bei Bestrahlung mit 540 MeV protonnen, Helv. Phy. Acta, 35, 553.

Bhandari N. (1969), A selective and versatile low level Beta-, X-, and Gamma-ray detector assembly, Nucl. Instr. Meths., 50, 251.

Bhandari N. (1969a), On orbital velocities of some stone meteorites, Proc. on 11th Symposium on cosmic rays, Astrophysics and Elementary Particle Physics, 11, 322.

Bhandari N., Bhat, S., Lal D., Rajagopalan G., Tamhane A.S. and Venkatavardan V.S. (1971), High resolution time averaged (millions of years) energy spectrum and chemical composition of iron group cosmic ray nuclei at 1 A.U. based on fossil tracks in Apollo samples, Proc. Lunar Sci. Conf. 2nd, 3, 2611.

Bhandari N., Goswami J.N., Lal D. and Tamhane A.S. (1973), Temporal variation of relative abundances of galactic VH and VVH nuclei., Proc. Int. Cosmic Ray Conf. 13th, 2, 1464.

Bhandari N., Bhattacharya S.K. and Padia J.T. (1975), The surface radioactivity of lunar rocks : Implications to solar activity in the past, Proc. Lunar Sci. Conf. 6th, 1913.

Bhandari N., Lal D., Trivedi J.R. and Bhatnagar A. (1976a), The Dhajala meteorite shower, Meteoritics, 11, 137.

Bhandari N., Bhattacharya S.K. and Padia J.T. (1976), Solar proton fluxes during the last million years, Proc. Lunar Sci. Conf. 7th, 513.

Bhandari N., Bhattacharya S.K. and Somayajulu B.L.K. (1978), Cosmogenic radio isotopes in Dhajala Chondrite : Implications to variations of cosmic ray fluxes in the interplanetary space, Earth Planet. Sci. Lett., 40, 194.

Bhandari N., Bhattacharya S.K. and Potdar M.B. (1979), Production profiles of radionuclides in chondrites and their solar cycle variation, Lunar & Planetary Science X, 107.

Bhandari N., Lal D., Nautiyal C.M., Padia J.T., Potdar M.B., Rao M.N. and Venkatesan T.R. (1980a), Determination of preatmospheric sizes of meteorites using neon isotopes and particle tracks, Meteoritics, 15, 265.

Bhandari N., Lal D., Rajan R.S., Arnold J.R., Marti K. and Moore C.B. (1980), Atmospheric ablation in meteorites : An experimental study based on cosmic ray track, Nuclear Tracks, 4, 213.

Bhandari N., Potdar M.B. and Suthar K.M. (1981), Multiple exposure history of chondrites (Abstracts), Meteoritical Society Meeting, Bern, Switzerland.

Bhandari N. and Potdar M.B. (1981), Cosmogenic ^{21}Ne and ^{22}Ne depth profiles in chondrite, Submitted to Earth & Planet. Sci. Lett.

Bhandari N., Potdar M.B. and P.N. Shukla (1981a), Induced radioactivity, tracks and rare gas studies in South Ray crater rocks, Lunar and Planetary Science XII, 62.

Bhattacharya S.K., Goswami J.N. and Lal D. (1973), Semi-empirical rates of formation of cosmic ray tracks in spherical objects exposed in space : Pre-atmospheric and post-atmospheric depth profiles, J.Geophys. Res., 78, 8356.

Bhattacharya S.K., Goswami J.N., Gupta S.K. and Lal D.(1973a), Cosmic ray effects induced in a rock exposed on the Moon or in free space : Contrast in patterns for "tracks" and "isotopes", Moon, 8, 253.

Bhattacharya S.K. and Bhandari N. (1975), Effects of exposure conditions on cosmic ray records in lunar rock, Proc. Lunar Sci. Conf. 6th, 1901.

Bhattacharya S.K. and Bhandari N. (1976), Modulation of galactic cosmic rays from the study of cosmogenic radioisotopes in meteorites, Proc. Symp. on Solar Planet. Phys., 2, 162.

Bhattacharya S.K. (1979), Cosmic ray characteristics based on induced radioactivity in lunar samples and meteorites, Ph.D. Thesis, Gujarat University, Ahmedabad, India.

Bhattacharya S.K., Imamura M., Sinha N. and Bhandari N. (1980), Depth and size dependence of ^{53}Mn activity in chondrites, Earth Planet. Sci. Lett., 51, 45.

Blake J.B., Paulikas G.A. and Freden S.C. (1969), Observation of solar protons aboard OV3-3 and ATS-1, in "Solar Flares and space research", (Ed.by C.de Jaeger and Z.Svestka), North Holland, p.266.

Blanchard D.P., Haskin L.A., Branon J.C. and Aboae E.L.(1977), Chemistry of soils and particles from Luna-24 (Abstracts) Conf. on Luna-24, 37.

Blanford D.E., Fruland R.M., Makay D.S. and Morrison D.A. (1974), Lunar surface phenomena; solar particle track gradients, micro-craters and accretionary particles, Proc. Lunar Sci. Conf. 3rd, 3557.

Burger J.J. and Swanenburg B.N. (1973), Energy dependent time lag in long-term modulation of cosmic rays, J. Geophys. Res., 78, 292.

Boeki R.S. (1972), A depth profile of ^{14}C in Lunar rock 12002, Earth Planet. Sci. Lett., 16, 269.

Bochsler P., Eberhardt, P., Geiss J. and Grogler N. (1969), Rare gas measurements in separate mineral phases of the Otis and Elenovka chondrites, in "Meteorite Research", (Ed. by P.Millman), D.Reidel, p.857.

Bogard D.D. and Cressy P.J., Jr. (1973), Spallation production of ^{3}He, ^{21}Ne and ^{38}Ar from target elements in Bruderheim chondrite, Geochim. Cosmochim. Acta, 37, 527.

Bogard D.D. and Gibson E.K., Jr. (1975), Volatile gases in Breccia 68115 (Abstracts), Lunar Science VI, 63.

Bogard D.D. and Hirsch W.C. (1978), Noble gases in Luna-24 core soils, in "Mare Crisium : The view from Luna-24" (Ed. by Merill and Pipike), Pergamon Press, N.Y., p.105.

Bogard D.D., Hirsch W.C. and Evans J.C. (1980), Cosmic ray exposure ages and shielding conditions of recently fallen chondrites (Abstracts), Lunar and Planetary Science XI,91.

Bostrom C.O., Williams O.J., Arens J.F. and Kohl J.W. (1967-1973), Solar proton monitor experiment, Solar Geophys. Data, 282-341.

Bourot-Denise M. and Pellas P. (1981), Cosmic ray track studies of Jilin (Kirin) chondrite (Abstracts), Meteoritical Society meeting, Bern, Switzerland.

Bronshtein V.A. (1964), Problems of movement of large meteoritic bodies in the atmosphere, NASA-TTF-247.

Cantelaube Y., Pellas P., Nordemann, D. and Tobailem J. (1969), Reconstitution de la meteorite Saint-Severin dans lespace, in "Meteorite Research" (Ed.by P.Millman), p.705.

Cephecha Z. (1961), Multiple fall of Pribram meteorite Photographed : 1, Double-station photographs of the fireball and their relations to the found meteorite, Bull. Astron. Soc. Czech., 12, 21.

Chupp E.L. (1971), Gamma ray and neutron emission from the sun, Sp. Sci. Rev., 12, 486.

Co-operation group, China (1977), Cosmogenic nuclides K^{40}, Mn^{54} and Co^{57} in Kirin meteorites and their depth distribution, Geochimica, 3, 173.

Cox J.P. and Giuli R.T. (1968), Principles of stellar structure, Gordon & Breach Science Publishers, N.Y.

Crozaz, R., Haak U., Hair M., Maurette M., Walker R. and Woolum D. (1970), Nuclear track studies of ancient solar radiation and dynamic lunar surface processes, Proc. Lunar Sci. Conf. 11th, 3, 2051.

Cressy P.J., Jr. (1964), Cosmogenic radionuclides in stone meteorites, Ph.D. Thesis, Carnegie Institute of Technology, Pittsberg, USA.

Cressy P.J., Jr. (1970), Multiparameter analysis of gamma radiation from Barwell, St. Severin and Tathlith meteorites, Geochim. Cosmochim. Acta, 34, 771.

Cressy P.J., Jr. (1971), The production rate of ^{26}Al from target elements in Bruderheim chondrite, Geochim. Cosmochim. Acta, 35, 1283.

Cressy P.J., Jr. (1971a), Cosmogenic radionuclides in the Lost City and Ucera meteorites, J.Geophy.Res., 76, 4072.

Cressy P.J., Jr. (1972), Cosmogenic radionuclides in Allende and Murchison carbonaceous chondrites, J.Geophys.Res.,77, 4905.

Ezer D. and Cameron A.G.W. (1972), Effects of sudden mixing in solar core on solar neutrinos and ice age, Nature, 240, 1280.

Finkel R.C. (1972), Depth profiles of galactic cosmic ray produced radionuclides in lunar samples., Ph.D. Thesis, University of California, San Diego, USA.

Finkel R.C., Kohl C.P., Marti K., Martinek B. and Rancetelli L. (1978), The cosmic ray record of the San Juan Capistrano meteorite, Geochim. Cosmochim. Acta., 42, 241.

Fireman E.L. and DeFelice J. (1961), Tritium, Argon-37 and Argon-39 in Bruderheim meteorite, J. Geophy. Res., 46, 3547.

Fireman E.L. (1966), Neutron exposure ages of meteorites, Z. Naturforsch., 21a, 1138.

Fleischer R.L., Price P.B., Walker R.M. and Maurette M.(1967), Origin of fossil charged particle tracks in meteorites, J. Geophy. Res., 72, 331.

Fleischer R.L., Hart H.R., Jr. and Comstock G.M. (1971), Very heavy solar cosmic rays : Energy spectrum and implications for lunar erosion, Science, 1971, 1240.

Fowler W.A. (1972), What cooks with solar nutrinos?, Nature 238, 24.

Freier P.S. and Webber W.R. (1963), Exponential rigidity spectrum for solar flare cosmic rays, J.Geophy. Res., 68,1605.

Fruchter J.S., Rancetelli L.A. and Perkins R.W. (1976), Recent and long-term mixing of lunar regolith based on ^{22}Na and ^{26}Al measurements in Apollo-15, 16, and 17 deep drill stems and drive tubes, Proc. Lunar Sci. Conf. 7th, 27.

Cressy P.J., Jr. and Bogard D.D. (1976), On the calculation of cosmic ray exposure ages of stone meteorites, Geochim. Cosmochim. Acta 40, 749.

Crozaz, R., Haak U., Hair M., Maurette M., Walker R. and Woolum D. (1970), Nuclear track studies of ancient solar radiation and dynamic lunar surface processes, Proc.Lunar Sci. Conf. 11th, 3, 2051.

D'Amico J., De Felice J., Fireman E.L., Jones C. and Spannagel G. (1971), Tritium and Argon radioactivities and their depth variation in Apollo-12 samples, Proc. Lunar Sci. Conf. 2nd, 1825.

Drozd R.J., Hohenberg C.M., Morgan C.J. and Ralston C.E., (1974), Cosmic ray exposure history at the Apollo-16 and other lunar sites : Lunar surface dynamics, Geochim. Cosmochim. Acta, 38, 1975.

Drozd R.J., Kennedy B.M., Morgan C.J., Podosek F.A. and Taylor G.J. (1976), The excess fission Xenon problem in lunar samples, Proc. Lunar Sci. Conf. 7th, 599.

Eberhardt P., Geiss J. and Lutz H. (1963), Neutrons in meteorites, in "Earth Science and Meteorites", (Ed.by J.Geiss and E.D. Goldberg), p.143.

Eberhardt P., Eugster O., Geiss J. and Marti K. (1966), Rare gas measurements in 30 chondrites, Z. Naturforsch. 21a, 414.

Eddy J.A. (1976), Mounder minimum, Science 1972, 1189.

Evans J.C., Rancetelli L.A., Reeves J.H. and Bogard D.D.(1979), Galactic cosmic ray variations during the period 1967 to 1978; Cosmogenic radionuclide production in meteorites (Abstracts), Conf.on Ancient Sun : Fossil records in the Earth, Moon and Planets, Boulder Colorado, 16-19 Oct.1979, p.28.

Fruchter J.S., Evans J.C., Reeves J.H. and Perkins R.W. (1981), Evidence from ^{26}Al profile for accretion of Apollo-15 double drive tube 15010/11, (Abstracts), Lunar and Planetary Science XII, 774.

Furukawa M., Shizuri K., Komura K., Satamoto K. and Tanaka S. (1971), Production of ^{26}Al and ^{22}Na from proton bombardment of Si, Al and Mg, Nucl. Phys. A., 174, 539.

Garcia-Munoz M., Mason G.M. and Simpson J.A. (1975a), The anomalous ^{4}He component in cosmic rays at $\lesssim$ 50 MeV per nucleon during 1972-74, Ap.J., 202, 265.

Garcia-Munoz M., Mason G.M. and Simpson J.A. (1975b), The low energy cosmic ray ^{2}H and ^{3}He spectra and the anomalous ^{4}He component, 14th Int. Cosmic Ray Conf., 1, 319.

Garcia-Munoz M., Mason G.M. and Simpson J.A. (1977a), New aspect of cosmic ray modulation in 1974-75 near solar minimum, Ap. J., 213, 263.

Garcia-Munoz M., Mason G.M. and Simpson J.A. (1977b), The appearance of superfluxes of quiet time cosmic rays, 15th Int. Cosmic Ray Conf., 3, 209.

Geiss J. and Oeshger H. (1960), The impact of cosmic radiation in meteorites, Space Research (Interscience, N.Y), 7, 1071.

Gensho R., Nitoh O., Makino T. and Honda M. (1977), Some long-lived and stable nuclides produced by nuclear interactions, Proc. 2nd Symposium on "Origin and Distribution of the chemical elements", Paris (IAGC), 11.

Goebel K., Schultes H. and Zahringer J. (1964), Production cross sections of Tritium and rare gases in various target elements, C.E.R.N.Report CERN-64-12, 7B.

Gopalan K. and Rao M.N. (1976), Rare gases in Bansur, Udaipur and Madhipura chondrites, Meteoritics, 11, 131.

Gopalan K., Rao M.N., Suthar K.M. and Venkatesan T.R.(1977), Cosmogenic and radiogenic noble gases in Dhajala chondrite, Earth Planet Sci. Lett., 36, 341.

Gosling J.T., Hansen R.T. and Bame J.S. (1971), Solar wind speed distributions 1962-1970, J.Geophy. Res., 76, 1811.

Goswami J.N., Lal D., Rao M.N., Sinha N. and Venkatesan T.R. (1978), Particle track and rare gas studies of Innisfree meteorite, Meteoritics, 13, 481.

Halliday I., Blackwell A.T. and Griffin A.A. (1978), Innisfree meteorite and the Canadian camera network, J.Roy. Astron. Soc. Canada, 72, 15.

Hampel W. (1971), Messung von γ-emitteren den radionucliden in den chondriten Chitado, Allende, Police, Lost City und Caserio Ucera, Diplomarbeit, Max-Planck-Institut fur Kernphysik, Heidelberg.

Heymann D. and Hubner W. (1974), Origin of inert gases in "Dusty Rock" 66095, Earth Planet. Sci. Lett., 22, 422.

Herzog G.F. and Anders E. (1971), Absolute scale for irridation ages of stony meteorites, Geochim. Cosmochim. Acta, 35, 605.

Heusser G., Kirsten T. and Ries D. (1979), Complex irradiation history of Kirin (H5) chondrite, Meteoritics, 14, 558.

Hsieh K.C., Mason G.M. and Simpson J.A. (1971), Cosmic ray ^{2}H from satellite measurements, 1965-69, Ap. J., 166, 221.

Hundhausen A.J. (1972), Coronal expansion and the solar wind, Springer-Verlag, Berlin, Heidelberg.

Honda M., Horie R., Imamura M., Nishiizumi K., Takaoka N. and Komura K., (1980), Irradiation history of the Kirin meteorite, Geochim. Jr., 14, 82.

Horz F., Brownlee D.E., Fechtig H., Hartung J.B., Morrison D.A., Neukum G., Schneider E., Vedder J.F. and Gault D.E. (1975), Lunar microcraters : Implications for the meteoroid complex, Planet. Space Sci., 23, 151.

Hutcheon I.O., McDougall J.D. and Price P.B. (1974), Improved determination of the long-term average Fe sepectrum from ~ 1 to ~ 460 MeV/nucleon, Proc. Lunar Sci. Conf. 5th, 2561.

Hoyt H.P., Walker R.M. and Zimmerman D.W. (1973), Solar flare proton spectrum averaged over last 5×10^3 years, Proc. Lunar Sci. Conf. 4th, 2289.

Intrigilator D.S. (1975), Measurement of large scale turbuleances in the solar system, Proc. 14th Int. Cosmic Ray Conf., 3, 1029.

Joint investigation group of Kirin meteorite shower (1977), A preliminary survey on Kirin meteorite shower, Scientia Sinica, 20, 502.

Kirsten, T., Krankovsky D. and Zahringer J. (1963), Edelgas und Kallium-Bustimmungen an enor groseren Zahl von Steinmeteoriten, Geochim. Cosmochim. Acta, 27, 13.

Kohl C.P. (1975), Galactic cosmic ray produced radioactivity in lunar and chondritic materials, Ph.D.Thesis, University of California, USA.

Kohman T.P. and Bender M. (1967), Nuclear production by cosmic rays in meteorites and on the moon, in "High Energy Nuclear Reactions in Astrophysics" (Ed. by B.S.P.Shen), 169.

King J.H. (1974), Solar proton fluences for 1977-1983 space missions, J. Space Craft and Rockets, 11, 401.

Kinsley J.H. (1969), A study of low energy cosmic rays at 1 A.U., NASA/GSFC report X-611-69-396, p.145.

Kohl C.P. Murrel M.T., Russ G.P., III and Arnold J.R.(1978), Evidence for constancy of cosmic ray flux over the past ten million years : ^{53}Mn and ^{26}Al measurements, Proc. Lunar Sci. Conf. 9th,2299.

Lal D. and Peters B. (1967), Cosmic ray produced radioactivity on the earth, Handbook der Physik (Ed. by S. Flugge), Springer-Verlag, p.551.

Lal D. (1969), Recent advances in the study of fossil tracks in meteorites due to heavy nuclei of cosmic radiation, Sp. Sci. Rev., 9, 623.

Lal D., Lorin J.C., Pellas P., Rajan R.S. and Tamhane A.S. (1969), On energy spectrum of iron group nuclei as deduced from fossil track studies in meteoritic minerals, in "Meteorite Research" (Ed. by P. Millman), D.Reidel, 275.

Lal D. and Marti K. (1977), On the flux of low energy particles in the solar system : The record in St.Severin meteorite, Nuclear Track Detection, 1, 127.

Lanzerotti L.J., Reedy R.C. and Arnold J.R. (1973), Alpha particles in cosmic rays over the last 80,000 years, Science, 179, 1232.

Lederer C.M. and Shirley V.S. (1978), Table of isotopes (VII Edition), Pub. By John Wiley and Sons, Inc.

Lezniak J.A. and Webber W.R. (1974), solar modulation of cosmic ray proton, helium nuclei and electrons, J.Geophys. Res., 76, 1605.

Lin R.P. and Hudson H.S. (1976), Non-thermal processes in large solar flares, Solar Phys., 50, 153.

Lingenfelter R.E., Canfield E.H. and Hampel V.E. (1972), The lunar neutron flux revisited, Earth Planet. Sci. Lett., 16, 355.

Lingenfelter R.E. and Hudson H.S. (1980), Solar particle fluxes and the ancient sun, Proc. Conf. on Ancient Sun, 69.

Marti K. (1967), Mass spectrometric detection of cosmic ray produced ^{81}Kr in meteorites and the Kr-Kr dating, Phy. Rev. Lett., 18, 264.

Marti K., Shedlovsky J.P., Lindstrom R.M., Arnold J.R. and Bhandari N.G. (1969), Cosmic ray produced radionuclides and rare gases near the surface of Saint-Severin meteorite, in "Meteorite Research", (Ed. by P.Millman) D.Reidel, p.246.

Marti K. and Lugmair G.W. (1971), ^{81}Kr-^{83}Kr and ^{40}K - ^{40}Ar ages, cosmic ray spallation products and neutron effects in lunar samples from oceanus procellarum, Proc. Lunar Sci. Conf. 2nd, 1591.

McCrosky R.E., Posen A., Schwartz G. and Shao C.P. (1971) Lost City meteorite : Its recovery and a comparison with other fireballs, J.Geophys. Res., 76, 4090.

McKibben R.B. (1977), The charge state of "anomalous" helium component as determined from rigidity dependence of short-term modulations of low energy galactic cosmic ray intensity, 15th Int. Cosmic Ray Conf., 3, 194.

Millman P. (1969), Astronomical information on meteorite orbits, in "Meteorite Research" (Ed. by P.Millman), D. Reidel, 541.

Mitchel J.M., Jr. (1976), An overview of climatic variability and its casual mechanisms, Quat. Res., 6, 481.

Modisettee J.L., Vinson T.M. and Hardy A.C. (1965), Model solar proton environments for manned spacecraft design, NASA/TND-2746, 23.

Moraal H. (1976), Observation of eleven year cosmic ray modulation cycle, Sp. Sci. Rev., 19, 845.

Muller O., Hampel W., Kirsten T. and Herzog G.F. (1980), Cosmic ray constancy and cosmogenic production rates in short-lived chondrites, Geochim. Cosmochim Acta, 45, 447.

Murali A.V., Pawaskar P.B., Reddy G.R. (1979), Chemical studies of two luna-24 regolith samples, Proc. Indian Nat. Sci. Academy, 45A, 2613.

Newkirk G. (1980), Solar variability on time scales of 10^5 years to $10^{9.6}$ years, Proc. Conf. on Ancient Sun, 293.

Niederer F., Wahlan M. and Geiss J. (1975), A search for energetic tritons in lunar samples, Meteoritics, 10, 466.

Nishiizumi K., Regnier S. and Marti K. (1980), Cosmic Ray exposure ages of chondrites, pre-irradiation and constancy of cosmic ray flux in the past, Earth Planet. Sci. Lett., 50, 156.

Nishiizumi K. and Arnold J.R. (1981), ^{53}Mn profiles and gardening process in lunar cores 60010 and 15011, (Abstracts), Lunar & Planetary Science XII, 306.

NOAA (1977), Solar Geophysical Data No.397, p.8.

Nordemann D., Tobailem J. de Lassus St.Genies CH. (1970), The St.Severin meteorite : Calculations of the atmospheric trajectory and orbit, commissariat and l'Energy atomique France, Report No.CEA-R-4045, 13.

Noon A.F., Fredriksson K., Jarosewich E. and Brenar P. (1976), Minerology and bulk, chondrite, size fraction chemistry of the Dhajala, India, Chondrite, Meteoritics, 11, 340.

Oeshger H. and Wahlen M. (1975), Low level counting techniques, Ann. Rev. of Nuclear Science, 25, 423.

Opik E.J. (1958), Physics of meteor flight in atmosphere, Pub. by Interscience, N.Y.

Paneth F.A., Reasbeck P. and Mayne K.I. (1953), Production by cosmic rays of Helium-3 in meteorites, Nature, 172, 700.

Perron C. (1975), Ph.D. Thesis, University of Paris sud, Orsay.

Potdar M.B. and Bhandari N. (1979), Natural radioactivity of Luna-24 and Apollo-16 soils, Proc.Indian Nat. Sci. Academy, 45A, 32.

Price P.B., Rajan R.S. and Tamhane A.S. (1967), On preatmospheric size and maximum space erosion rate of Patwar stony-iron meteorite, J.Geophy. Res., 72, 1377.

Raisbeck G.M. and Yiou F. (1974), Cross sections for spallation production of ^{10}Be in target N, Mg and Si, and their astrophysical applications, Phy. Rev., C9, 1385.

Raisbeck G.M., Boersling P., Klapisch R. and Thomas T.D. (1975) Li, Be and B production in the 3-GeV proton bombardment of Ni Phy. Rev., C12, 527.

Rajan R.S., ReVelle D.O. and Wetherill G.W. (1977), Preatmospheric velocities of meteorites, Meteoritics, 13, 604.

Rancetelli L.A., Perkin R.W., Cooper J.A., Kaye J.H. and Wogman N.A. (1969), Radionuclide composition of the Allende meteorite from non-destructive gamma-ray spectrometric analysis, Science, 166, 1269.

Reedy R.C. and Arnold J.R. (1972), Interaction of solar and galactic cosmic ray particles with the Moon, J.Geophy. Res., 77, 537.

Reedy R.C., Herzog G.F. and Jessberger E.K. (1979), The reaction Mg(n, α) Ne at 14.1 and 14.7 MeV : Cross sections and implications for meteorites, Earth Planet. Sci. Lett., 44, 341.

Reedy R.C. (1980), Lunar radionuclide records of average cosmic ray fluxes over the last ten million years, Proc. Conf. on Ancient Sun, 365.

Regnier S., Lagarde M. and Simonoff G.W. (1973), Production de ^{26}Al dans Fe et Si par protons de 0.6 et 24 GeV, Earth Planet. Sci. Lett., 18, 9.

ReVelle D.O. (1979), A quasi-simple oblation model for large meteorite entry : Theory versus observations, J.Atmosph. Terr. Phys., 41, 453.

Rowley J.K., Cleveland B.T., Davis R., Jr., Hampel V.E. and Kirsten T. (1980), The present and past solar neutrino luminosity of the sun, Proc. Conf. on Ancient Sun, 45.

Schwarzchild M. (1958), Structure and evolutionary history of stars, Princeton University Press, N.J.

Schaeffer O.A. and Heymann D. (1965), Comparison of ^{36}Cl-^{36}Ar and ^{38}Ar-^{39}Ar cosmic ray exposure ages of dated fall of iron meteorites, J.Geophy. Res., 70, 215.

Schaeffer O.A. (1975), Constancy of galactic cosmic rays in time and space, Proc. 14th Int. Cosmic Ray Conf., 11, 3508.

Shedlovsky J.T., Honda M., Reedy R.C., Evans J.C., Lal D., Lindstrom R.M., Delany A.C., Arnold J.R., Loosli H.H., Fruchter J.S. and Finkel R.C. (1970), Pattern of bombardment produced radionuclides in rock 10017 and in lunar soil, Proc. Lunar Sci. Conf. 11th, 2, 1503.

Schultz L., Signer P., Lorin J.G. and Pellas P. (1972), Complex irradiation history of Weston chondrite, Earth Planet. Sci. Lett., 15, 403.

Schultz L. and Signer P. (1976), Depth dependence of spallogenic helium, neon and argon in St.Severin chondrite, Earth Planet. Sci. Lett., 30, 191.

Silberberg R. and Tsao C.H. (1973), Partial cross-sections in high energy nuclear reactions and astrophysical applications, Targets with Z 28, Ap. J. Suppl. 220, 25, 315.

Simonenko A.N. (1978), Orbital elements of 45 meteorites, Pub. by Academy of USSR, Moscow, 1975.

Spergel M.S., Reedy R.C., Lazareth O.W. and Levy P.W. (1981), Cosmogenic nuclide production in small spherical meteoroids, Lunar and Planetary Science XII, p.1026.

Stetler A., Eberhardt P., Geiss J., Grogler N. and Mauner P. (1973), Ar-39-Ar-40 ages and Ar-37-Ar-39 exposure ages of lunar rocks, Proc. Lunar Sci. Conf. 4th, 1865.

Tobailem J., Charles Henri de Lassus St. Genies (1977), Sections efficacies des reactions nucleaires induites par protons, deutons, particles alpha, IV-Aluminium, Note CEA-N-1466 (4), 45.

Trivedi B.M.P. and Goel P.S. (1969), Productions of ^{22}Na and ^{3}H in a thick slicate target and its application to meteorites J.Geophys. Res., 74, 3909.

Van Ginneken A., and Turkevich A. (1970), Production of manganese 54 and zinc 65 from copper in thick targets by 0.45 GeV, 1.0 GeV, and 3-GeV protons, J.Geophy. Res., 75,5121.

Van Hollebeke M.A.I., Wang J.R. and McDonald F.B. (1972), Modulation of low energy galactic cosmic rays over solar maximum (cycle 20), J.Geophys. Res., 77, 6881.

Van Schmus W.R. and Wood J.A. (1967), A chemical and petrological classification for chondritic meteorites, Geochim. Cosmochim. Act, 31, 747.

Venkatesan T.R., Nautiyal C.M., Padia J.T. and Rao M.N.(1980), Solar (flare) cosmic ray proton fluxes in the recent past, Proc. Lunar Sci. Conf. 11th, 1271.

Voshage H. and Hintenberger H. (1963), The cosmic ray exposure ages of iron meteorites as derived from isotopic composition of potassium and production rates of cosmogenic radionuclides in the past, in "Radioactive dating and methods of low level counting", IAEA, 367.

Wahlen M., Finkel R.C., Imamuma M., Kohl C.P. and Arnold J.R. (1973), ^{60}Co in lunar samples, Earth Planet. Sci. Lett., 19, 315.

Waldmeir M. (1961), The sunspot activity in the years 1610-1960, Pub. by Zurich Schulthess & Co. AG.

Walton J.R. (1974), Production of Helium, Neon, Argon in lunar material by solar cosmic ray protons, Ph.D. Thesis, Michigan University, U.S.A.

Walton J.R., Heymann D., Yaniv A., Edgerly D. and Rowe M.W. (1976), Cross sections for He and Ne isotopes in natural Mg, Al and Si, He isotopes in CaF_2, Ar isotopes in natural Ca and radionuclides in natural Al, Si, Ti, Cr and stainless steel induced by 12- to 45 - MeV protons, J.Geophys. Res., 81, 5689.

Wanke H. (1974), Chemical composition of the Moon, in "Topics in Current Chemistry" (Ed. by A.Davison et al.), Springer-Verlag, Heidelberg.

Wasson J.T. (1974), Meteorites : Classification and properties, Springer-Verlag, Heidelberg.

Wdowczyk J. and Wolfendale A.W. (1979), Diffusion of highest energy cosmic rays from Virgo Cluster, Nature, 281, 356.

Webber W.R. (1966), An evaluation of solar-cosmic ray events during solar minimum, The boeing company report D2-84274-1 (DDC document number AD-821677), 44.

Webber W.R. (1967), The spectrum and charge composition of the primary cosmic radiation, Handbook der Physik (Ed. by S. Flugee) 46, 181.

Weddel J.B. and Haffner J.W. (1966), Statistical evaluation of radiation from solar flares, North American Aviation Report SID 66-424 (N 67-13210; NASA-CR-80531),172.

Wetherill G.W. (1980), Multiple cosmic rays exposure ages of chondrites, Meteoritics, 15, 386.

Whipple F.L. and Hawkins G.S. (1959), Meteors, Handbook of Phys. (Ed. by S. Fluggee), Springer-Verlag, 518.

Wolfendale A.W. (1975), Possible explanation of the spectral shape, in "Origins of Cosmic Rays" (Ed. by Osborne J.L. and Wolfendale A.W.), D.Reidel, p.221.

Woolum D.S., Burnett D.S., Marian F. and Weiss J.R. (1975), Measurement of lunar neutron density profile, The Moon,12,231.

Wright R.J., Simms L.A., Reynolds M.A. and Bogard D.D.(1973), Depth variation of cosmogenic noble gases in the 120-kg Keyes chondrite, J.Geophy. Res., 78, 1308.

Yaniv A. and Marti K. (1981), Detection of stopped solar flare helium in lunar rock 68815, Ap.J. Lett., 247, L143.

Zook H.A. (1980), On lunar evidence for a possible large increase in solar activity $\sim 2\times10^4$ years ago, Proc. Conf. on Ancient Sun, 245.

&&&&&&&&&&&&&&

LIST OF PUBLICATIONS

1. Bhandari N., Bhattacharya S.K. and Potdar M.B. (1979), Production Profiles of Radionuclides in chondrites and their Solar Cycle Variation; Lunar and Planetary Science X, 107.

2. Potdar M.B. and Bhandari N. (1979), Natural Radioactivity of Luna-24 and Apollo-16 Soils, Proc. Indian Nat. Sci. Academy 45A, 32.

3. Bhandari N. and Potdar M.B. (1981), Cosmogenic ^{21}Ne and ^{22}Ne depth profiles in chondrites, To be published in Earth Planet. Sci. Lett.

4. Bhandari N., Potdar M.B. and Shukla P.N. (1981), Induced radioactivity, tracks and rare gas studies in South Ray Crater rocks, Lunar and Planetary Science XII, 62.

5. Bhandari N., Lal D., Nautiyal C.M., Padia J.T., Potdar M.B., Rao M.N. and Venkatesan T.R. (1980), Determination of preatmospheric sizes of meteorites using neon isotopes and particle tracks, Meteoritics, 15, 265.

6. Bhandari N., Potdar M.B. and Suthar K.M. (1981), Multiple exposure history of chondrites (Abstracts), Meteoritical Society Meeting, Bern, Switzerland.